



**Politecnico  
di Torino**

**Politecnico di Torino**

Thesis for Master of Science in Mechanical Engineering  
Department of Mechanical and Aerospace Engineering (DIMEAS)

# **Multibody modelling and handling analysis of a 1/5 scale vehicle**

**Advisor:**

Prof. Alessandro VIGLIANI (DIMEAS)

**Candidate:**

Aravind NARAYAN BABU (S271932)

**External Advisors:**

Ing. Angelo Domenico VELLA (DIMEAS)

Ing. Daniele CATELANI (Hexagon SPA)

Ing. Mauro VESCO (Hexagon SPA)

## Table of Contents

I.	<b>Index</b> .....	2
II.	<b>List of figures</b> .....	4
III.	<b>List of tables</b> .....	7
IV.	<b>Abstract</b> .....	8

### 1. Introduction

1.1.	The multibody approach and an introduction to ADAMS solver.....	9
1.1.1.	Newton – Raphson method.....	9
1.2.	Definitions related to the ADAMS environment.....	10
1.2.1.	Generalized co-ordinates.....	10
1.2.2.	Joints and motions in ADAMS.....	11
1.3.	Types of analyses in ADAMS.....	12
1.3.1.	Initial Condition (IC) Analysis.....	13
1.3.1.1.	Positional IC Analysis.....	13
1.3.1.2.	Velocity IC Analysis.....	14
1.3.1.3.	Force and Acceleration IC Analysis.....	14
1.3.2.	Kinematic Analysis.....	14
1.3.2.1.	Positional Kinematic Analysis.....	14
1.3.2.2.	Velocity Kinematic Analysis.....	15
1.3.2.3.	Force and acceleration Kinematic Analysis.....	15
1.3.3.	Dynamic Analysis.....	15
1.3.4.	Static Analysis.....	16

### 2. Vehicle specifications

2.1.	Losi 5T 2.0 specifications.....	17
------	---------------------------------	----

### 3. Template and subsystem modelling

3.1.	Front suspension.....	19
3.1.1.	Properties.....	19
3.1.2.	Template.....	22
3.2.	Rear suspension.....	23
3.2.1.	Properties.....	23
3.2.2.	Template.....	24
3.3.	Steering.....	25
3.3.1.	Description.....	25
3.3.2.	Template.....	26
3.4.	Brakes.....	27
3.5.	Driveline.....	27
3.6.	Chassis.....	30
3.7.	Powertrain.....	31
3.8.	Anti-roll Bars (ARB).....	32
3.8.1.	Finite Element (FE) part theory.....	32
3.8.2.	Loads in FE Part.....	33

3.8.3. Comparison of FE Part method vs other methods.....	33
3.8.4. Templates.....	34
3.9.Tires.....	35
3.9.1. Fiala Tire model.....	35
3.9.2. Templates.....	37
<b>4. Assembly creation and Full Vehicle modelling</b>	
4.1. Front suspension assembly.....	38
4.2. Rear suspension assembly.....	39
4.3.Full vehicle assembly.....	40
<b>5. Simulation setups</b>	
5.1.Suspension simulation setups.....	42
5.1.1. Front suspension simulations.....	42
5.1.1.1. Parallel wheel travel.....	42
5.1.1.2. Opposite wheel travel.....	43
5.1.1.3. Steering simulations.....	43
5.1.2. Rear suspension simulations.....	44
5.1.2.1. Parallel wheel travel.....	44
5.1.2.2. Opposite wheel travel.....	45
5.2. Full vehicle simulation setups.....	46
5.2.1. Static equilibrium test.....	46
5.2.2. Ramp steer.....	47
5.2.3. Step steer.....	48
<b>6. Results</b>	
6.1.Suspension Analysis results.....	49
6.1.1. Parallel wheel travel.....	49
6.1.1.1. Computation of installation ratios.....	49
6.1.1.2.Influence of spring stiffnesses.....	50
6.1.1.3.Influence of camber angle.....	52
6.1.1.4.Influence of toe angle.....	56
6.1.2. Opposite wheel travel.....	57
6.1.2.1.Influence of ARBs.....	57
6.1.2.2.Influence of spring stiffnesses.....	60
6.1.3. Steering simulation results.....	62
6.2.Full vehicle analysis results.....	63
6.2.1. Static equilibrium test.....	63
6.2.2. Ramp steer results.....	63
6.2.3. Step steer results.....	68
6.2.3.1.Influence of spring stiffnesses.....	68
6.2.3.2.Influence of ARBs.....	71
<b>7. Conclusions and further scope of work.....</b>	<b>75</b>
V. <b>Appendix.....</b>	<b>76</b>
VI. <b>References.....</b>	<b>80</b>
VII. <b>Acknowledgements.....</b>	<b>81</b>

## List of figures

Fig. 2.1 - Basic dimensions - Losi 5ive T 2.0 - Top View.....	17
Fig. 2.2 - Basic dimensions - Losi 5ive T 2.0 - Side View.....	17
Fig. 3.1- Front suspension- Losi 5iveT 2.0.....	19
Fig. 3.2 - Front suspension Template.....	22
Fig. 3.3 - Losi 5iveT 2.0 rear suspension.....	23
Fig. 3.4 – Rear suspension template.....	24
Fig. 3.5 - Steering CAD model.....	26
Fig. 3.6 - Steering template on ADAMS/Car.....	26
Fig. 3.7 - Brakes template.....	27
Fig. 3.8 - Driveline template.....	28
Fig. 3.9 - Chassis template.....	30
Fig. 3.10 - Powertrain template .....	31
Fig. 3.11 – Front anti-roll bar (ARB) template.....	34
Fig. 3.12 - Rear anti-roll bar (ARB) template.....	35
Fig. 3.13 - Front tires template.....	37
Fig. 3.14 – Rear tires template.....	37
Fig. 4.1- Front suspension assembly.....	38
Fig. 4.2 – Rear suspension assembly.....	39
Fig. 4.3 – Full vehicle assembly.....	40
Fig. 5.1 - Parallel wheel travel setup – Front.....	42
Fig. 5.2 – Opposite wheel travel setup – Front.....	43
Fig. 5.3 – Steering simulation setup.....	44
Fig. 5.4 – Parallel wheel travel setup – rear.....	45
Fig. 5.5 – Opposite wheel travel setup – rear.....	45
Fig. 5.6 – Static Equilibrium Test setup .....	46
Fig. 5.7 – Ramp steer test setup.....	47
Fig. 5.8 – Step steer test setup.....	48

Fig 6.1 – Installation ratios for the front suspension assembly.....	49
Fig. 6.2 – Installation ratios for the rear suspension assembly.....	50
Fig 6.3 – Total roll rate variation vs wheel travel for front suspension.....	51
Fig. 6.4 – Scrub radius variation due to spring stiffnesses in front suspension.....	52
Fig. 6.5 – Camber variation in front suspension vs wheel travel.....	53
Fig. 6.6 – Camber variation in rear suspension vs wheel travel.....	53
Fig. 6.7 – Scrub radius vs wheel travel for front suspension.....	54
Fig. 6.8 – Lateral distance to roll centre from tire patch for front suspension vs wheel travel	55
Fig. 6.9 – Lateral distance to roll centre from tire patch for rear suspension vs wheel travel.	55
Fig. 6.10 – Total roll rate variation vs wheel travel for different camber angles in front suspension.....	56
Fig. 6.11 – Scrub radius vs vertical wheel travel for different toe angles in front suspension.....	57
Fig. 6.12 – Normal tire forces in front suspension for opposite wheel travel.....	57
Fig. 6.13 – Variation of normal tire forces in rear suspension for opposite wheel travel.....	58
Fig. 6.14 – Total roll rate for front suspension vs wheel travel.....	59
Fig. 6.15 - Total roll rate for rear suspension vs wheel travel.....	59
Fig. 6.16 – Tire normal forces for front suspension with different spring stiffnesses vs wheel travel .....	60
Fig. 6.17 – Tire normal forces for rear suspension with different spring stiffnesses vs wheel travel.....	60
Fig. 6.18 – Variation in total roll rate for different springs in front suspension vs wheel travel.....	61
Fig. 6.19 – variation in total roll rate for rear suspension with different spring stiffnesses vs wheel travel.....	61
Fig. 6.20 – Steering input vs steering angle at wheels.....	62
Fig. 6.21 – Wheel load variation in ramp steer manoeuvre with ARB.....	63
Fig. 6.22 – Wheel load variation in ramp steer manoeuvre without ARB.....	63
Fig. 6.23 – Steering angle vs lateral acceleration during ramp steer.....	64
Fig. 6.24 – Sideslip angle vs lateral acceleration during ramp steer manoeuvre.....	65
Fig. 6.25 – Chassis roll angle vs lateral acceleration during ramp steer manoeuvre.....	66
Fig. 6.26 – Time evolution of chassis roll angle during ramp steer.....	67

Fig. 6.27 – Time evolution of lateral acceleration during step steer manoeuvre for different spring stiffnesses.....	67
Fig. 6.28 Time evolution of chassis roll angle during step steer manoeuvre for different spring stiffnesses.....	68
Fig. 6.29 – Time evolution of sideslip angle during step steer manoeuvre for different spring stiffnesses.....	69
Fig. 6.30 – Time evolution of yaw rate during step steer manoeuvre for different spring stiffnesses.....	69
Fig. 6.31 – Handling diagram depicting the steer angles (solid lines) and corresponding sideslip angles (dashed lines) for the analysis of effect of spring stiffness.....	70
Fig. 6.32 – Effect of ARB on temporal evolution of lateral acceleration for step steer manoeuvre.....	71
Fig. 6.33 – Effect of ARB on temporal evolution of chassis roll for step steer manoeuvre...	72
Fig. 6.34 – Effect of ARB on the temporal evolution of sideslip angle during step steer manoeuvre.....	72
Fig. 6.35 – Effect of ARB on temporal evolution of yaw rate for step steer manoeuvre.....	73
Fig. 6.36 – Handling diagram for the analysis on the effect of ARB during step steer with steer angles (solid lines) and sideslip angles (dashed lines) vs lateral acceleration.....	74
Fig. A.1 – Three-dimensional (3D) Beam particle depiction.....	76
Fig. A.2 – Depiction of coordinates of beam element.....	77

## List of Tables

Table 1.1 – Joints and associated constraints in ADAMS environment.....	12
Table 2.1 - Basic dimensions of Losi 5iveT 2.0.....	18
Table 2.2 - Mass and Inertia Properties.....	18
Table 3.1 – Damper properties of Losi 5iveT 2.0.....	20
Table 3.2 – Front spring properties.....	21
Table 3.3 - Constraints in the front suspension template.....	22
Table 3.4 - Rear spring properties.....	24
Table 3.5 - Constraints in the rear suspension template.....	25
Table 3.6 – Constraints in the steering template.....	27
Table 3.7 – Constraints in the driveline template.....	29
Table 3.8 – Constraints in the chassis template.....	31
Table 3.9 – Constraints in the powertrain template.....	31
Table 3.10 – Constraints in the ARB template.....	34
Table 3.11 – Parameters required for the FIALA tire model.....	36
Table 4.1 - Different spring configurations for the full vehicle assembly.....	41
Table 6.1 - Installed spring lengths for each full vehicle configuration.....	63

## **Abstract**

The aim of the thesis work that is presented here is to describe the multibody model of a remote controlled (RC) scaled vehicle and study its handling behaviour at different driving conditions with the help of building tools and simulations in the Adams/Car work environment. The multibody model will help in ascertaining the validity of such experimental tests that can be performed on the scaled vehicle in the future by comparing with the simulation results presented here. The effect of Finite element (FE) anti-roll bar subsystems in the suspension and full vehicle assemblies will, in particular, be addressed in the results section.

The work here consists of the following broad sections; the first section will present the reader with an overview of the multibody approach to vehicle dynamics and the Adams/Car environment. It will more specifically have a discussion on how the solver works and will be followed by a section with an elaborate discussion on the scaled vehicle and its depiction on the software environment. Each template and subsystem that has been modelled will be explained in detail, carrying information about the different properties and constraints. The following section will deal with the different simulations that were set up to be performed on the complete vehicle and suspension assemblies and the final section will deal with the results and the consequent interpretation of said results which will aid in understanding the behaviour of the vehicle. The discussions also include an outline on the behaviour of the front and rear suspension systems of the scaled vehicle making use of the suspension test-rig available within the ADAMS/Car environment.

The other software programs that were majorly used for the actualization of this thesis work are SolidWorks and Matlab. A SolidWorks model of the steering system already available with the research group was used to understand the mechanism and create a viable translation of the same on Adams/Car and Matlab was primarily used for characterizing the damper and spring behaviour needed for Adams/Car and for post processing of results obtained from the full-vehicle and suspension simulations.



## 1. Introduction

### 1.1. The multibody approach and an introduction to the ADAMS solver

This chapter aims to introduce the Adams multibody environment and the method that the ADAMS solver uses for performing simulations based on user defined inputs. The following section is summarized from the discussions on the same topic in “ADAMS/Solver and MSS”<sup>[1]</sup> and “ADAMS/Solver Primer”<sup>[2]</sup>.

ADAMS stands for Automated Dynamic Analysis of Mechanical Systems. ADAMS/Car is a part of the ADAMS package and range of software and is a multi-body software that is very extensively used in the automotive industry to realize suspension, tire and full vehicle designs among others. It is a powerful tool to understand vehicle dynamics and kinematics parameters.

The ADAMS/Solver is common across ADAMS/View and ADAMS/Car and uses the same procedure to solve and simulate the systems concerned. The solver makes use of the Newton-Raphson iterative method to provide solutions for systems that are not linear. A brief description of this algorithm is given below as the full description of the functioning of the solver is beyond the scope of this thesis and this section has been added only to give a rudimentary background on it to the reader.

#### 1.1.1. Newton – Raphson Method:

It is an iterative method that is employed by the ADAMS/Solver to obtain results in a quick and robust manner. As already stated, the Newton – Raphson method is applicable to solve non-linear equation by finding the equation’s associated root. If  $f(x) = 0$  is the differentiable function considered, an initial root approximation  $x^{(0)}$  is taken into account and a new root  $x^{(1)}$  is obtained which is ideally closer to the actual root  $x^*$ . This computation is as follows

$$x^{(1)} = x^{(0)} - \frac{f(x^{(0)})}{f'(x^{(0)})} \quad (1.1)$$

where we can see that the derivative of the function is utilized in order to get a closer approximation with each iteration. This is made possible by linearizing the function considered at  $x^{(0)}$  and so

$$f(x) \approx f(x^{(0)}) + f'(x^{(0)})(x - x^{(0)}) \quad (1.2)$$

The root of this function instead leads to a linear equation whose root is given by the definition of  $x^{(1)}$  shown above in the equation. This is carried on till the actual root is found with the quadratic convergence rate that is obtained from this method. The only condition is that the first guess or approximation is close to the actual root. ADAMS allows the user to define how often the derivative is to be updated as it is an expensive operation. This is done by using the PATTERN setting that is a part of the INTEGRATOR statement in the Solver. If the frequency of updating the derivative is low on the other hand, it could lead to errors because the convergence follows a linear trend and not a quadratic trend. The linear trend takes more time and steps to reach the solution when compared to the quadratic

convergence. Therefore, it is required to find a balance in defining the number of Jacobians (derivatives) required for a simulation.

Since there are multiple unknowns in the non-linear system that is considered, the root is replaced by the n-dimensional vector  $q \in \mathbb{R}^n$  and therefore the system to be solved becomes of the form

$$f(q) = \begin{bmatrix} f_1(q) \\ f_2(q) \\ \vdots \\ f_{n-1}(q) \\ f_n(q) \end{bmatrix} = 0 \quad (1.3)$$

The approach for this is similar to the one-dimensional function case shown previously, first the function is linearized and then equated to zero before the new values of  $q$  are obtained ultimately finding  $q^*$ .

## 1.2. Definitions related to the ADAMS environment:

The simulations in ADAMS give the time evolution of the mechanical system taken into consideration. The position, orientation, and the velocities of the different parts of the system can be indicated using the solver.

### 1.2.1. Generalized co-ordinates:

The position of a particular part in the model is given by its generalized co-ordinates. The co-ordinates in the model can be global or local and could be Cartesian or spherical. If an arbitrary rigid body  $p$  is to be defined, then it is defined by three coordinates in the Cartesian system

$$p = [x \quad y \quad z]^T \quad (1.4)$$

Meanwhile, the orientation is given by the array

$$\mathcal{E} = [\psi \quad \varphi \quad \theta]^T \quad (1.5)$$

where the orientation is defined by Euler angles that conform to the 3-1-3 sequence rotation and the generalized set of co-ordinates for the rigid body is

$$q = [p \quad \mathcal{E}]^T \quad (1.6)$$

The longitudinal and angular velocities can be derived by differentiating the co-ordinates with respect to time.

$u = \dot{p}$  is the longitudinal velocity and  $\bar{\omega} = B\dot{\mathcal{E}}$  is the body angular velocity.

B is given by

$$B = \begin{bmatrix} \sin\phi\sin\theta & 0 & \cos\phi \\ \cos\phi\sin\theta & 0 & -\sin\phi \\ \cos\theta & 1 & 0 \end{bmatrix} \quad (1.7)$$

Using this matrix, it is possible to relate the angular velocity with the generalized co-ordinates. An orientation matrix A is defined which is related to the angular velocity as follows

$$\dot{A} = A\tilde{\omega} \quad (1.8)$$

The matrix A is given by

$$A = \begin{bmatrix} \cos\psi\cos\phi - \sin\psi\cos\theta\sin\phi & -\cos\psi\sin\phi - \sin\psi\cos\theta\cos\phi & \sin\psi\sin\theta \\ \sin\psi\cos\phi + \cos\psi\cos\theta\sin\phi & -\sin\psi\sin\phi + \cos\psi\cos\theta\cos\phi & -\cos\psi\sin\theta \\ \sin\theta\sin\phi & \sin\theta\cos\phi & \cos\theta \end{bmatrix} \quad (1.9)$$

A matrix is defined in accordance with the Euler rotation sequence 3-1-3 as seen above and is useful to finding the derivatives associated with a rotating body.

### 1.2.2. Joints and Motions in ADAMS:

Joints in ADAMS are represented as constraints in particular co-ordinates according to the behaviour required by the body. For a mechanical system with x bodies, a vector has to be defined that will give the position and orientation at a given time frame in the system. This vector is defined as

$$q = [q_1^T \ q_2^T \ \dots \ q_x^T]^T = [q_1 \ q_2 \ \dots \ q_n]^T \quad (1.10)$$

Where  $n = 6.x$

If a co-ordinate is supposed to be constrained in the above vector, it becomes the following expression

$$\Phi(q) = 0 \quad (1.11)$$

If we take all constraints in a body into account, it is denoted by

$$\Phi(q) = [\Phi_1^T(q) \ \Phi_2^T(q) \ \dots \ \Phi_{n_j}^T(q)]^T = [\Phi_1(q) \ \Phi_2(q) \ \dots \ \Phi_m(q)]^T \quad (1.12)$$

where  $n_j$  is the number of joints and  $m$  is the number of constraints in the body. The number of constraints is usually lesser than the number of generalized co-ordinates that are used to define the model that is taken into consideration.

The time derivatives of the constraint equation give us the velocity and acceleration kinematic constraint equations associated with the model.

A motion, whereas, can be defined as a constraint equation that is dependent on time and can be represented as

$$\Phi(q, t) = 0 \quad (1.13)$$

and similarly, the velocity and the acceleration kinematic motions can be given by the derivatives of  $\Phi(q, t)$  with respect to time.

The following table gives an insight on the types of connections available and the number of constraints and the type of motion they enable.

*Table 1.1 – Joints and associated constraints in ADAMS environment*

<b>Joint</b>	<b>Number of constraints</b>	<b>Motion allowed</b>
Fixed	6	No motion allowed
Translational	5	Translation of parts with respect to one another along one axis
Revolute	5	Rotation of one part with respect to another around one axis
Cylindrical	4	One rotational and one translational motion of one part with respect to another along an axis
Con-vel	4	Two co-incident rotations of one part with respect to another at a constant velocity
Hooke	4	Two co-incident rotations of one part with respect to another
Spherical	3	Three rotations of one part with respect to another
Planar	3	Planar translation of the xy plane and of a body with respect to another body and rotation in its plane
Orientation	3	Three translational motions of one part with respect to the other
Inline	2	One translation and three rotations of one part with respect to another
Parallel axes	2	Three translations and one rotation of a part with respect to another
Perpendicular	1	Three translations and two rotations
Inplane	1	Two translations and three rotations

### **1.3.Types of Analyses in ADAMS:**

The types of analyses in ADAMS can broadly be classified into the following categories

- (i) Static analysis
- (ii) Initial Condition (IC) analysis
- (iii) Kinematic Analysis
- (iv) Dynamic Analysis

A brief description of each type of analysis is given in this section.

### 1.3.1. Initial Condition (IC) Analysis:

As the name suggests, this analysis is done at the beginning of any simulation and deals with finding the consistent configuration of the assembly and its parts.

The condition to satisfy the assembling of the parts is that the constraint equations need to be satisfied at the start time by the generalized co-ordinates. In mathematical terms, this condition is given by

$$\Phi(q, t_0) = 0 \quad (1.1)$$

Likewise, the condition for consistent generalized co-ordinates is given by the following kinematic constraint equation.

$$\Phi_q(q, t) \cdot \dot{q} = -\Phi_t(q, t) \quad (1.2)$$

The IC analysis is performed on the position, velocity and the acceleration and forces acting on the model.

#### 1.3.1.1. Positional IC Analysis:

The position analysis is done based on the input the user wants to give when defining the position of the model. Based on this input, the model is assembled and then the IC analysis is performed. The function is given by

$$f(q_1, \dots, q_n) = \frac{1}{2} w_1 (q_1 - q_1^0)^2 + \dots + \frac{1}{2} w_n (q_n - q_n^0)^2 \quad (1.3)$$

with the constraint equations for positional IC analysis taken into consideration. In the function above,  $w_i$  are the weight factors and  $q_i^0$  are the initial co-ordinates that define the initial configuration of the overall model. The weight factors are assigned large values to some entries related to the corresponding entries in the  $q^0$  array if they are considered as exact. The other weight factors are assigned with the value 1. The constrained optimization problem solution will not change the IC values that have been assigned by the user with this approach.

The matrix  $W$  is the weight matrix and is given by

$$W = \text{diag} (w_1, w_2, w_3, \dots, w_n) \quad (1.21)$$

During the IC analysis, certain constraints can be considered as redundant by the solver. If such a constraint that is identified as redundant is consistent, then there are no issues in running the simulation. Otherwise, they can affect the simulation performance and give rise to unexpected eigen vectors. Redundant constraints are usually a result of too many joints in the model that is being analysed and so it is advisable to model the body with just the required number of joints.

### 1.3.1.2.Velocity IC analysis:

This IC analysis is a simple application of the algorithm used in the position IC analysis. It is a continuation of sorts as the model has the constraint equations that are linearized from the position IC analysis and so it is a simple analysis for the solver to carry out and it removes the need to linearize the constraints. The solution is found out in one iteration

### 1.3.1.3.Force and Acceleration IC analysis:

If the system does not undergo friction, then this analysis makes use of the solution of the linear system's equations of motion and is in line with the kinematic acceleration constraint equations mentioned in equation (). The resulting system is

$$\begin{bmatrix} M & \Phi_q^T(q^0) \\ \Phi_q(q^0) & 0 \end{bmatrix} \begin{bmatrix} \ddot{q} \\ \lambda \end{bmatrix} = \begin{bmatrix} F \\ \tau \end{bmatrix} \quad (1.22)$$

With M being the generalized mass matrix.

In this linear system, convergence is seen in one iteration. The initial acceleration conditions are calculated based on the initial position and initial velocity analyses.

The joints produce forces and torques on the bodies they connect based on their type and the number of degrees of freedom they constrain.

## 1.3.2. Kinematic Analysis:

Kinematic analysis requires, in addition to independent constraint equations, certain constraints which must be time dependent. Kinematic analysis also can be done at the position level, velocity level and acceleration level.

### 1.3.2.1. Positional Kinematic Analysis:

The positional kinematic analysis deals with finding the position of the part or model considered at a time that is greater than the initial time ( $t_1 > t_0$ ). The Newton Raphson method is employed to find  $\Phi(q_1, t_1)$ . The constraint equations are subject to linearization using the Taylor's series expansion. The position of  $\Phi(q_1, t_1)$  is given by

$$\Phi(q_1, t_1) = \Phi(q_0, t_1) + \Phi_q(q_0, t_1)(q_1 - q_0) \quad (1.23)$$

The constraint matrix is square and invertible. The initial configuration is determined thanks to the use of an explicit integrator and the iteration is carried out till the correction and residual become sufficiently small. The following expression represents this

$$\Phi_q(q_0, t_1)\Delta^{(j)} = -\Phi(q_1^{(j)}, t_1) \quad (1.24)$$

Where  $\Delta^{(j)}$  is the correction and  $j \geq 0$  at each iteration.

### 1.3.2.2. Velocity Kinematic Analysis:

The kinematic constraints with respect to velocity are linear and so this is fairly simple in comparison to the other analyses. The analysis makes use of the position  $q_1$  available from the positional kinematic analysis to find  $\Phi_q(q_1, t_1)$  which then is used to find the new velocity of the model considered.

### 1.3.2.3. Acceleration Kinematic Analysis:

At time  $t_1$  the analysis is performed and the generalized acceleration  $\ddot{q}$  is obtained which is useful to compute the Lagrange multipliers to find the solution of the system given below

$$\Phi_q^T \lambda = F - M\ddot{q} \quad (1.25)$$

Which represents the equations of motion.

### 1.3.3. Dynamic Analysis:

For dynamic analysis, the following parameters need to be defined

$$K = \frac{1}{2}u^T M u = \frac{1}{2}\bar{\omega}^T \bar{J} \bar{\omega} \quad (1.26)$$

Where K is the kinetic energy

M is the generalized mass matrix

$\bar{J}$  is the generalized inertia matrix with respect to a local frame of reference

$\lambda \in R^m$  is the array containing the Lagrange multipliers. The value of  $m$  depends on the number of constraint equations coming from the joints in the system.

$\mathbb{F}(q, \dot{q}, t) = \begin{bmatrix} f \\ \bar{n} \end{bmatrix} \in R^6$  is used to represent the vector of the applied forces, where  $f$  is the vector in the global frame of reference and the applied torque in the local frame of reference is given by  $\bar{n}$ .

$Q(q, \dot{q}, t) \in R^6$  is used to represent generalized body forces.

The equations of motion formulated using the Lagrange approach is of the order two and is as follows

$$\frac{d}{dt} \left[ \left( \frac{\partial K}{\partial \dot{q}} \right)^T \right] - \left( \frac{\partial K}{\partial q} \right)^T + \Phi_q^T \lambda = Q \quad (1.27)$$

$$\frac{d}{dt} \left( \frac{\partial K}{\partial u} \right)^T = M \dot{u} \quad (1.28)$$

The angular momentum is defined as

$$\Gamma \equiv \frac{\partial K}{\partial \zeta} = B^T \bar{J} B \zeta \quad (1.29)$$

Each rigid body is represented by a set of 15 equations that contain the necessary information to perform dynamic analysis of the system considered.

The additional point to note is that constraint equations must be satisfied by the set of differential equations, and this makes the analysis more complex. A set of Differential and Algebraic Equations (DAE) is defined with an index which gives the number of times it has to be differentiated to make the set of equations into ordinary differential equations. The higher the number of differentiations needed to be performed, the more complex the system is to solve. For dynamic analysis problems, this index is 3. The solver has two more methods and the most common one in ADAMS is the direct index 3 DAE solver associated with the differential equations. This is the basis of the working of the GSTIFF-I3 solver. It is briefly discussed below

The 3 DAE index uses the Backward Euler formulation which provides the information required for higher order methods. The time derivative  $\dot{y}_1$  is replaced with

$$\dot{y}_1 = \frac{1}{h} y_1 - \frac{1}{h} y_0 \quad (1.30)$$

The solution is found by obtaining  $y(t_1)$  which is equal to  $y_1$  by discretizing the following system

$$\frac{1}{h} y_1 - \frac{1}{h} y_0 - g(t_1, y_1) = 0 \quad (1.31)$$

The function  $g$  is non-linear and so a non-linear system is required to be solved in order to find  $y_1$ . This can be achieved by the Newton Raphson method.

The more refined second method deals with reducing the index to 2 from 3. Therefore, in this method, instead of the position constraint equations, the velocity kinematic equations are solved. This is called the SI2 algorithm, which is more accurate and robust. It will not be discussed here as it is beyond the scope of this work.

#### 1.3.4. Static Analysis:

The static analysis involves the solver finding the static equilibrium of the overall model without any external loads/forces acting on it.

The STATIC approach is used to perform the static analysis by the C++ solver. The Newton-Raphson method is used by the solver in this case as well to find the solution of a set of non-linear equations. The key point to note in the STATIC approach is that all time derivatives must be equal to zero, which implies that the body or in our case, a vehicle is at rest or at equilibrium.



## 2. Losi 5iveT 2.0 Specifications

### 2.1. Mass and geometrical properties:

Losi 5ive T 2.0 is a radio controlled (RC) short course off-road truck scaled to a fifth of the actual size of vehicles in the category. It is a successor to the Losi 5ive T and has upgrades in the areas of new bar-styled steering rack with adjustable Ackermann steering and aspects related to radio control that fall beyond the scope of discussion of this thesis. Some of the important geometric and mass parameters of Losi 5ive T 2.0 are listed below

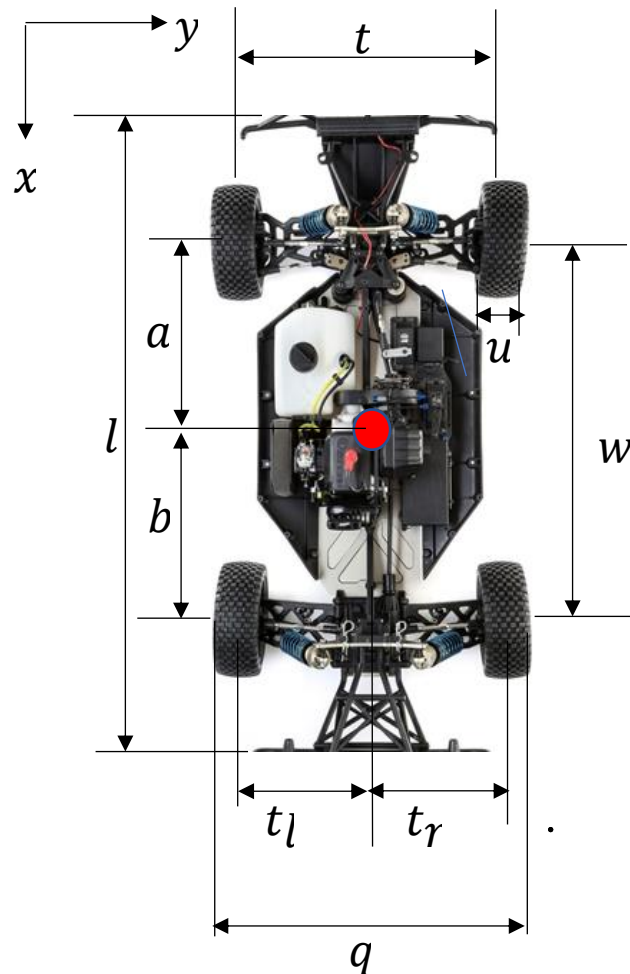


Fig. 2.1 - Basic dimensions - Losi 5ive T 2.0 - Top View

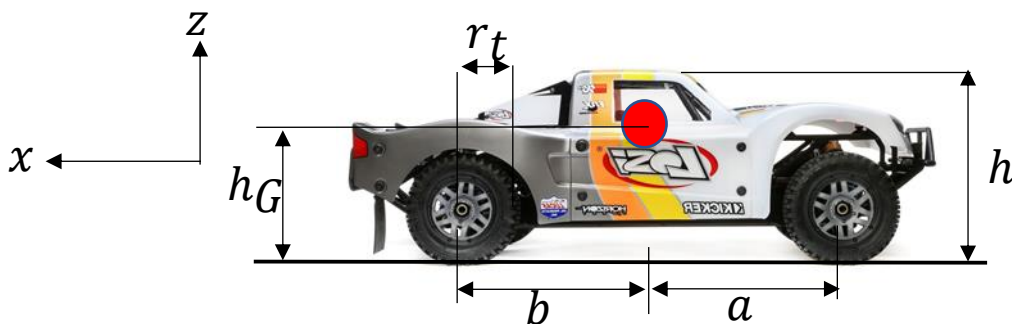


Fig. 2.2 - Basic dimensions - Losi 5ive T 2.0 - Side View

*Table 2.1 - Basic dimensions of Losi SiveT 2.0*

<b>Dimension</b>	<b>Description</b>	<b>Value [m]</b>
$l$	Length	0.965
$q$	Width	0.527
$h$	Height	0.311
$w$	Wheelbase	0.610
$t$	Trackwidth	0.456
$r_t$	Tire radius	0.181
$u$	Tire width	0.071
$a$	Centre of Gravity (CoG) distance to front axle	0.305
$b$	CoG distance to rear axle	0.305
$t_l$	Left semi-track	0.228
$t_r$	Right semi-track	0.228
$h_G$	CoG height	0.095

*Table 2.2 - Mass and Inertia Properties*

<b>Property</b>	<b>Description</b>	<b>Value</b>
$m_s [kg]$	Sprung mass	11.95
$m_u [kg]$	Un-sprung mass	1.495
$J_x [kg m^2]$	Sprung mass moment of inertia around x axis	0.112
$J_y [kg m^2]$	Sprung mass moment of inertia around y axis	0.722
$J_z [kg m^2]$	Sprung mass moment of inertia around z axis	0.745

The vehicle is powered by a 32cc pull-start petrol engine and employs a 4WD transmission system. The steering and throttle are actuated by means of respective 1/5 scale radio-controlled servomotors. The vehicle possesses an 800cc fuel tank. A detailed discussion on each subsystem of the vehicle and the equivalent Adams/Car model will follow in the next chapter.

### 3. Template and subsystem modelling

In this section, different subsystems of the vehicle and their relevant templates built on Adams/Car will be discussed in detail. The vehicle subsystems can be divided into

- Front suspension
- Rear suspension
- Steering
- Brakes
- Driveline
- Chassis
- Powertrain
- Tires
- Anti-rollbars

The individual subsystems are built from the corresponding templates and are in turn used to build the complete vehicle model. The templates are built in the “Template builder” environment of Adams/Car and the subsystems and assemblies are created in the “Standard Interface” environment, as already discussed earlier. A detailed explanation of each subsystem and the corresponding models is as follows

#### 3.1. Front suspension

##### 3.1.1. Properties:

The Losi 5ive T 2.0 is composed of the double-wishbone suspension geometry for both the front and rear suspension systems. The picture below depicts the front suspension.

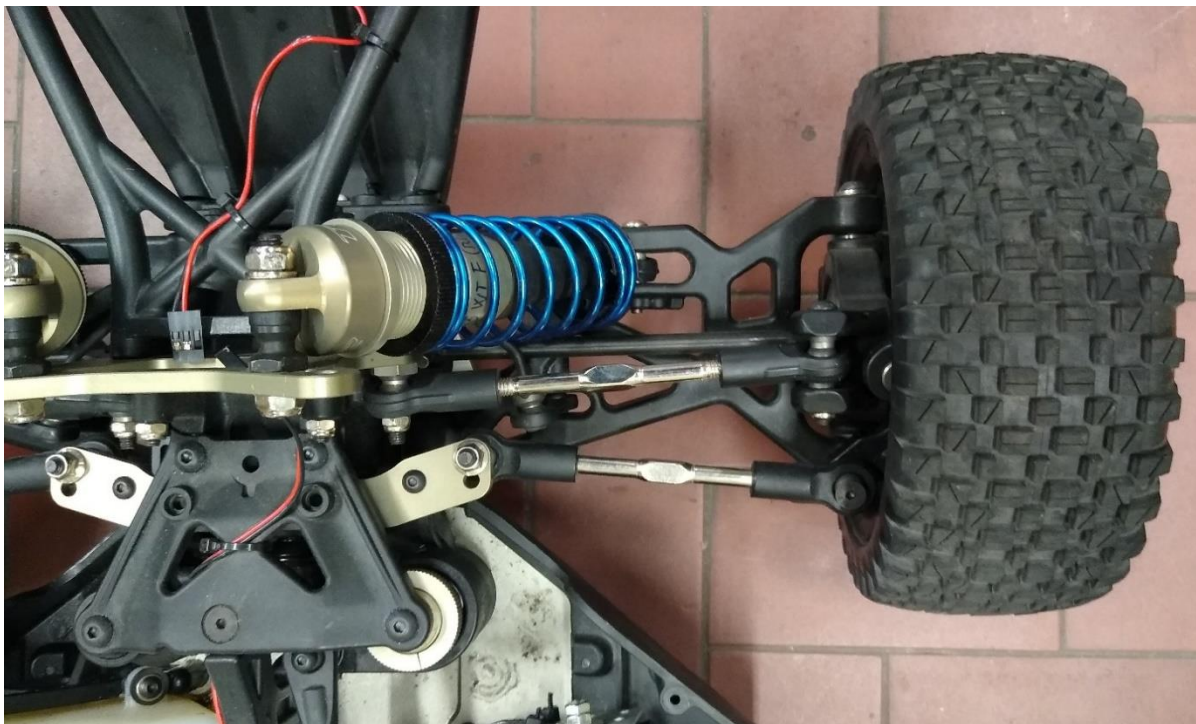


*Figure 3.1- Front suspension- Losi 5iveT 2.0*

Losi 5iveT 2.0 comes with 11 different grades of damper oil with varying damping coefficients. These damping coefficients were already available after being obtained from previous experimental tests.

The damping force as a function of velocity for each oil grade was calculated using the following formula. The damping coefficients of oils of different velocities are reported in the table below

$$F_d = c\dot{x} \quad (3.1)$$

where  $F_d$  is the damping force

$c$  is the damping coefficient of the specific oil grade

$\dot{x}$  is the relative velocity between the piston and cylinder of the damper

The resultant maximum damping force for each damping coefficient as a function of velocity when it ranges from 0 to 0.1 m/s is reported below

*Table 3.1 – Damper properties of Losi 5iveT 2.0*

<b>Oil Viscosity [wt]</b>	<b>Experimental Damping Coefficient <math>c</math> [Ns/m]</b>
20	96.73
25	109.09
30	136.45
35	144.73
45	194.23
50	237.16
60	248.58
70	246.50
80	271.25
90	301.84
100	331.89

Similarly, the vehicle comes with set of springs for the front suspension with varying stiffnesses. The spring force can be calculated using the following formula

$$F_s = k * x \quad (3.2)$$

where  $F_s$  is the spring force

$k$  is the spring stiffness

$x$  is the relative spring displacement

The maximum spring force for different values of spring stiffnesses when the relative displacement between the top and bottom part of the spring is between 0 to 0.05m is tabulated and plotted below

*Table 3.2 – Front spring properties*

<b>Code</b>	<b>LOSB2964</b>	<b>LOSB2965</b>	<b>LOSB2966</b>	<b>LOSB2967</b>
<b>Spring Colour</b>	Yellow	Blue	Red	Orange
<b>Stiffness</b> <b><math>k</math> [N/m]</b>	1817	2046	2276	2505

The suspension is composed of two spring-damper systems, two lower control arms and two upper control arms, upright-hub assemblies on either side attached to steering tie-rods as its principal components. The upper ends of the spring-damper systems are constrained to the body and the lower ends are constrained to the lower control arms. The upright is held between the ends of the two control arms and the tie-rods which transmit the steering motion are connected to the uprights. The figure shows the equivalent template in the Adams/Car “template builder” environment.

The steering and anti-roll bar templates are also discussed separately in individual templates in the following paragraphs. The table below depicts the type of constraints between different parts in the front suspension template. This is important to understand as the overall degrees of freedom of the front subsystem depend on these constraints.

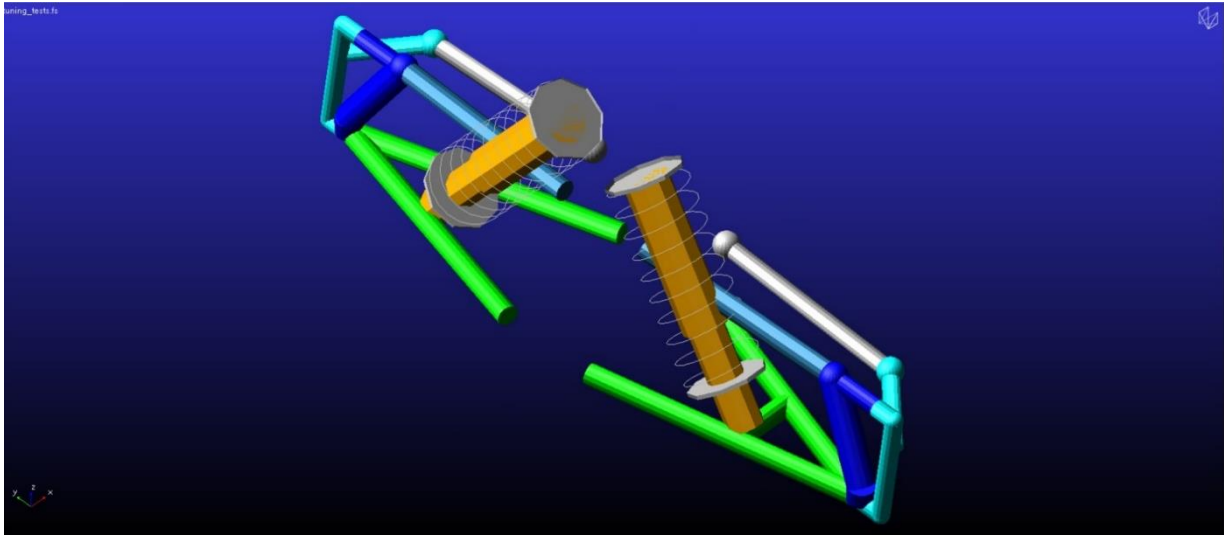


*Figure 3.2 - Front suspension Template*

*Table 3.3 – Constraints in the front suspension template*

<b>S. No.</b>	<b>Type of Joint</b>	<b>Number of dofs constrained</b>	<b>Parts Linked</b>
1.	Revolute	5	Lower control arm (LCA) to body
2.	Revolute	5	LCA to upright
3.	Spherical	3	Upper control Arm (UCA) to upright
4.	Hooke	4	UCA to body
5.	Spherical	3	Tie-rod to revolving knuckle
6.	Revolute	5	Upright to revolving knuckle
7.	Con-vel or hooke	4	Tie-rod to steering
8.	Hooke	4	Upper strut to body
9.	Hooke	4	Lower strut to LCA
10.	Cylindrical	4	Between upper and lower strut
11.	Spherical	3	Spindle to upright
12.	Revolute	5	Wheel center to spindle

The springs and dampers have their properties defined by default from the Adams/Car shared database whenever a new suspension template is created and therefore the important aspect of the suspension modelling is to ensure that the characteristics of the spring and dampers are updated according to the specifications of the vehicle. The damper force and spring force as functions of relative velocity and displacement are the parameters that need to be updated in the respective property files.

The bump-stops in the template were removed as we do not have the concerned data. The template is as shown below

## 3.2.Rear suspension

### 3.2.1. Properties:

The actual rear suspension in the yz plane looks as follows



*Figure 3.3 - Losi FiveT 2.0 rear suspension*

The damper properties for the rear suspension are the same as the ones reported for the front suspension. Specific oils with different coefficients can be selected for different simulations as required, the effect of which has been explained in the subsequent sections of this paper.

The suspension kit for the actual vehicle comes with a different set of springs with stiffnesses that vary in comparison to the front springs that were presented earlier. The rear spring stiffnesses are reported in the table below and the corresponding maximum spring forces when the displacement is assumed to be from 0 to 0.05m have been plotted and tabulated.

*Table 3.4 – Rear spring properties*

Code	LOSB2970	LOSB2972	LOSB2971	LOSB2973
<b>Spring Colour</b>	Yellow	Blue	Red	Orange
<b>Stiffness</b> <i>k</i> [N/m]	1200	1411	1641	1888
<b>Spring Force</b> <i>F<sub>s</sub></i> [N]	60	70.55	82.05	94.4

The only significant difference between the front and rear suspension systems of Losi 5ive T 2.0 is that only the front wheels are steered and consequently there is no need for tie-rods in the rear suspension template, which results in slight changes in the constraints between the uprights and the control arms as described in the table below

### 3.2.2. Template:

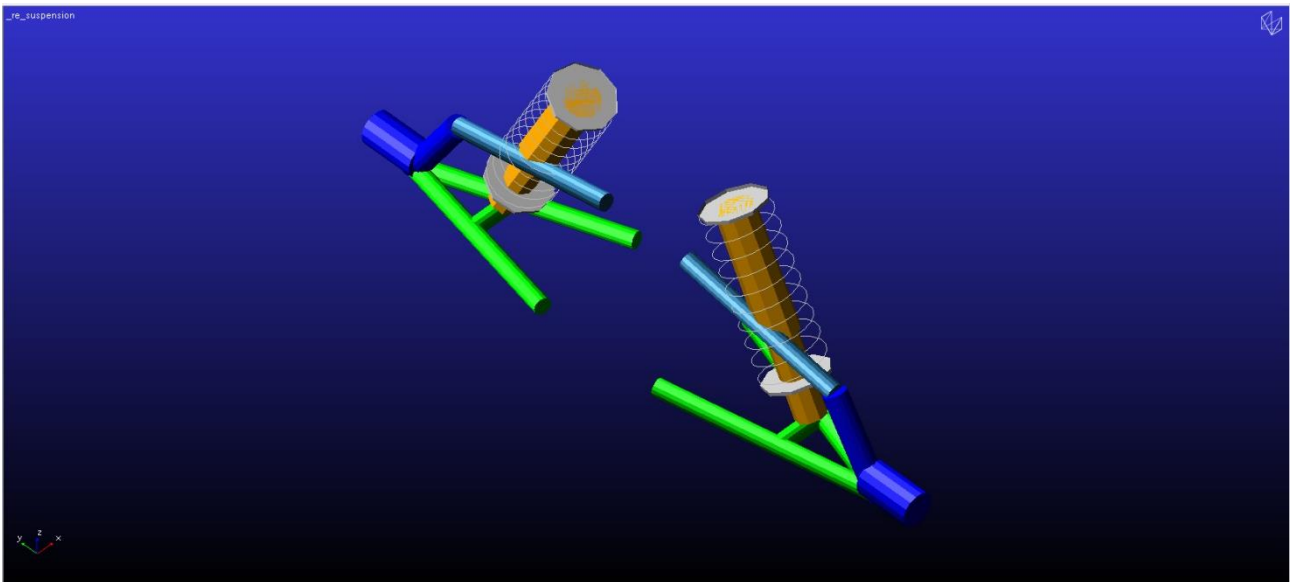


*Figure 3.4 – Rear suspension template*

The constraints in the model are as follows.



*Table 3.5 – Constraints in the rear suspension template*

<b>S. No.</b>	<b>Type of Joint</b>	<b>Number of dofs constrained</b>	<b>Parts Linked</b>
1.	Revolute	5	LCA to body
2.	Revolute	5	LCA to upright
3.	Hooke	4	UCA to body
4.	Spherical	3	UCA to upright
5.	Revolute	5	Spindle to wheel
6.	Spherical	3	Upright to spindle
7.	Cylindrical	4	Upper strut to lower strut
8.	Hooke	4	Lower strut to LCA
9.	Hooke	4	Upper strut to body

### **3.3. Steering**

#### **3.3.1. Description:**

The Losi 5ive T 2.0 is a scaled radio-controlled vehicle and so the steering input is through a servomotor. The CAD model of the steering system was available, and it was used as the preliminary point of study to build the steering template on ADAMS/ Car. The CAD model is depicted in the figure

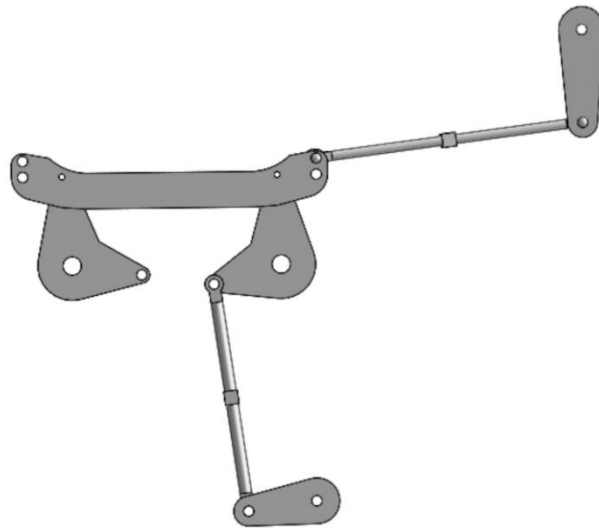


*Figure 3.5 - Steering CAD model*

The steering input link rotates through an angle of  $90^\circ$  to produce end to end steer at the wheels. The steering model on Adams/car was modelled to replicate this behaviour as closely as possible using geometric measurements. The model is shown below.

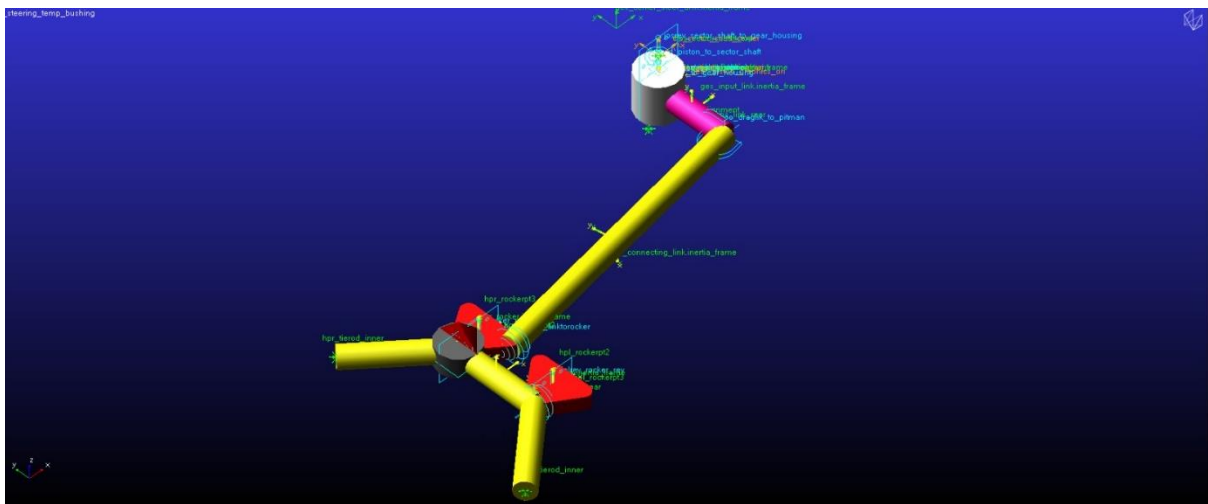


*Figure 3.6 - Steering template on ADAMS/Car*

As seen in the picture, the steering system is different from conventional steering templates in the sense that there is no depiction of a steering wheel or column and intermediate steering shafts. The revolute joint connected to the frame and the input link is defined as the steering wheel joint to ensure the steering input is provided there.

*Table 3.6 – Constraints in the steering template*

<b>S. No.</b>	<b>Type of Joint</b>	<b>Number of dofs constrained per joint</b>	<b>Parts linked</b>
1.	Spherical (2)	3	Rockers with the centre steer arm
2.	Perpendicular (Kinematic)	1	Rocker on the right side with centre steer arm
3.	Revolute (2)	5	Rocker to body
4.	Spherical	3	Intermediate link to right side rocker
5.	Hooke	4	Intermediate link with input link
6.	Revolute	5	Steering motor input to body
7.	Translational	5	Functionality of rack
8.	Revolute	5	Body to input link
9.	Bushing (inactive in kinematic mode)	5	Rocker to the centre steer arm

### **3.4.Brakes**

The brake template is depicted in the figure. It was relatively simple, as the modifications were again made on existing template and the only changes were the radii of the discs and the redefinition of the wheel centres were done to be compatible with the scale of the vehicle. The braking force on each wheel is predefined in the form of point torques and the default values were used in this process.

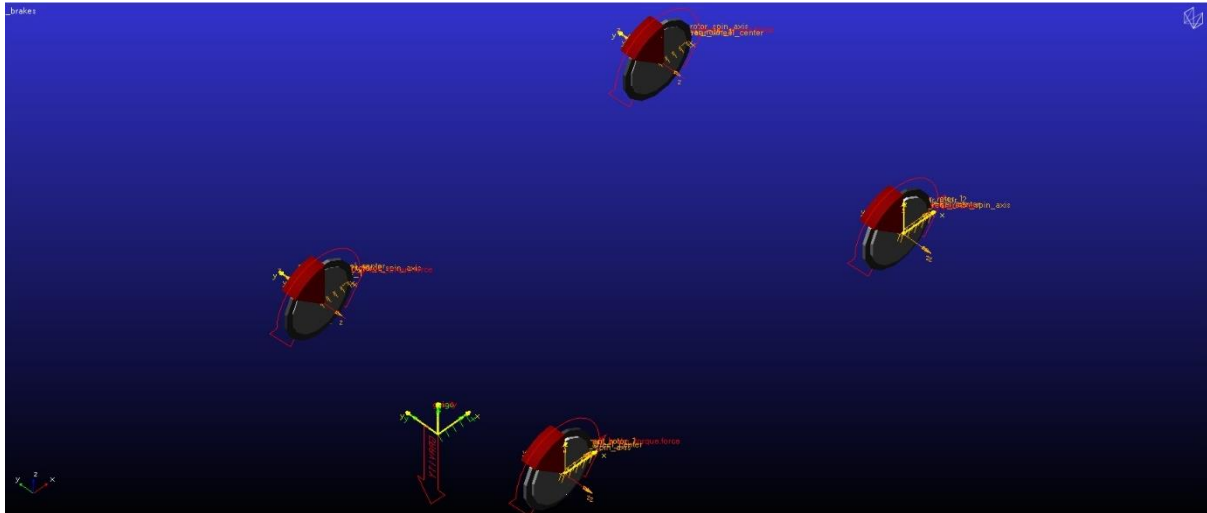


*Figure 3.7 - Brakes template*

### 3.5. Driveline

As already discussed, Losi 5iveT 2.0 employs a 4-WD system so the driveline was introduced by modifying the default AWD template on the Adams/Car database. Again, the important aspect that had to be taken care of was the scaling to ensure compatibility with the actual vehicle dimensions. The position of the power input to the driveline from the engine was also adjusted to ensure it replicates the actual vehicle assembly. The output from the driveline is given to the front and rear wheels via the spindle. The constraints in the driveline template are described in the table below.

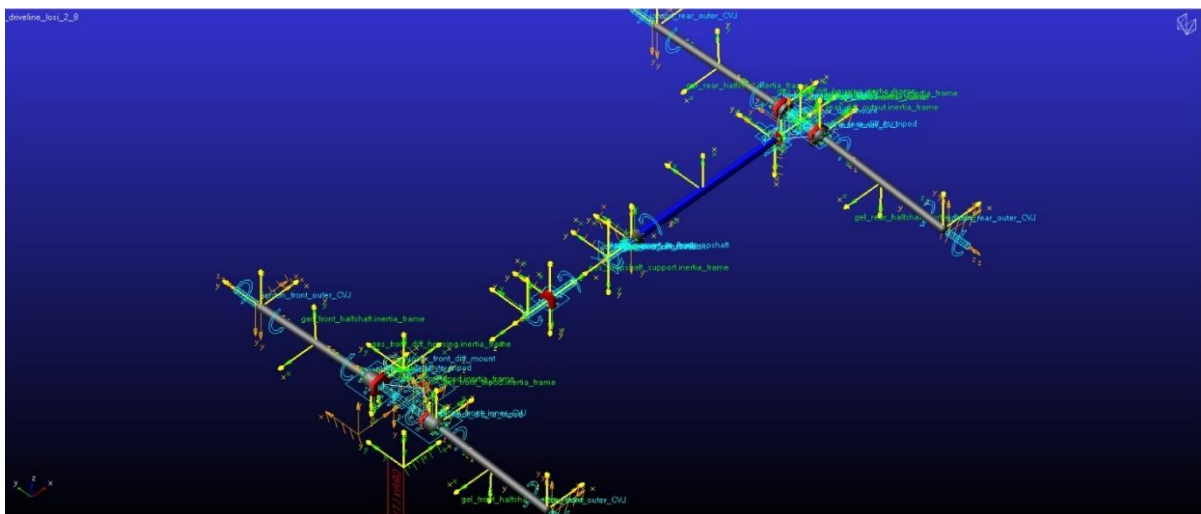


*Figure 3.8 - Driveline template*

*Table 3.7 – Constraints in the driveline template*

<b>S. No.</b>	<b>Type of constraint</b>	<b>Number of dofs constrained per joint</b>	<b>Parts linked</b>
1.	Fixed	6	Front differential housing to body
2.	Fixed	6	Rear differential housing to body
3.	Translational (2)	5	Front differential output to front tripod
4.	Translational (2)	5	Rear differential output to rear tripod (right and left)
5.	Convel (2)	4	Right and left front tripods to front half-shafts
6.	Convel (2)	4	Right and left front half-shafts to front spindles
7.	Convel (2)	4	Right and left rear tripods to rear half-shafts
8.	Convel (2)	4	Right and left rear half-shafts to rear spindles
9.	Revolute (2)	5	Front differential housing to front right and left differential outputs
10.	Revolute (2)	5	Rear differential housing to right and left rear differential outputs
11.	Revolute	5	Front differential input to front differential housing
12.	Revolute	5	Rear differential input to rear differential housing

13.	Revolute	5	Powertrain to propeller shaft input
14.	Translational	5	Slip yoke to rear propeller shaft
15.	Hooke	4	Rear propeller shaft to rear differential input
16.	Con-vel	4	Front propulsion shaft to slip yoke
17.	Con-vel	4	Propulsion shaft input to front propulsion shaft
18.	Inline	2	Front propulsion shaft to support
19.	Inline (kinematic)	2	Propulsion shaft support to body
20.	Inplane	1	Propulsion shaft support to body
21.	Orientation	3	Propulsion shaft support to body

### 3.6.Chassis

The chassis of the Losi 5ive T 2.0 is made of aluminium and the outer trim mass is made of plastic. On Adams/Car, the chassis was introduced as a rigid body f and the definitions that were required were the hardpoints related to the wheel centres, CoG position and the trim mass position. Once these were defined, the mass properties were updated according to the materials that needed to be considered using the in-built calculation tool available in the software.

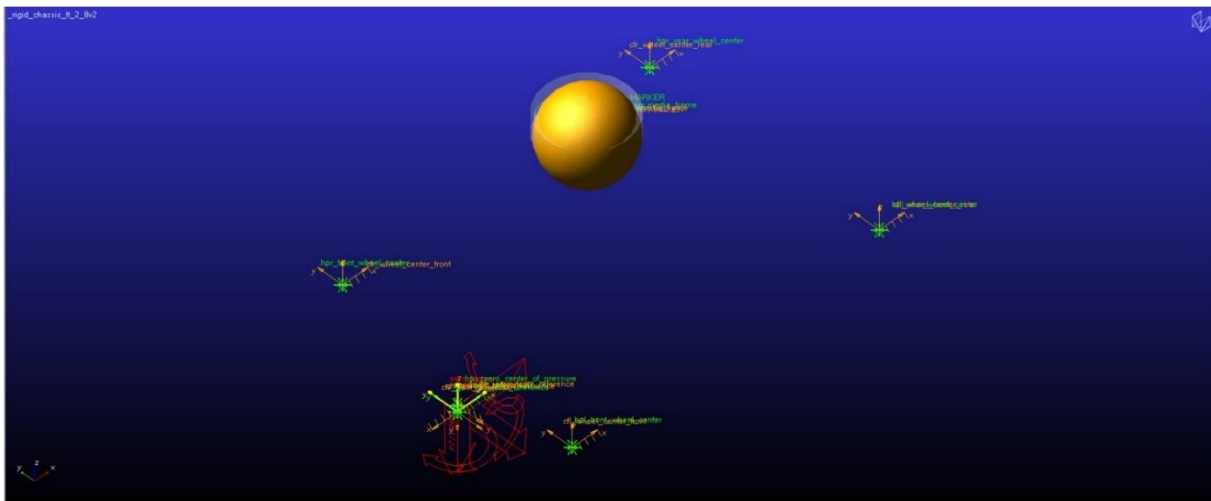


*Figure 3.9- Chassis template*

The chassis is depicted in a simplistic way in the template above. Adams/Car takes the mass and inertia properties of the part into consideration. The simplification lies in modelling the

rigid body as a sphere with the equivalent mass of the actual chassis. Similarly, the trim mass is also added as a cylinder with the appropriate mass equivalent to that of the actual plastic part. They are connected to each other with the help of a fixed joint as there is no relative motion between the chassis and the trim mass. The template also requires us to define the position of the wheel centres in terms of hardpoints. There is also a provision to define the aerodynamic parameters as parameter variables and subsequently as communicators which give additional information about the model that the solver handles.

*Table 3.8 – Constraints in the chassis template*

S. No.	Type of joint	Number of dofs constrained	Parts constrained
1.	Fixed	6	Trim mass and chassis

### 3.7.Powertrain

In Adams/Car, the engine template can be defined with the engine mounting points are the output torque which feeds the wheels directly in the case of a 2WD or feeds the driveline in case of AWD or 4WD. In our case, the engine torque feeds the driveline defined earlier and so the modifications were made to existing Adams/Car engine transmission template in order to replicate the actual vehicle. The mounting points were defined as hardpoints according to their actual position in the vehicle and a fixed joint is used to constrain the powertrain to the body.

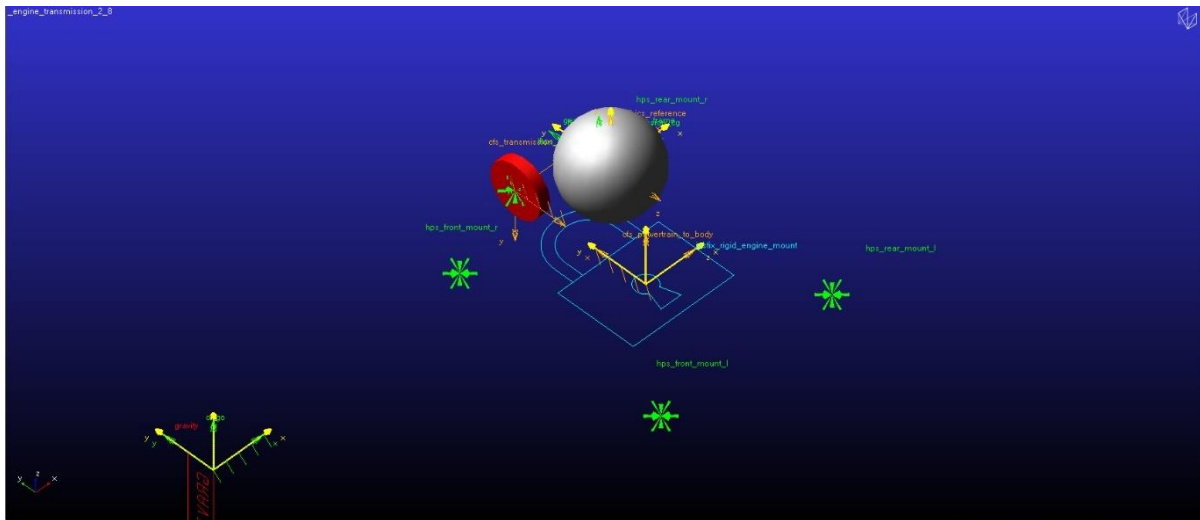


*Figure 3.10 - Powertrain template*

*Table 3.9 – Constraints in the powertrain template*

S. No.	Type of constraint	Number of dofs constrained	Parts connected
1.	Fixed	6	Powertrain to body

### **3.8. Anti-Roll Bars**

The anti-roll bars are 3 mm in diameter and are made of steel. They are fixed to the lower control arms of the suspension in both the front and the rear, and the upper part is constrained to the body. The Adams/ Car model of both the front and rear anti-roll bars were realised using the pre-existing anti-roll bar template as a point of reference. It was decided to model the anti-rollbars using Finite Element Method (FEM) elements in order to understand the stress at different regions while simulating both suspension and full vehicle tests, whereas the drop-links that connect the anti-rollbar to the lower control arms are modelled as rigid parts. A short theory about the FE part creation and simulation is given in this section after which the anti-roll bar templates are explained with their constraints.

#### **3.8.1. FE part theory:**

This part is a summary of the theoretical discussion “Welcome to the FE Part” by MSC Software [3].

The Finite Element part (FE Part) is an object developed to completely suit the Adams environment and is particularly suitable for analysis of large deformation cases. The results obtained for such simulations have a high degree of accuracy when compared to the linear Flex body method in Adams when it comes to such high deformation cases. The FE part can be created directly within a template using the FE part wizard, unlike the Flex body approach, which requires one to create and make use of a Modal Neutral File (MNF). Another key difference is the requirement of inertia properties to define the FE part using constant, symmetric, consistent mass matrices.

The FE part method allows two types of formulations. They are 2-dimensional (2D) and 3-dimensional (3D) beam formulations. The FE part is most effective for studying objects which have or undergo geometric non-linearities due to large deformations. The 3D beam representation, which this work has made use of, provides the user information and the effects due to deformations in all three co-ordinates and includes behaviours like stretching, bending, and torsion.

A much more detailed overview of the 3D beam element can be seen in the appendix.

As in any other FE analysis software, the FE part method in Adams makes use of finite elements which are defined by the position of nodes present in the structure that is to be analysed. For a near perfect replication of the structure that is being modelled both in terms of geometry and structural behaviour, a large number of nodes need to be defined.

The FE part uses the following information in order to simulate the behaviour of the structure under analysis.

- (i) The material of the structure gives important information about it like the stress-strain characteristics and the mass properties in accordance with the geometry



defined. This is done by constants whose number varies depending on whether the material is isotropic, orthotropic, or anisotropic.

- (ii) The nodes define the beam's neutral axis. The neutral axis passes through the origin of each node that constitutes the part. The nodes also provide information regarding the degree of freedom of the FE part. In case of a 3D beam.

$$DOF = 3 * ((4 * number\ of\ nodes) - 1) \quad (3.3)$$

- (iii) The section properties values give us the information regarding the moments of inertia of the beam.

### 3.8.2. Loads in FE parts:

After analysis, the result sets will contain the forces and torques in each direction at each node and its midpoints (FX, FY, FZ, TX, TY, TZ). The node where load is applied is numbered as S = zero and next is the load applied midway between the node at S=0 and the next nearest node in increasing S (FX1, FY1 and so on); this is followed by the load applied on the next nearest node in increasing S (FX2, FY2 and so on); this continues in increasing S over locations at nodes and midpoints between nodes until the node at S=1.

### 3.8.3. FE part comparison with other methods

Structures with geometric non-linearity can be modelled using other approaches like using MNF files or by using discrete flexible links. In the multi-MNF file method, we use an appropriate number of MNF files defining the flexible bodies. These bodies are connected using joints or bushings.

In the case of Discrete flexible links, the rigid bodies are connected using bushings or Adams Solver BEAM, FIELD.

Some of the advantages that can be noticed when using the FE part method when compared to the alternatives stated above is as follows:

- (i) There is no necessity for a lumped mass approach or for including linear flexible components.
- (ii) It is easier to modify and parametrize the FE part when compared to the other two methods.
- (iii) It is less time consuming and offers a greater degree of accuracy as already stated.
- (iv) The refinement is easier as it is related to increasing the number of nodes in the part. It can also be coarsened similarly by decreasing the number of nodes when defining the part. In this sense, it is easier than the other approaches for non-linear beam formulation.

The only noticeable disadvantage is that there is no support for animated contour plots for the FE parts as it only supports the X-Y plots in the postprocessor for stress and strain recovery.

### 3.8.4. Template description

The front anti-roll bar can be seen here along with the table containing the constraints in the template.

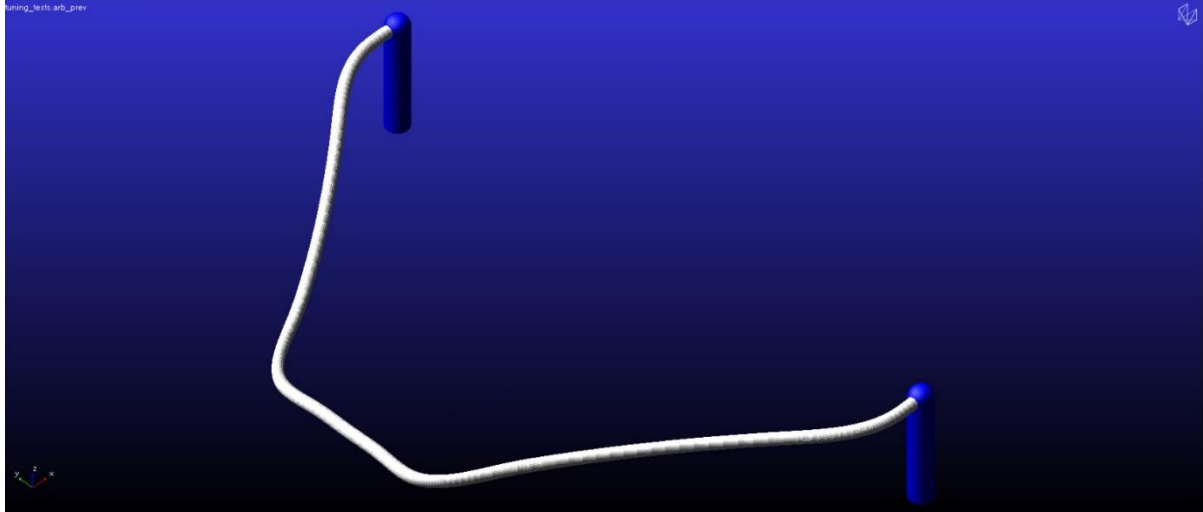


*Table 3.10 – Constraints in the ARB templates*

*Figure 3.11 - Front anti-roll bar template*

S. No.	Type of Joint	Number of dofs constrained	Parts connected
1.	Spherical (2)	3	Drop-link to LCA
2.	Con-vel (2)	4	Drop-link to FE anti-roll bar part
3.	Revolute	5	FE anti-rollbar part to body

The rear anti-roll bar is similarly modelled with the same constraints as the one in the front. The drop-links are modeled as rigid parts while the anti-roll bar itself is once again modeled as an FE part.

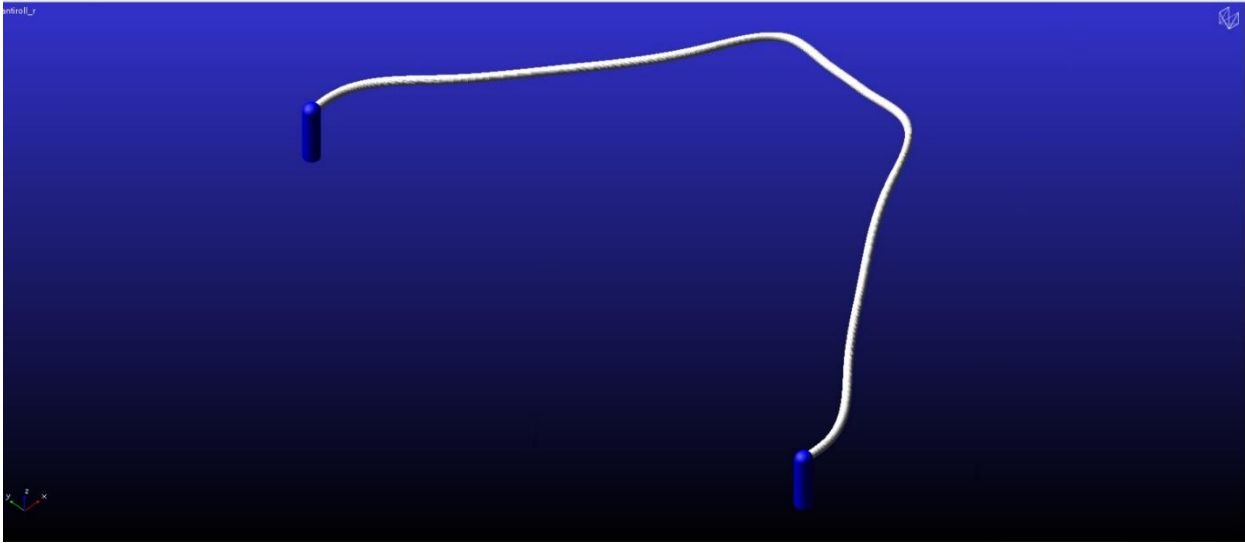


*Figure 3.12 - Rear anti-roll bar template*

### **3.9.Tires**

The tires of Losi 5ive T 2.0 are slightly unique when compared to conventional tires of an automobile. Usually, automobile tires are pneumatic, but the Losi tires are filled with a specific type of foam inside the tire carcass. This property of the tires under consideration makes the usage of conventional tire models like the Pacejka model, for example, difficult to represent the tires in the Adams/Car environment. The Pacejka and Smithers models are based on empirical datasets from experiments and are applicable to pneumatic tires, taking parameters like tire pressure into consideration. But since there is no experimental data and since as already explained, the tires are not pneumatic, other simpler tire models were explored and required to replicate the actual tires.

The tire model chosen ultimately was the Fiala model. It is a simple tire model that is available in the Adams/Car software as a .tir file and it requires basic tire data related to geometry and stiffness and damping characteristics. Since it allows us to modify the tire geometry according to our convenience, it was picked as the model to represent the tires to be added to the full vehicle model.

The Fiala model is compatible for handling analysis and less so for the purposes related to durability analysis of a vehicle. A short theoretical description of the model taken from the Hexagon online help for Adams <sup>[4]</sup> is as follows.

#### **3.9.1. Fiala Tire Model:**

The Fiala tire model, also known as the Fiala Handling Force Model, has a few important assumptions to be taken into consideration. They are as follows

- (i) The tire carcass exhibits the behaviour of a beam on an elastic base and is modelled accordingly

- (ii) The contact with the road is provided by brush elements (brush tire model in the lateral direction)
- (iii) The contact patch of the tire is rectangular in shape and experiences a uniform pressure distribution across it.
- (iv) The tire forces are independent of the camber angle.

As mentioned earlier, this model offers the convenience of not requiring experimental datasets to define the tire in the Adams environment. The requirements are basic and are largely related to the geometrical and inertial properties of the tire. They have been illustrated in the following table

*Table 3.11 – Parameters required for the FIALA tire model*

<b>Input Quantity</b>	<b>Description</b>	<b>Source</b>
$M_t$	Tire mass	User defined
Alpha	Slip angle	Adams Solver
$S_s$	Longitudinal slip ratio	Adams Solver
Pen	Tire deflection	Adams Solver
V_pen	Deflection rate	Adams Solver
Vertical_damping	Vertical damping coefficient	Tire property file
Vertical_stiffness	Vertical tire stiffness	Tire property file
CSLIP	Partial derivative of longitudinal force (Fx) with respect to the longitudinal slip ratio at zero slip	Tire property file
CALPHA	Partial derivative of lateral force (Fy) with respect to slip angle (alpha) at zero slip angle	Tire property file
UMIN	Friction coefficient at full slip condition	Tire property file
UMAX	Friction coefficient at zero slip condition	Tire property file
Rolling resistance	Coefficient of rolling resistance	Tire property file

Certain parameters are taken directly from the Adams solver and the rest are obtained from the tire property file which can be modified by the user according to requirement. Once these input parameters are defined, the solver uses it to calculate the tire forces.

### 3.9.2. Adams/Car Tire template:

For modelling in Adams/Car, it was preferred to build the tire models using the modified property file for the Fiala model. The required communicators were created, and the model was verified after a communicator test was performed with relevant templates which helped ensure that all required communicators were properly defined.

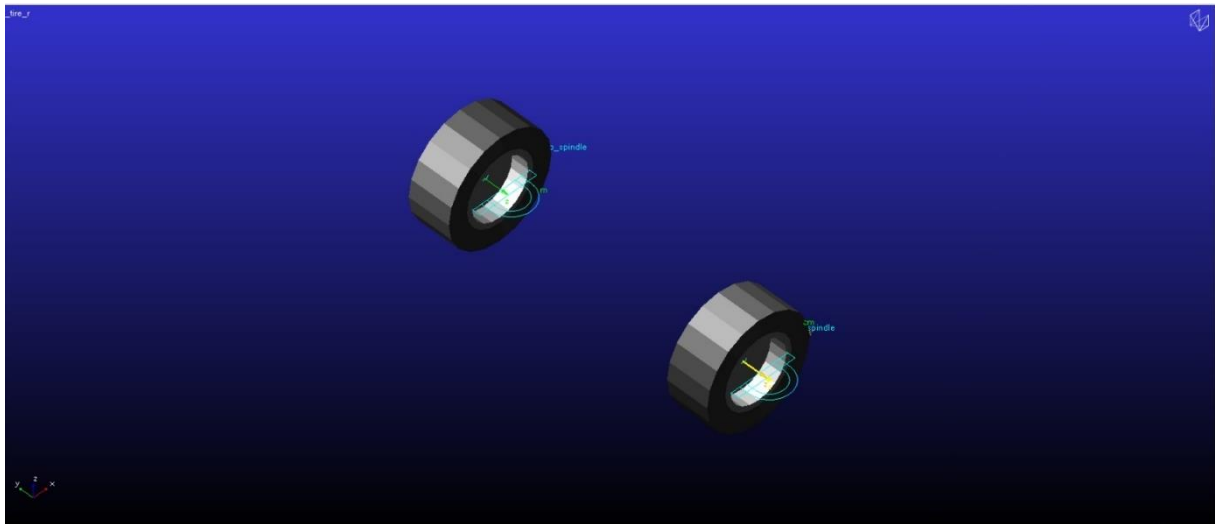


*Figure 3.13 - Front tires template*

The constraints in the tires are with the spindle and they are constrained to each spindle with a fixed joint. Therefore, the rotation of the spindles allows for the rotation of the wheels attached to them.

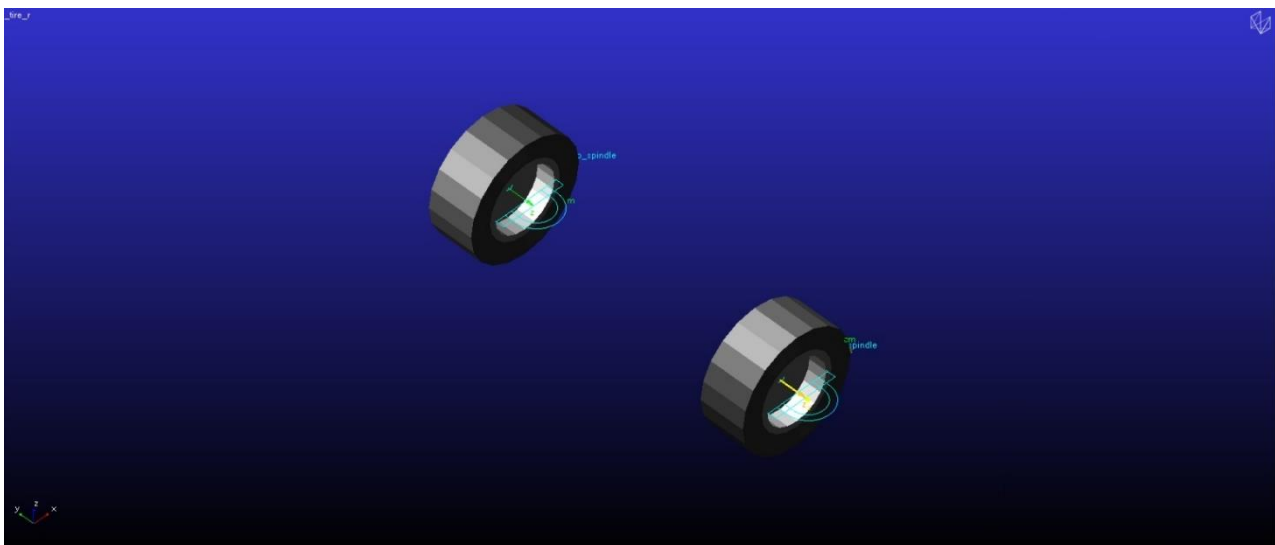


*Figure 3.14 - Rear tire template*

#### 4. Assembly Creation and full vehicle modelling

Once the templates were created, the Adams/Car Standard Interface environment was utilized in order to create subsystems and assemblies. The subsystems are created using the templates and it is necessary to define if the subsystem is of “front”, “rear” or “any” type according to the application. For example, in our vehicle model, the front suspension, anti-rollbars and steering are considered as “front” subsystems. The subsystems like rear suspension and rear anti-rollbar are defined as “rear” and subsystems like engine, driveline, chassis, and brakes are defined as “any” as they are common for the whole vehicle.

Following the definition and saving of the subsystems in the working database, the required assemblies were created by combining relevant subsystems that were created in the Standard Interface. The assemblies have been discussed and depicted as described below.

##### 4.1. Front Suspension Assembly:

Adams/Car allows us to create suspensions assemblies or full vehicle assemblies according to the requirement. The suspension assemblies are created using the suspension subsystem along with additional subsystems like anti-roll bar and steering depending on the vehicle configuration. The suspension assembly allows for extensive suspension-related simulations and analyses like parallel wheel and opposite wheel travel and steering. These simulations are realised using the suspension test rig that is inbuilt in the software and contains its own set of input and output communicators that communicate with the ones in the assembly.

The front suspension assembly was created, and it consists of the following templates

- (i) Front suspension subsystem
- (ii) Front anti-roll bar subsystem
- (iii) Steering subsystem
- (iv) The test-rig

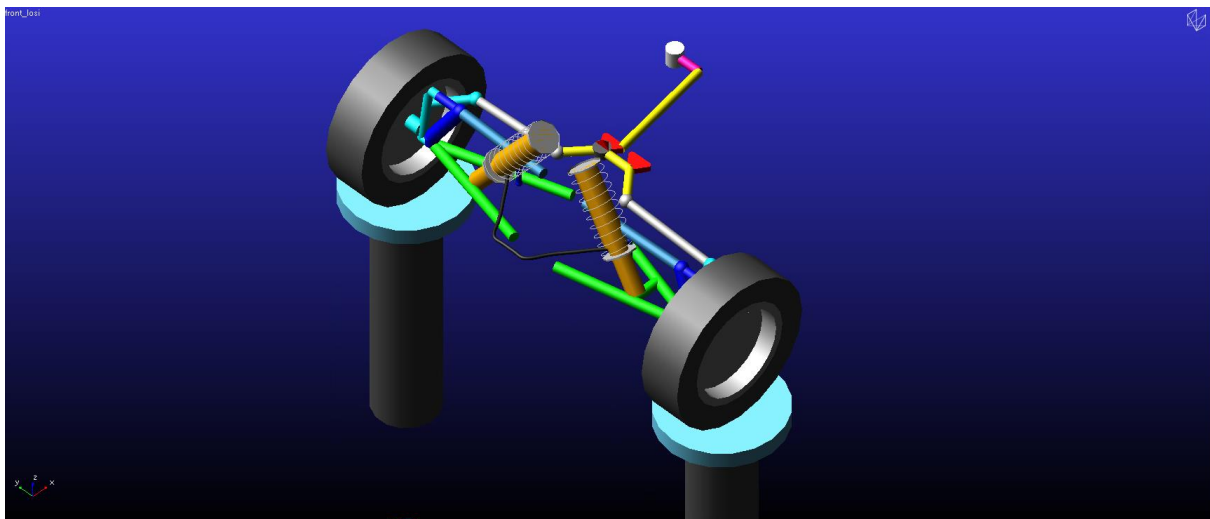


*Figure 4.1 - Front suspension assembly*

The assembly is as shown in the figure above.

This assembly has aided in suspension analysis and verifying the behaviour of the model. The simulation setup and results will be discussed in the latter sections of the paper.

#### 4.2.Rear Suspension Assembly:

The rear suspension assembly was also created with intention to achieve the same goals as the ones for the front suspension. As already stated, the vehicle is front wheel steered so there is no steering template when creating the rear suspension assembly. Therefore, the analyses are restricted to parallel and opposite wheel travel for this assembly. The subsystems that are included in the assembly are

- (i) Rear suspension subsystem
- (ii) Rear anti-roll bar subsystem
- (iii) Suspension test-rig

The rear suspension assembly is depicted in the figure

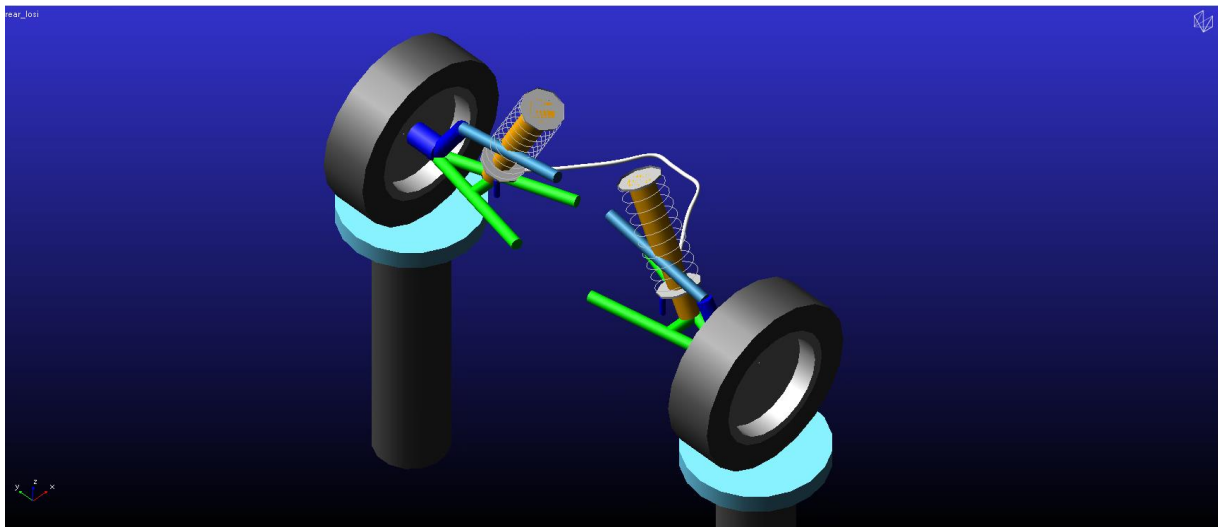


*Figure 4.2 - Rear suspension template*

Obviously, it is not possible to perform a steering simulation for this assembly but there was scope for performing simulations like parallel and opposite wheel travel, the setup and results of which have been discussed in the subsequent parts of this work.

### 4.3.Full vehicle assembly:

The full vehicle assembly was created similarly on the Adams/Car Standard Interface environment with the following subsystems

- (i) Front suspension
- (ii) Rear Suspension
- (iii) Front anti-roll bar
- (iv) Rear anti-roll bar
- (v) Front steering
- (vi) Front wheels
- (vii) Rear wheels
- (viii) Brakes
- (ix) Chassis
- (x) Powertrain
- (xi) Driveline

The full vehicle assembly is shown in the figure below

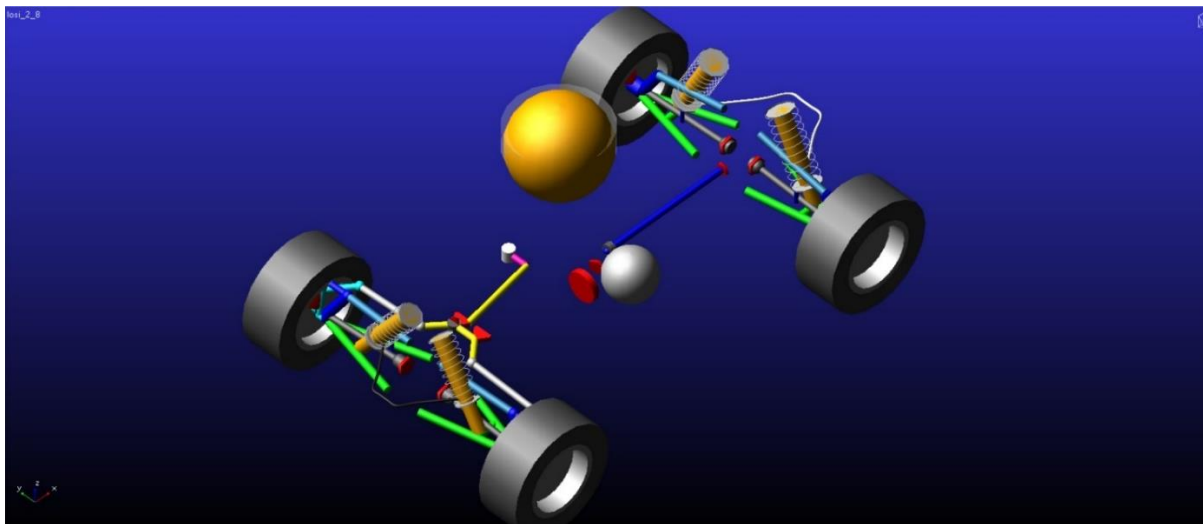


*Figure 4.3 - Full vehicle assembly*

Based on the different spring stiffnesses of both the front and rear springs, there can be 16 different configurations of the vehicle, and each of this can have a configuration without the anti-roll bar. Considering that it is redundant to elaborate the results for each of these configurations, a few of these configurations have been picked with one of them as baseline and the other as the configurations to be compared with the baseline. The baseline configuration is chosen to be the one in which both the front and rear suspension subsystems are equipped with comparable stiffnesses (1<sup>st</sup> configuration in the following table), details of which can be found in the previous chapters. Against the results obtained from this, an effort has been to compare the results obtained from the following configurations.



*Table 4.1 – Different spring configurations for the full vehicle assembly*

<b>S. No.</b>	<b>Configuration</b>	<b>Front</b>	<b>Rear</b>
1.	Baseline	Soft	Extra-hard
2.	2	Soft	Hard
3.	3	Extra-hard	soft

The reasoning behind the selection of these specific configurations is simple. The first configuration is the baseline, considering that the values of both front and rear spring stiffnesses mentioned earlier are comparable in terms of magnitude but the rear stiffness is slightly higher. In the second configuration, we keep the front suspension with soft springs again but change the rear to its hard springs, and in terms of stiffness, the value of the front spring is now slightly higher than the rear springs. In the third case, we pick an extreme condition in which the front suspension is with its stiffest springs and the rear with its softest. There is no means to perform a simulation with the rear springs being way stiffer than the fronts considering the values and therefore that could be interpreted through the baseline results.

Secondly, to understand the effect of anti-roll bars, the full model has been modified in three ways

- (i) With only front ARB
- (ii) With only rear ARB
- (iii) With no ARB

These conditions have been applied and compared again against our baseline configuration (with soft front spring and Extra-hard rear spring) which has both ARBs present. This is to understand the effect of additional stiffness due to the presence or lack thereof due to the absence of ARBS.

## 5. Simulation Setups

### 5.1. Suspension simulation setups:

#### 5.1.1. Front Suspension assembly:

As already stated, the first simulations to be performed on the suspension assemblies are parallel wheel travel. These simulations have been performed to analyze the effect of toe, camber and the spring stiffnesses, the results of which will be discussed in the next chapter.

##### 5.1.1.1. Parallel Wheel Travel:

This simulation involves the suspension system being subjected to vertical loads on both the wheels simultaneously and therefore both wheels are either in bump or rebound position together. The simulation setup has to set the bump and rebound travel to 20mm. The number of steps required to run the simulation was set to 50 as shown in the image.

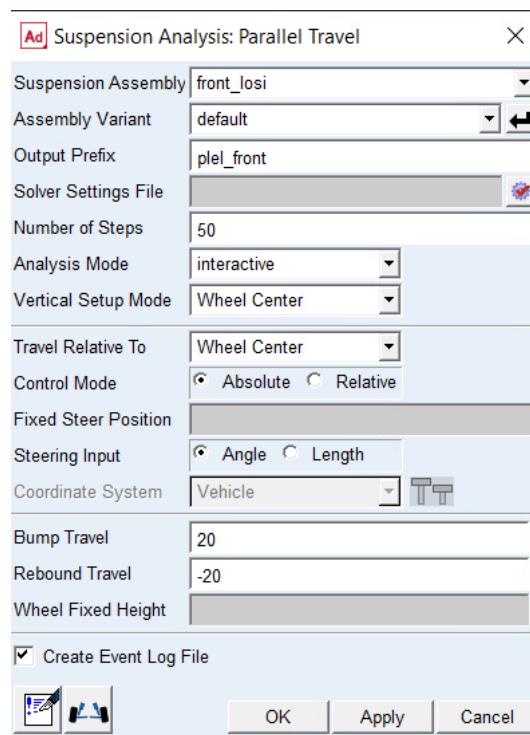


*Figure 3.1 - Parallel wheel travel setup - Front*

##### 5.1.1.2. Opposite Wheel travel:

For the opposite wheel travel, the vertical displacements on the wheels are applied alternatively, and as a result, when one wheel is in the bump position, the other wheel is in the

rebound position. The bump and rebound cases were once again set to be 25mm and the number of steps also remained the same as for the parallel wheel travel simulation at 50 steps.

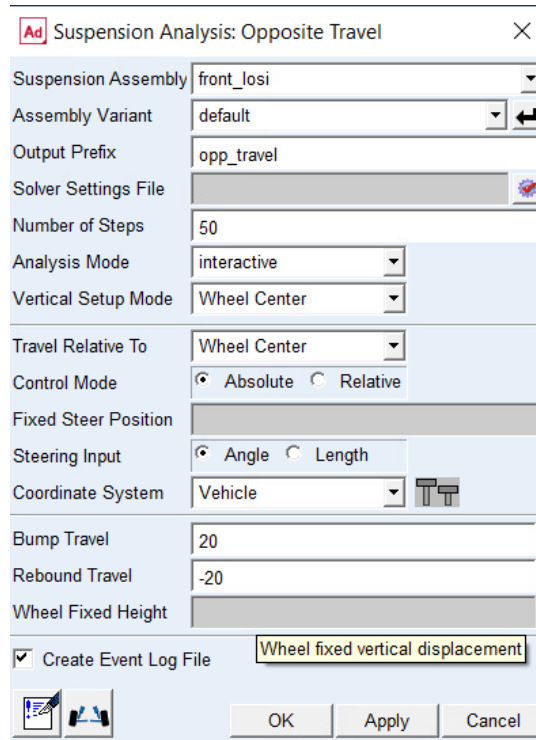


*Figure 5.2 – Opposite wheel travel setup - Front*

### 5.1.1.3. Steering simulation:

As already seen, the vehicle is front wheel steered and therefore a suspension steering test is performed on it to understand the extent of steer that is transferred to the wheels when a steering input is given at a static condition. The setup is as shown in the figure below.

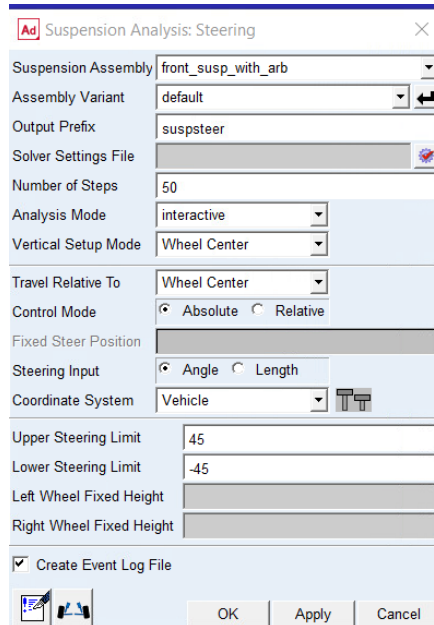


*Figure 5.3 – Suspension steering simulation setup*

## 5.1.2. Rear Suspension Assembly

The simulations on the rear suspension assembly were performed, like for the front assembly, with and without the FE anti-roll bar and by varying the spring stiffnesses.

### 5.1.2.1. Parallel wheel travel:

As in the case with the front suspension assembly, the bump and rebound travel values were fixed at 25mm for the rear assembly as shown below. The remainder of the values were again filled out and included the undeformed tire radius, brake and drive ratios, wheel-base and tire mass.

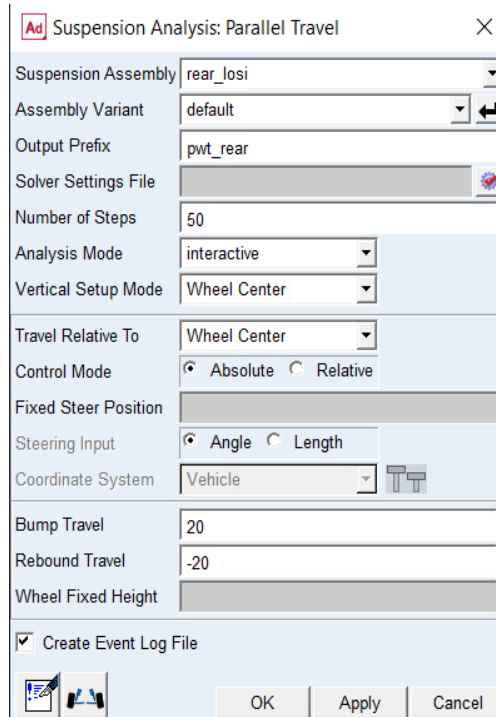


**Figure 5.4 – Parallel wheel travel setup – rear**

### 5.1.2.2. Opposite wheel travel

Again, the same setup parameters as the one for the front assembly opposite wheel travel were used here and can be seen below.

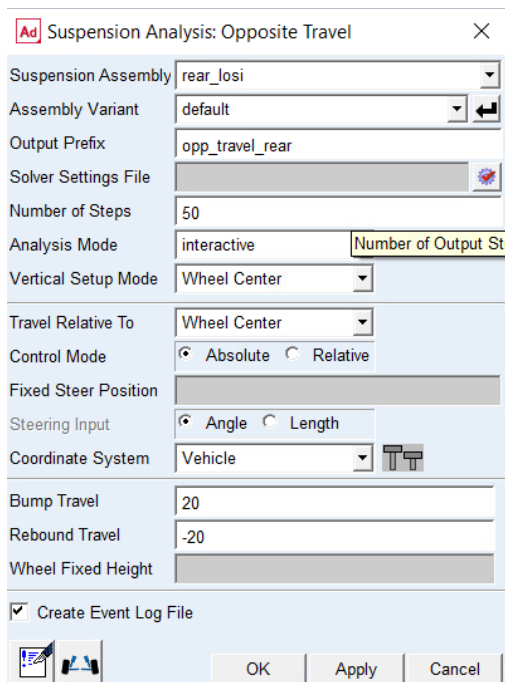


**Figure 5.5 – Opposite wheel travel - rear**

These tests for the front and rear suspension assemblies were repeated without the anti-roll bar to understand the impact it has on the results. The simulations were also repeated for different values of spring stiffness and damping values to understand their effect on the various parameters and the results will be discussed in the subsequent sections.

## 5.2. Full vehicle simulation setups

The principal focus of the full model is to understand the handling behaviour of the vehicle. To this end, the open loop testing methods are useful and therefore, the manoeuvres like step steer, ramp steer, swept steer, impulse steer, sine swept steer and J steer were to be performed on the full model. But before this, the first step is to verify the static equilibrium of the model, and this is realized using the static equilibrium test for the full vehicle.

### 5.2.1. Static Equilibrium Test:

In order to realize this, certain changes were made to the solver considering the complexity of the full model and the presence of FE parts. The maximum number of Newton-Raphson iterations (MAXIT) in the settings was increased to 500 from the default value of 25. The setup for the static analysis is as shown in the figure.

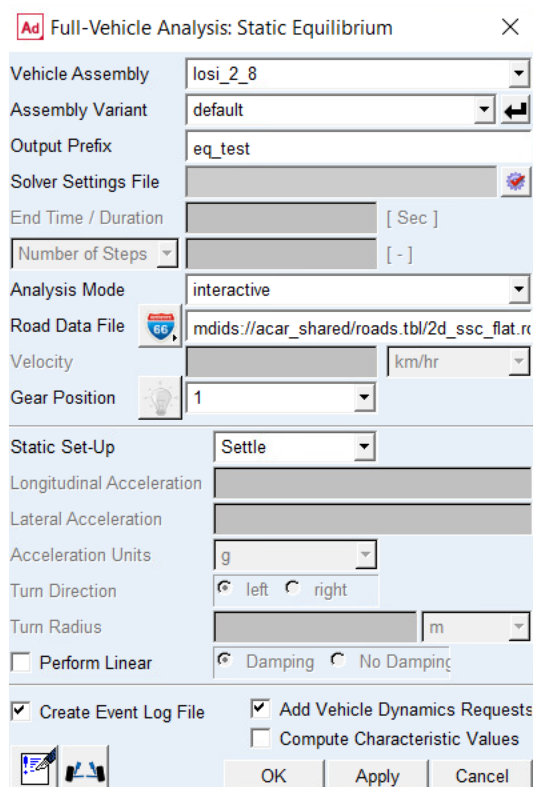
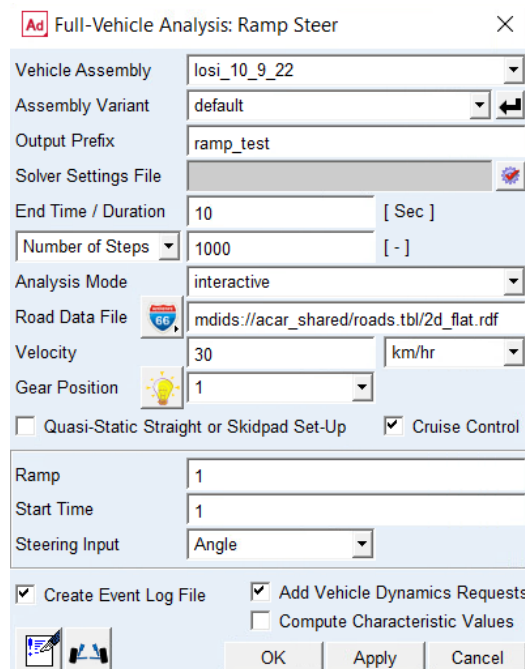


Figure 5.6 – Full vehicle static equilibrium test setup

The simulation was successful, and the convergence was achieved for the static equilibrium within the number of iterations specified. This static equilibrium is to be performed for all the configurations of the full assembly mentioned in the previous chapter. This is important to understand the tuning of the vehicle's springs in terms of installed length, as each configuration needs this adjustment to prevent over-squatting or diving of the vehicle in the static position. The next step was to perform the open loop testing methods mentioned above. The set up for each of these manoeuvres along with the description is as follows.

### 5.2.2. Ramp Steer:

Ramp steer is a manoeuvre where the steering input rate increases while the velocity is kept constant. This rate of change in steering input is constant and alters the turning radius of the vehicle as the steer input changes. This manoeuvre was simulated with the following setup conditions for all the configurations mentioned. The velocity is also supposed to be constant and therefore the cruise control has been flagged for this setup.



*Figure 5.4 – Ramp steer setup*

### 5.2.3. Step Steer:

Step steer is a dynamic manoeuvre in which, from equilibrium conditions, the vehicle is driven on a straight line and there is an instantaneous increase in the steering angle at an appreciably high rate. The setup conditions for this manoeuvre are as follows.

Vehicle Assembly	losi_10_9_22
Assembly Variant	default
Output Prefix	step_steer
Solver Settings File	
End Time / Duration	10 [ Sec ]
Number of Steps	1000 [ - ]
Analysis Mode	interactive
Road Data File	mdids://acar_shared/roads.tbl/2d_flat.rdf
Velocity	30 km/hr
Gear Position	1
<input type="checkbox"/> Quasi-Static Straight or Skidpad Set-Up	<input type="checkbox"/> Cruise Control
Turn Direction	<input checked="" type="radio"/> left <input type="radio"/> right
Steering Control Mode	<input type="radio"/> Absolute <input checked="" type="radio"/> Relative
Method	Steering Wheel Angle
Final Steer Value	8
Step Start Time	1.0
Duration of Step	0.7
Steering Input	Angle
<input checked="" type="checkbox"/> Create Event Log File	<input checked="" type="checkbox"/> Add Vehicle Dynamics Requests
	<input type="checkbox"/> Compute Characteristic Values

*Figure 5.5 – Step Steer setup*

These two open steer simulation techniques will be applied as stated to the various configurations already mentioned and the results have been discussed in the next chapter.



## 6. Results

After the completion of the simulations, Matlab has been used to do the post-processing and the plotting of the data of interest after extracting them from ADAMS as spreadsheets containing the result sets. Some of the important observations have been presented in this chapter, with the aim of throwing as much light as possible on the behaviour of the suspensions and the full vehicle models in different conditions. The results of the suspension analyses have been presented before the ones of the full vehicle analysis. For the suspension analyses, as stated in the previous chapter, the front suspension and rear suspension assemblies have been subject to multiple parallel wheel travel simulations and opposite wheel travel simulations. The simulations have been set up in a way that the effects of spring stiffnesses and certain suspension geometry like camber and toe, and the effect of the presence of the ARB in opposite wheel travel simulations in the suspension assemblies are discussed. Since the model is a front-wheel steered one, certain parameters related to steering are not applicable for the rear and so are not discussed here. To avoid redundancy, in certain cases plots with similar trends for front and rear will not be discussed as it is implied to the reader.

### 6.1. Suspension Analyses:

#### 6.1.1. Parallel wheel travel results:

##### 6.1.1.1. Computation of installation ratio:

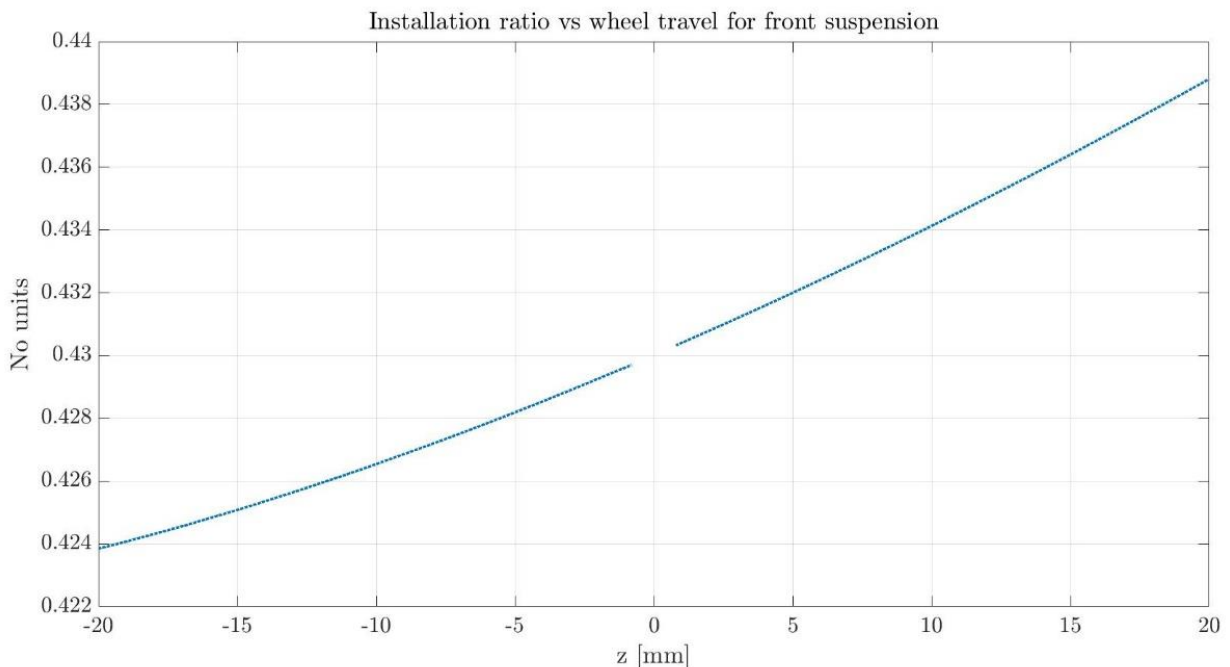


*Figure 6.1 – Installation ratios for the front suspension assembly*

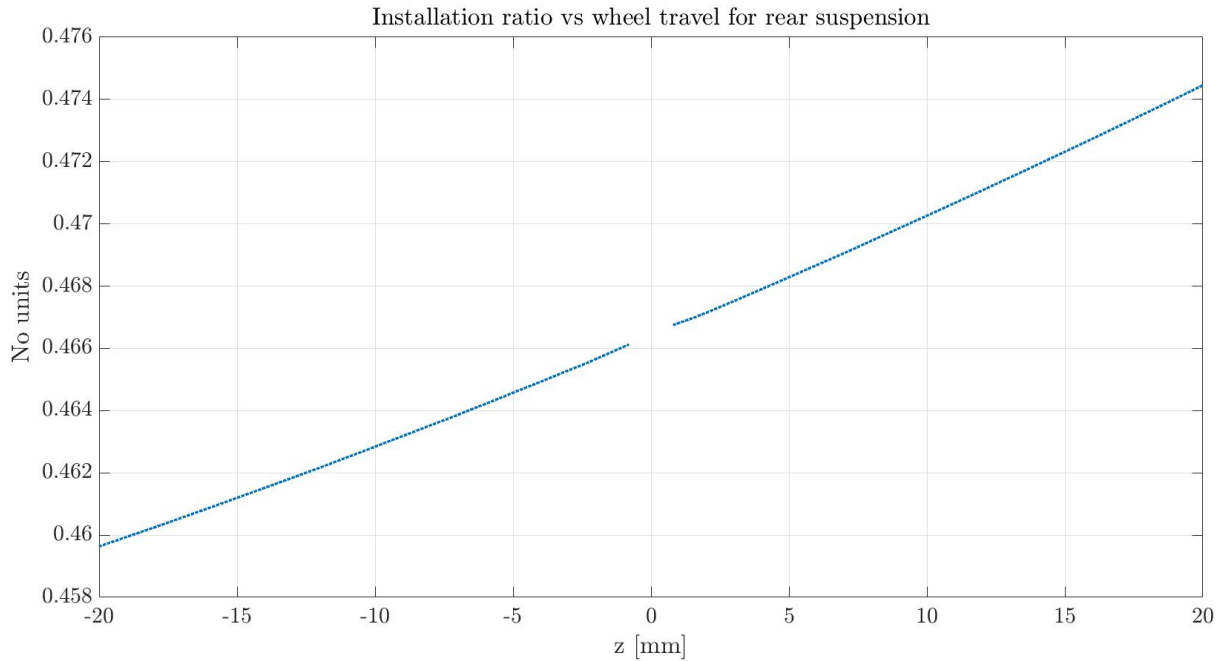


**Figure 6.2 – Installation ratios for rear suspension assembly**

Installation ratio is defined as the ratio of change in length of a spring or a shock absorber to a change in vertical wheel travel <sup>[4]</sup>. It is an important parameter that helps determine the spring and suspension characteristics to find the ride and roll rates associated with it.

In the plots above, we can see the installation ratio associated with the front and rear suspensions in rebound and bounce conditions. For our model, it is seen that the installation ratio increases with the increase in bounce and decreases with the increase in rebound for both the front and rear suspensions. Therefore, the parameters like ride and roll rates associated with it follow a similar trend, and this will be exhibited in the subsequent results and plots. The installation ratio at zero displacement is undefined since there is neither a change in spring displacement nor a change in wheel vertical travel.

**6.1.1.2. Effect of spring stiffnesses:**

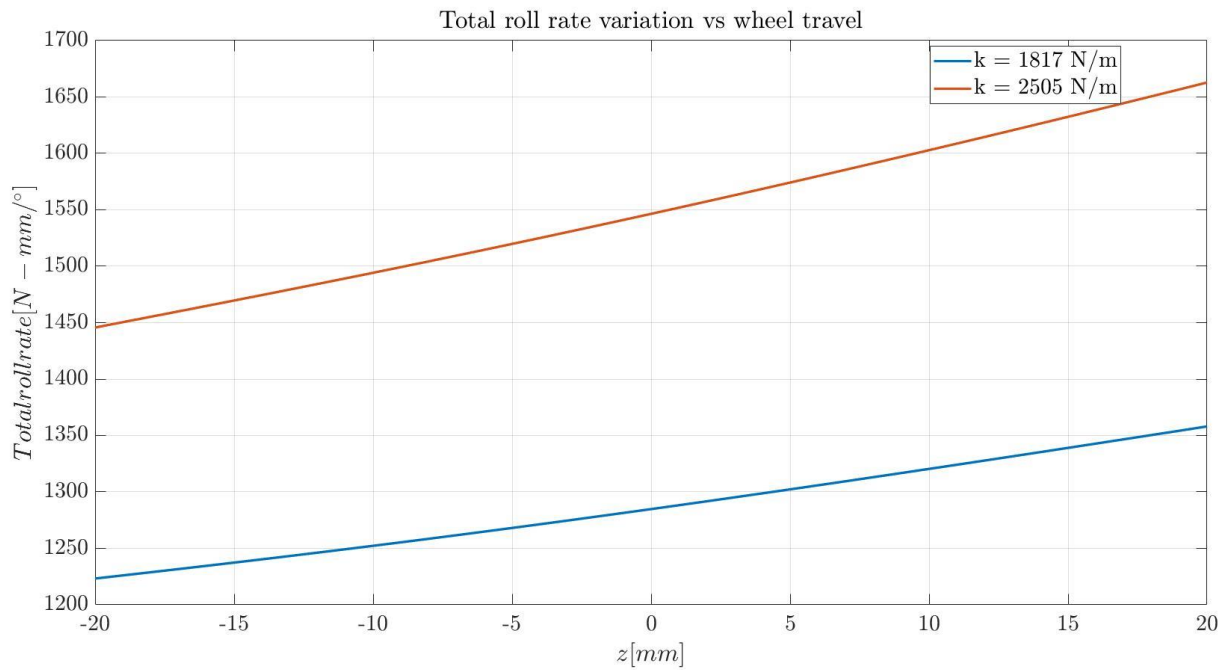


**Figure 6.3 – Total roll rate variation vs wheel travel for front suspension**

Quite evidently, we see here that for the same parallel wheel travel conditions, the front suspension modified with harder springs has higher total roll rate values throughout the course of the vertical wheel travel when compared to the baseline front suspension here which is provided with softer springs. Total roll rate is the effective stiffness offered by the suspension against roll motion by a torque that provides this resistance <sup>[4]</sup>, and it is evident that stiffer the springs, higher is this value.

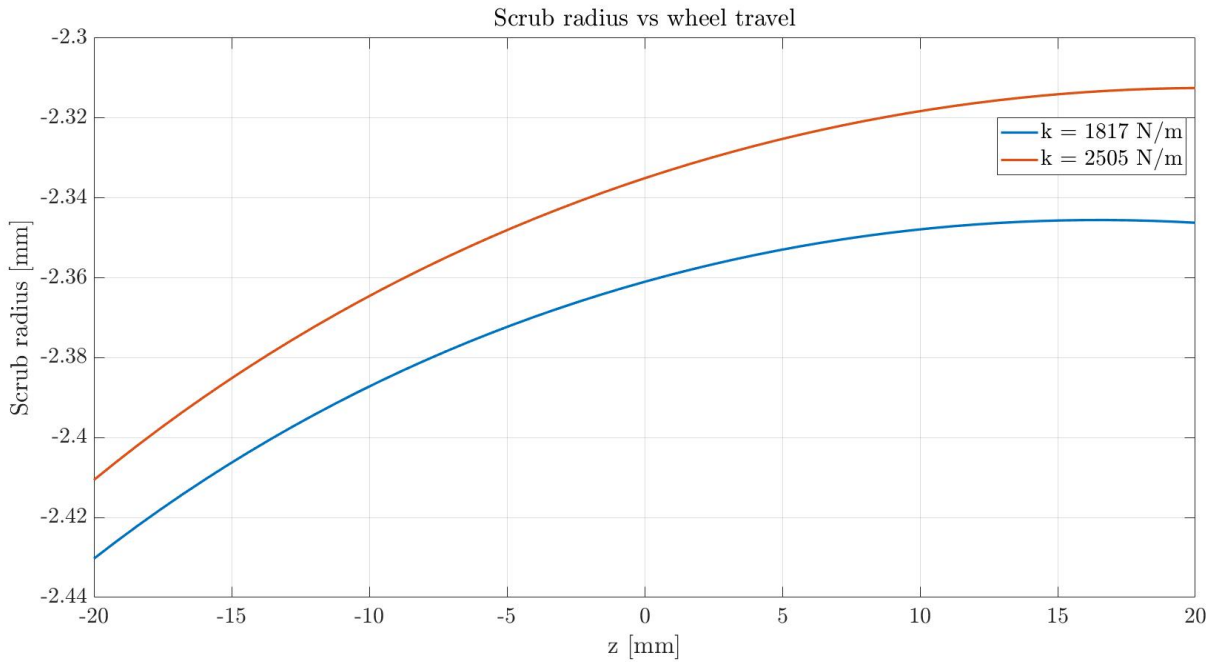


**Figure 6.4 – Scrub radius variation due to spring stiffnesses in front suspension**

The plot above shows the effect of spring stiffness on scrub radius during a parallel wheel travel test. The stiffer spring is compressed less and therefore the negative value of the scrub radius at zero vertical displacement is lesser than that in the baseline configuration and the two configurations have a similar trend throughout the vertical wheel travel between the two extremities defined in the simulation setup.

#### **6.1.1.2. Influence of camber angle:**

Next, we discuss the influence that the camber angle has on certain parameters with some plots shown below.

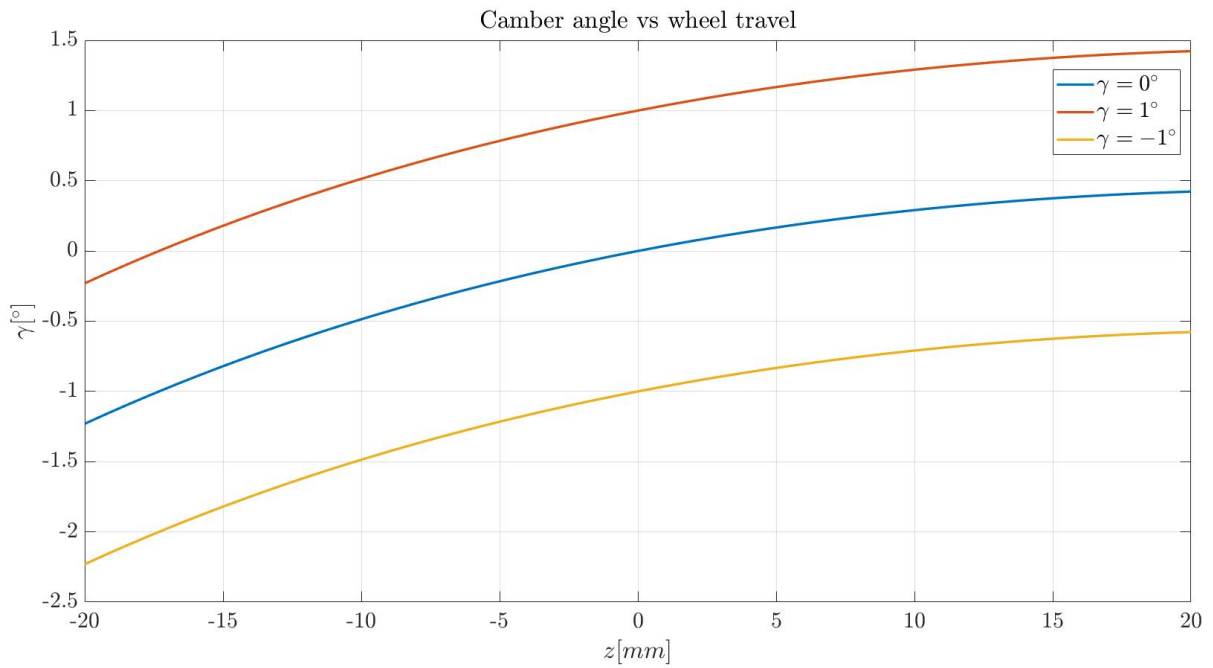


**Figure 6.5 – Camber variation in front suspension vs vertical wheel travel**

Firstly, the evolution of the camber angle throughout the course of wheel travel in the front suspension is shown in three conditions, baseline, positive camber of  $1^\circ$  and a negative camber of  $1^\circ$ . The three trends have similar evolutions.

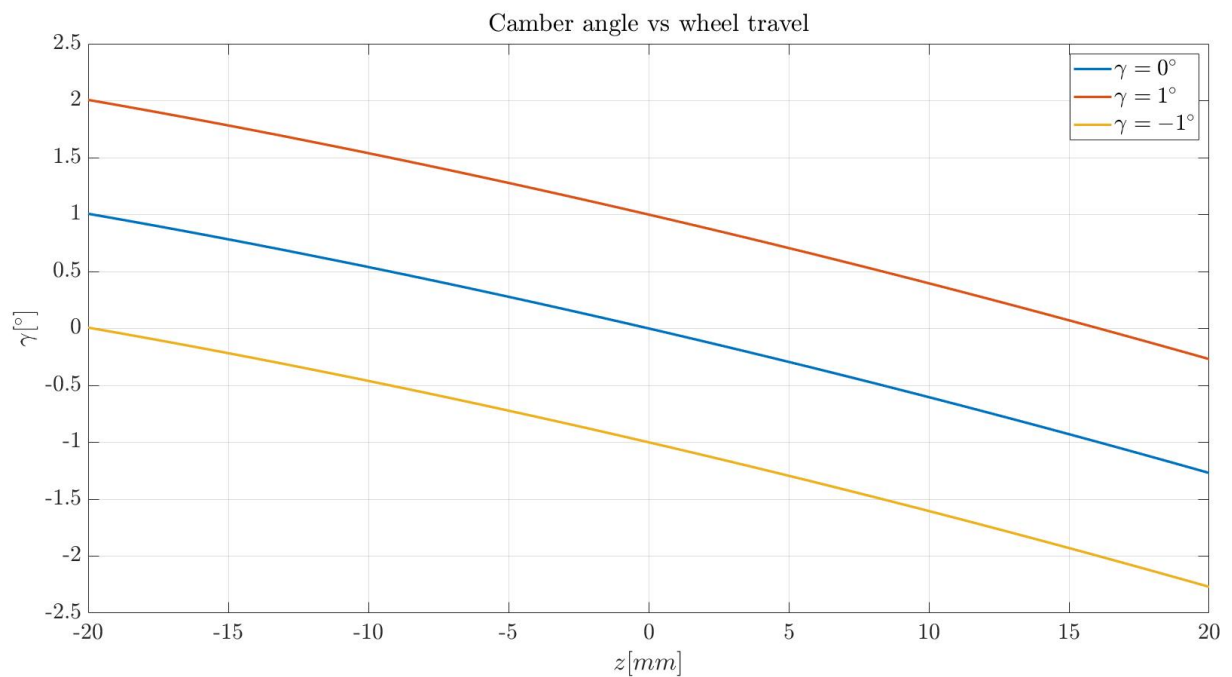


**Figure 6.6 – Camber angle variation in rear suspension vs vertical wheel travel**

The camber angle evolution of the rear suspension (*Fig. 6.4.*) shows a slightly different behaviour as the rear suspension differs from the front one due to the absence of steering system connected to it. Therefore the degree of freedom associated with steering of the wheels is considered “locked” resulting in the behaviour shown above. It is seen that the camber angle decreases during bounce and reaches higher values during rebound of the wheel in the vertical direction. In simpler terms, the front suspensions move towards a positive camber condition in bounce and a negative camber condition in rebound. The converse is true in the case of the rear suspensions.

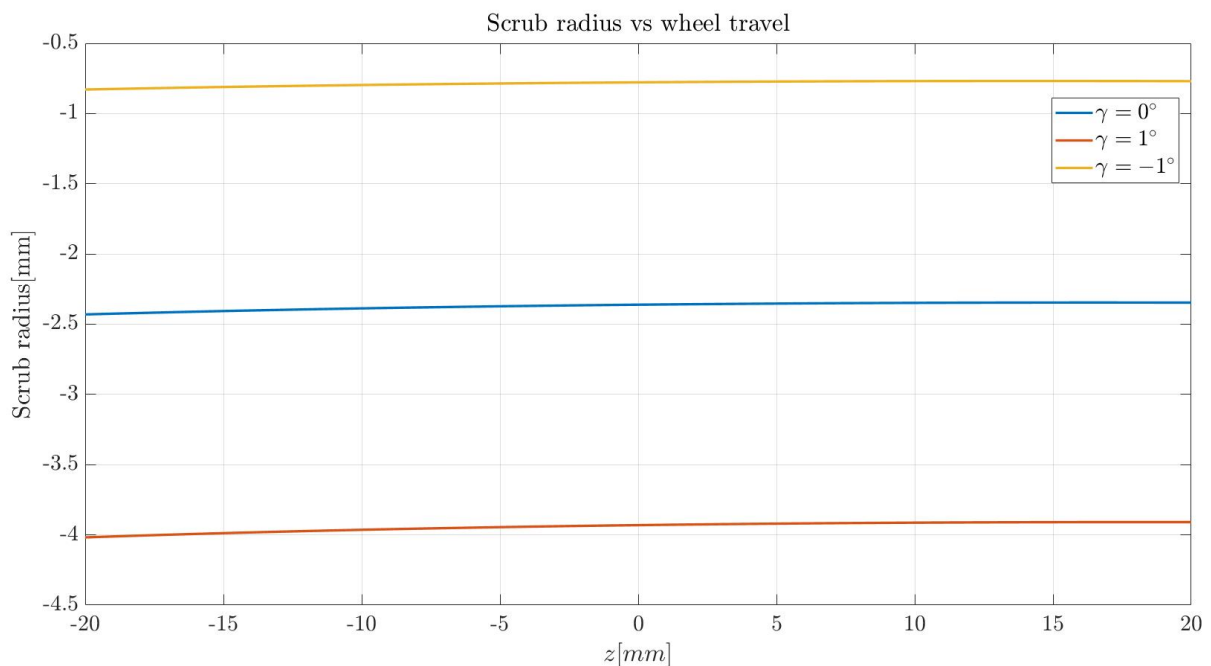


**Figure 6.7 – Scrub radius vs wheel travel for front suspension**

The camber influence on the scrub radius can be seen here again for the front suspensions. Since positive camber is the outward inclination of the wheel and consequently, the scrub radius in this configuration is higher. The converse is true for the condition with negative camber, and the zero-camber configuration has a scrub radius between the two values.

As a consequence, the same logic can be applied to understand the effect on the lateral distance between the contact patch and the roll centre for the front suspensions. In a positive camber, the top of the tire is inclined outward and so the bottom of the tire which is in contact with the ground is inclined towards the vehicle. Therefore, it has a smaller lateral distance to the roll centre in comparison to the other two conditions.

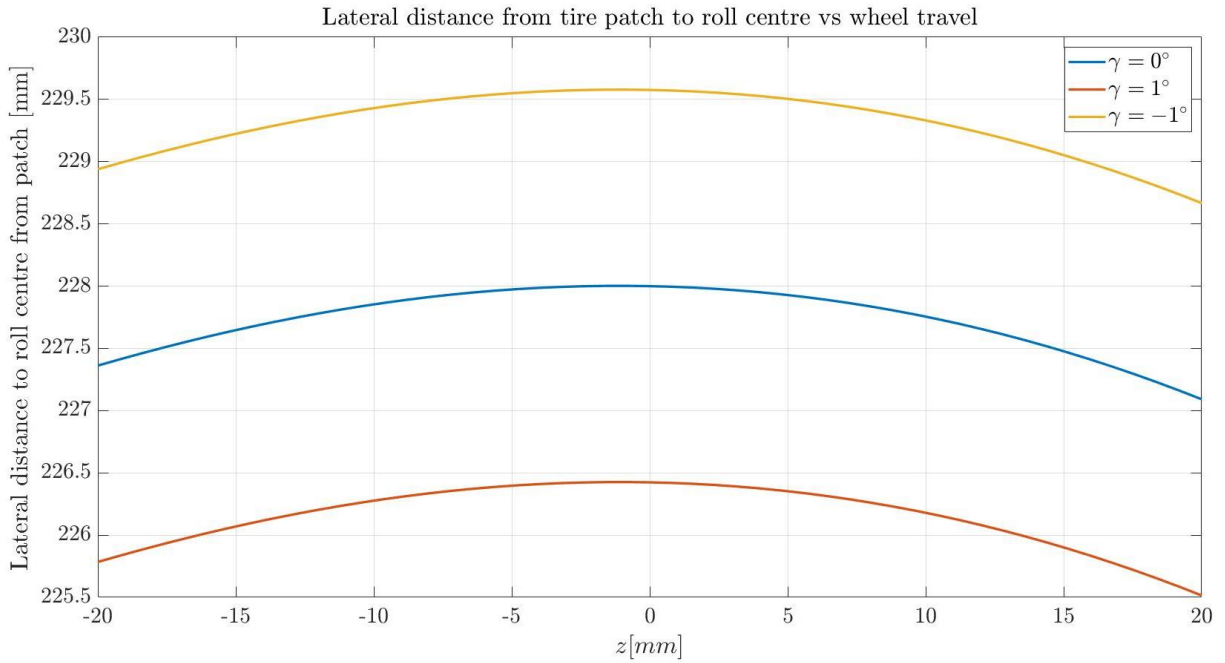


**Figure 6.8 – Lateral distance to roll centre from tire patch vs wheel travel for front suspension**

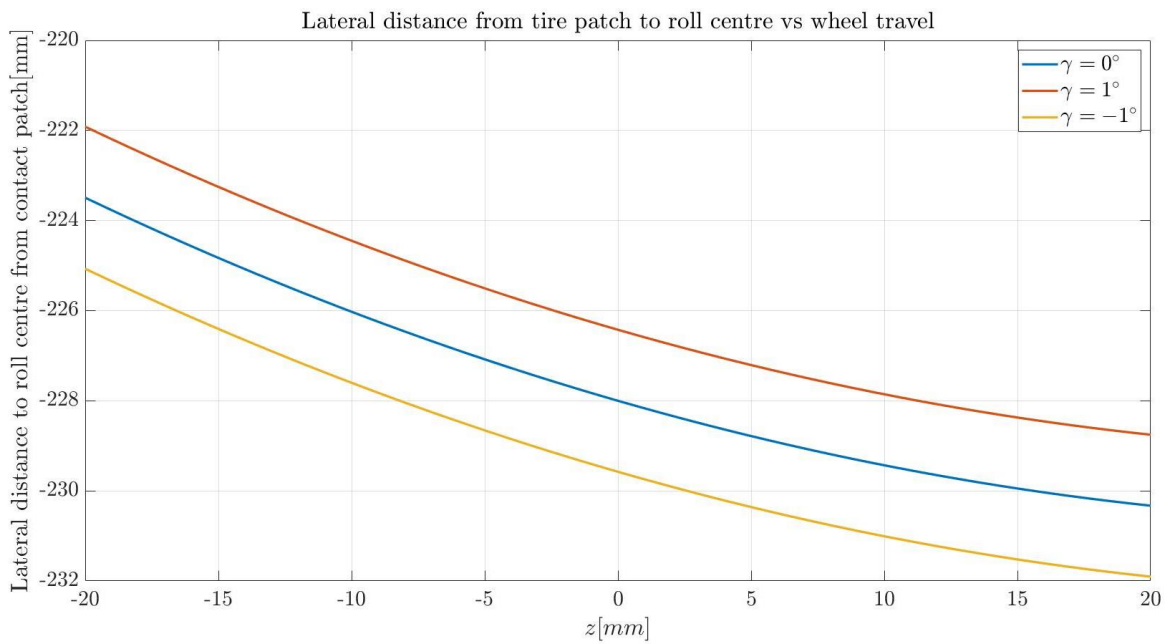


**Figure 6.9 - Lateral distance to roll centre from tire patch vs wheel travel for rear suspension**

However for the reasons explained earlier, the evolution of the lateral distance to contact patch in the rear suspension assembly follows a different trend, as shown above in the figure, to that

of the same feature in the front. It is observed that in all three conditions, during bounce, the lateral distance reduces between the roll centre and wheel patch, while it increases during rebound phase. This is again related to the degrees of freedom available to the rear suspension.

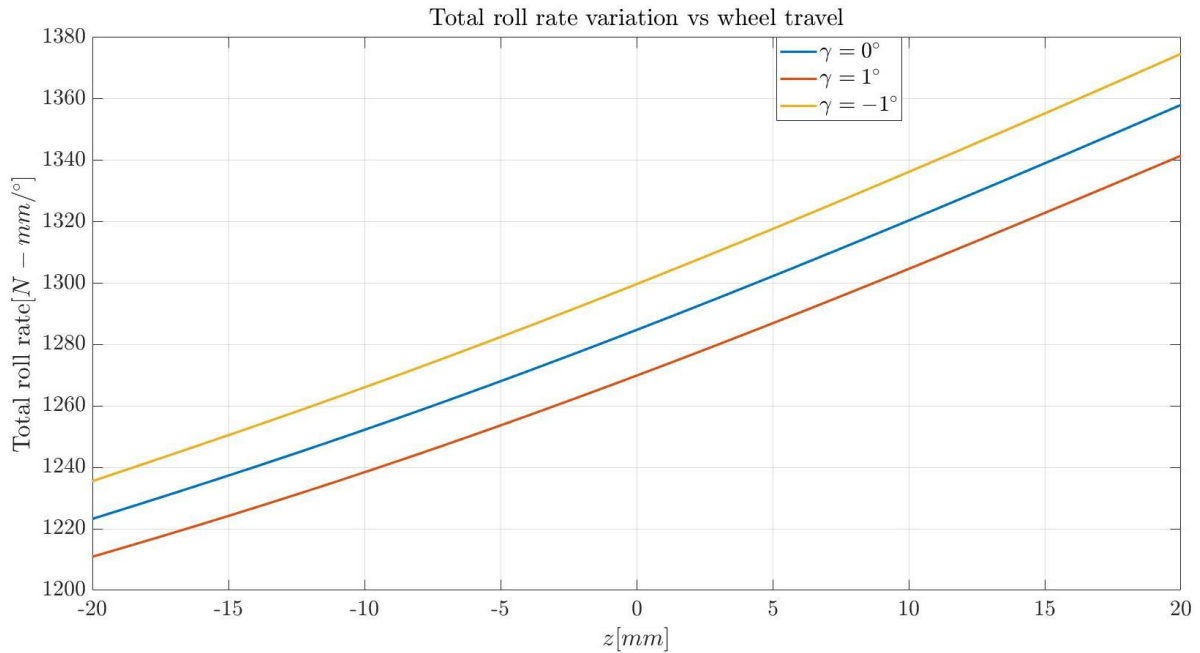


**Figure 6.10 – Total roll rate variation vs wheel travel for different camber angles in front suspension**

Lastly, the camber influence on the roll rate variation is shown. The positive camber allows for a slightly higher dive of the front suspension due to the position of the wheels and consequently has a marginally lower roll rate than the zero camber or the negative camber condition. The negative camber, offers greater resistance to roll as shown in the plot and is preferred to achieve smooth cornering at higher speeds.

### 6.1.1.3. Influence of toe angle:

The toe angle also has an influence on the scrub radius of the vehicle in the front as shown in the figure below. Positive toe or toe in is defined as the inward inclination of the tire when observed from the top in comparison to the vehicle's centreline, while negative toe or toe out is the outward inclination with respect to the centreline. And so, consequently, it is seen that toe in increases the scrub radius while toe out decreases it with respect to the baseline condition of no-toe.



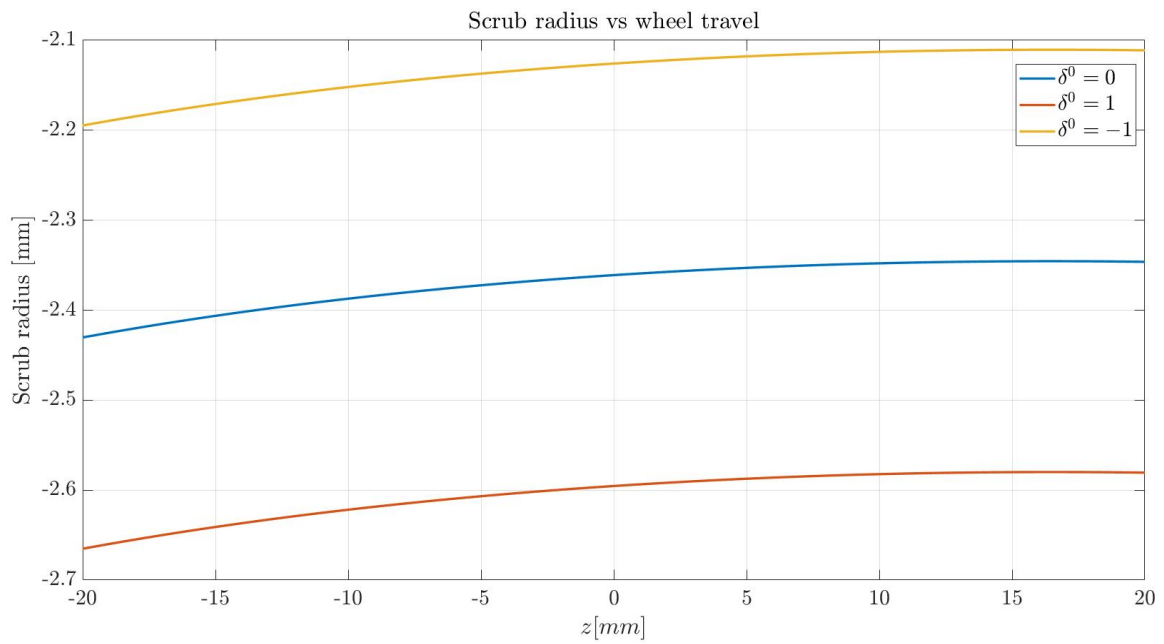


*Figure 6.11 -Scrub radius vs vertical wheel travel for different toe angles in front suspension*

## 6.1.2. Opposite wheel travel:

### 6.1.2.1. Influence of addition of ARB:

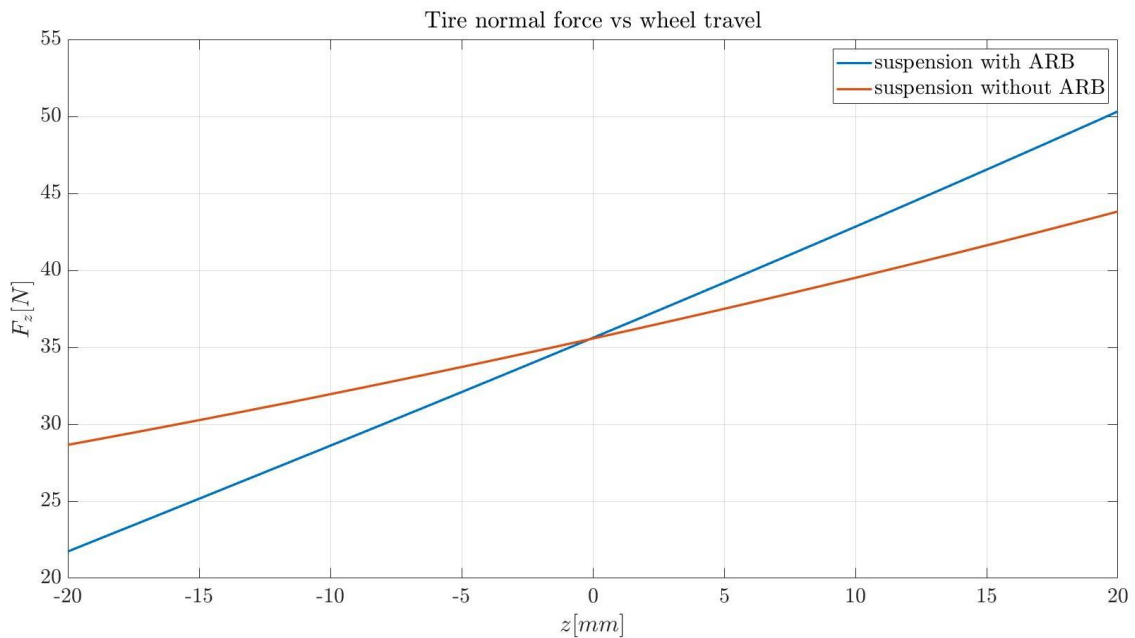


*Figure 6.12 – Normal tire forces in front suspension for opposite wheel travel*

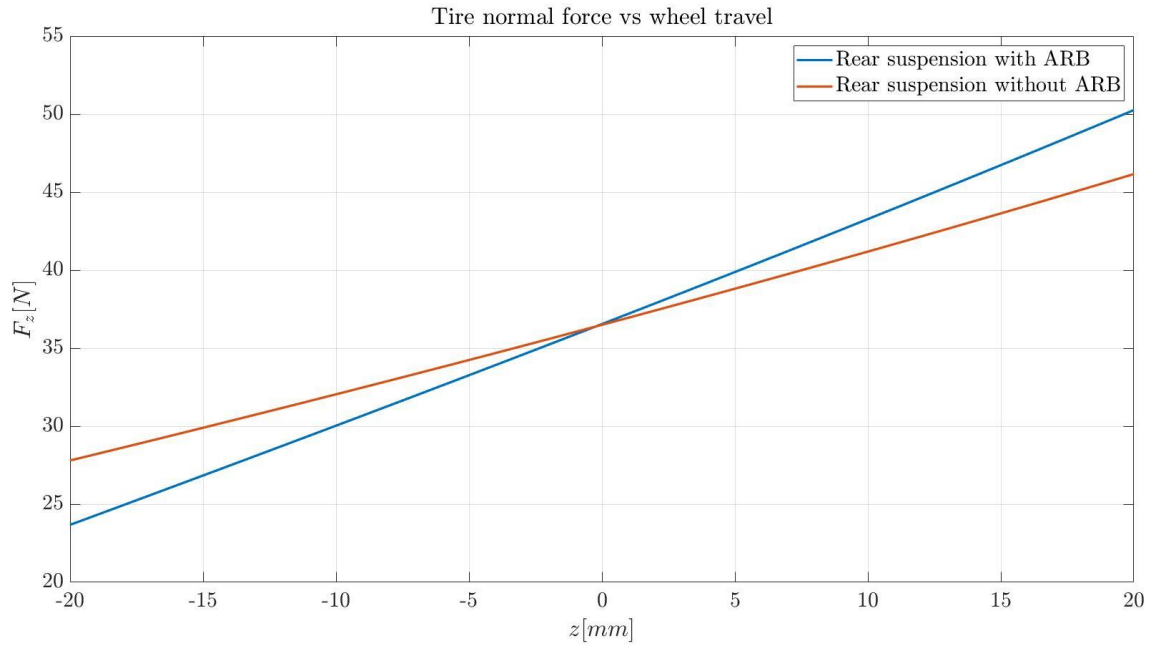


**Figure 6.13 – Variation of normal tire forces in rear suspension for opposite wheel travel**

While performing the opposite wheel travel simulation, it is observed that for a given tire (left or right) the suspension assembly with ARB experiences a lower vertical wheel load in the rebound position while it is higher in the bounce position in comparison to the suspension without ARB. In opposite wheel travel, when one wheel is in bounce condition, the other wheel is fully in rebound. The presence of the ARB allows for a better load distribution along the lateral direction, which aids in increasing the stability of the vehicle and enhancing its handling capabilities. This aspect will be explored further in the section dedicated to the discussion of the results pertaining to the full vehicle simulations.

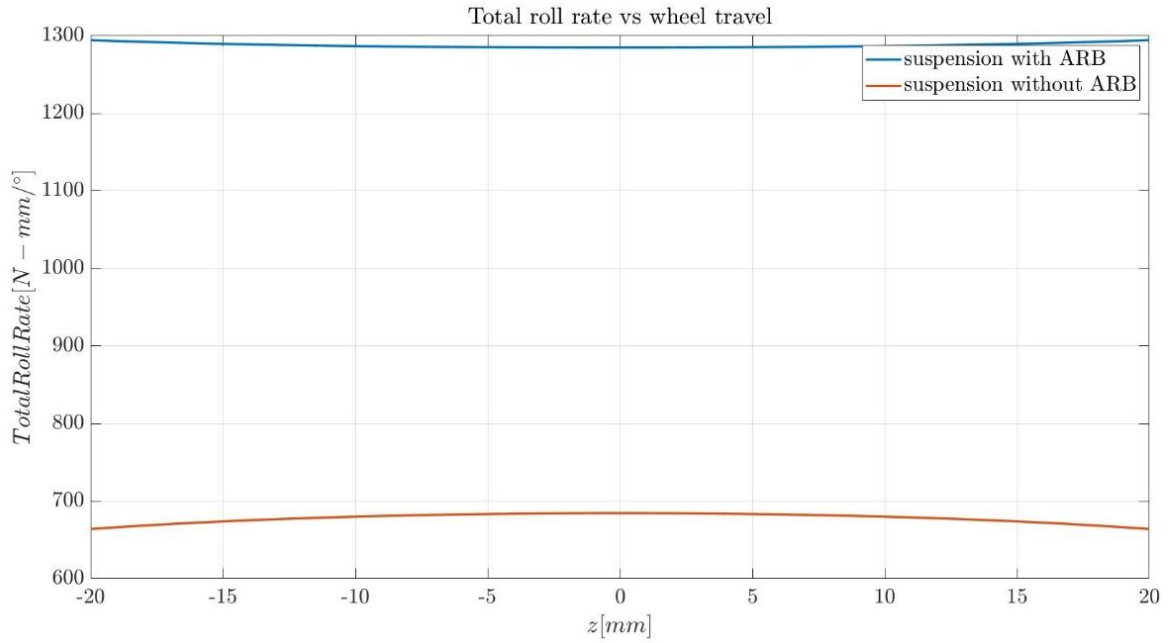


**Figure 6.14 – Total roll rate for front suspension vs wheel travel**

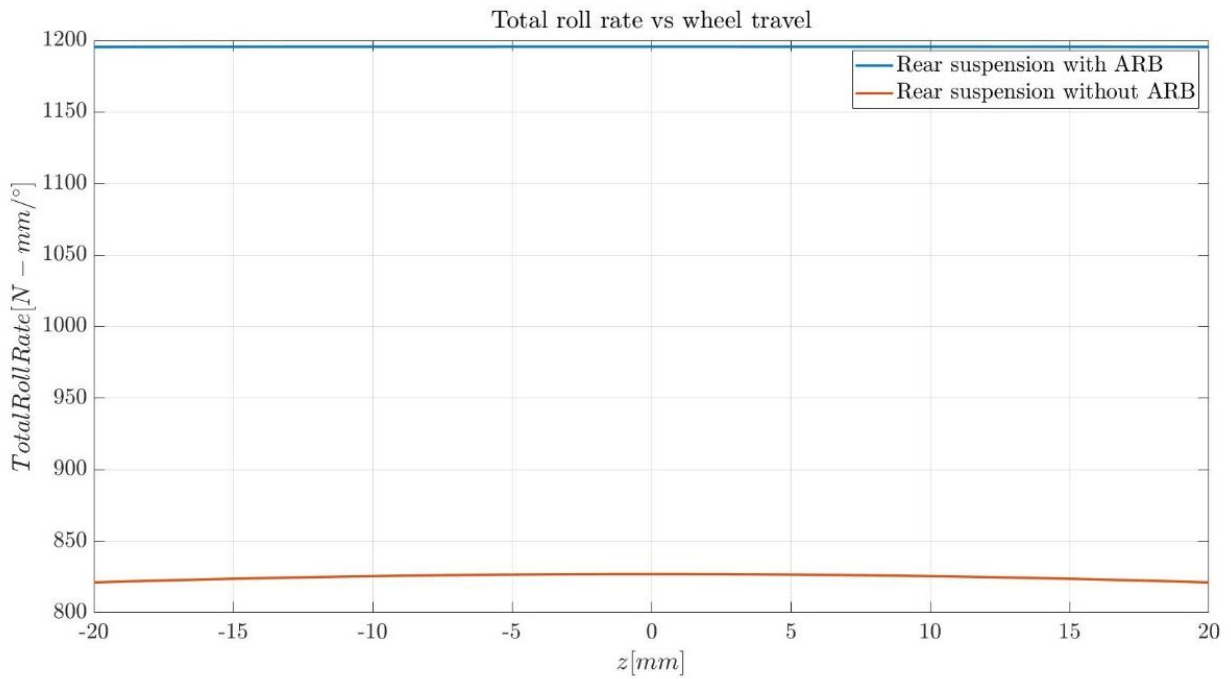


**Figure 6.15 – Total roll rate for rear suspension vs wheel travel**

Another noticeable influence of the ARB is the contribution to various stiffness parameters like ride rate, total roll rate etc. The ARB configuration is stiffer and hence it guarantees greater stability for a given suspension assembly. The plots depict the total roll rate of the front and rear suspensions with and without their respective ARBs in the assembly.

### 6.1.2.2. Influence of spring stiffness:

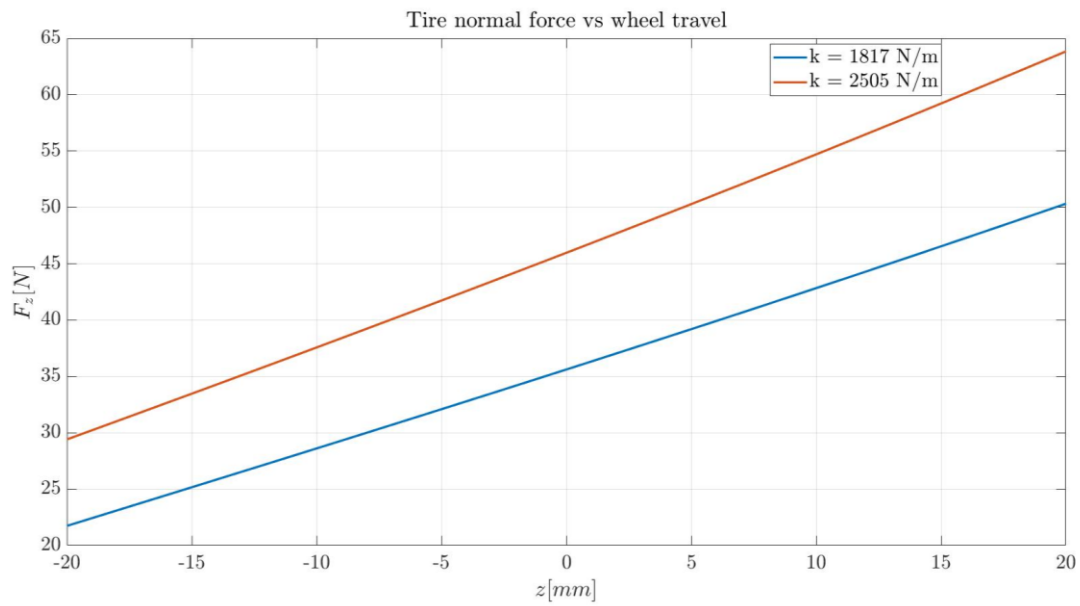


Figure 6.16 – Tire normal forces for front suspension with different spring stiffnesses vs wheel travel

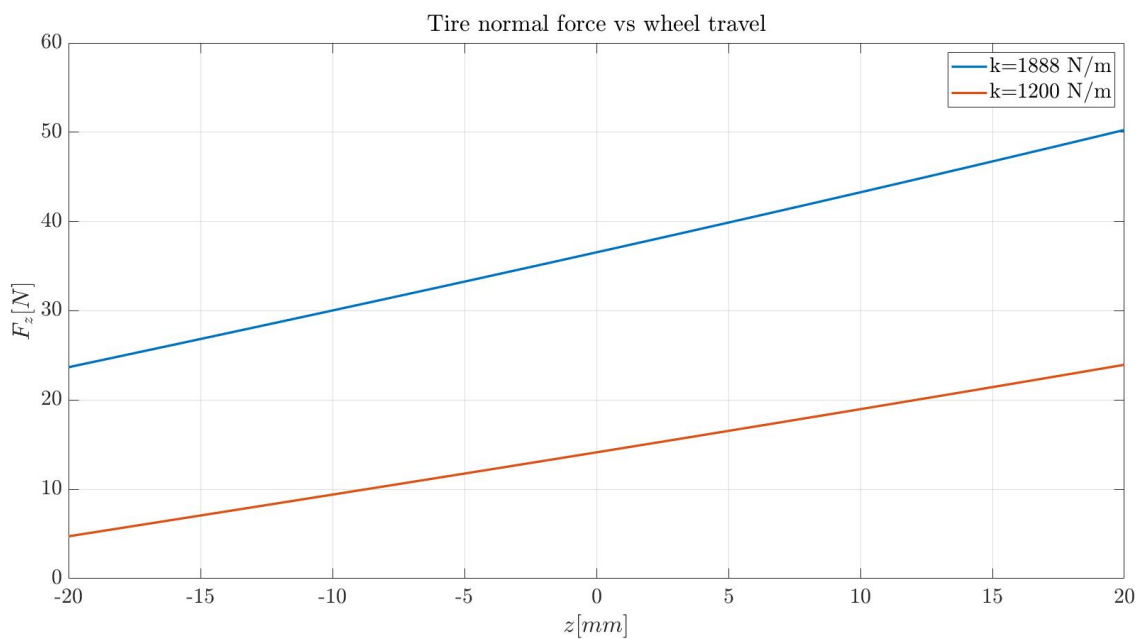
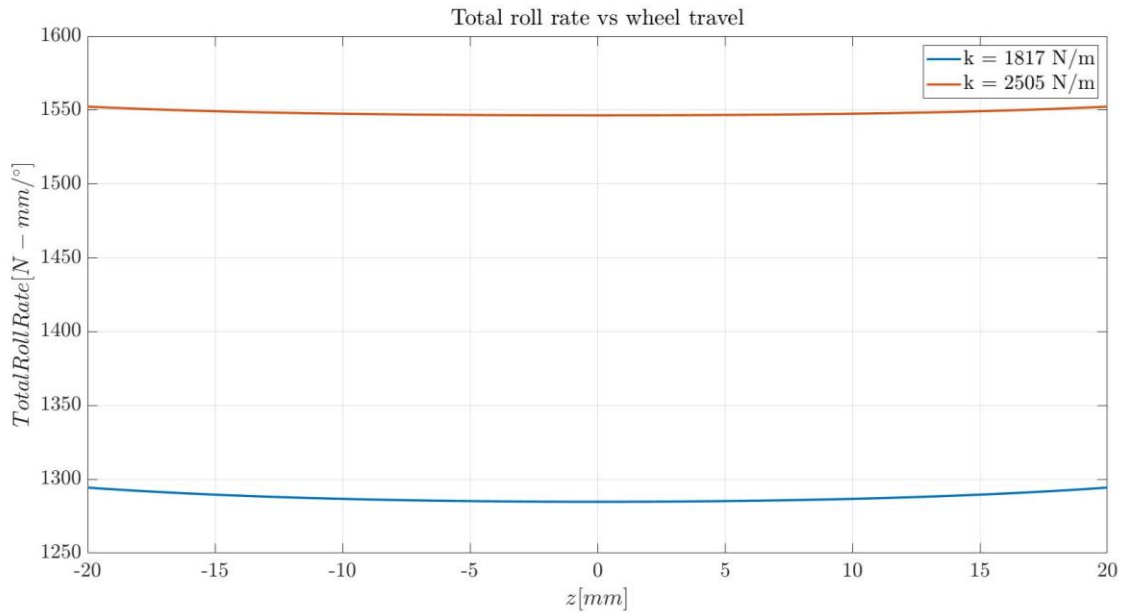
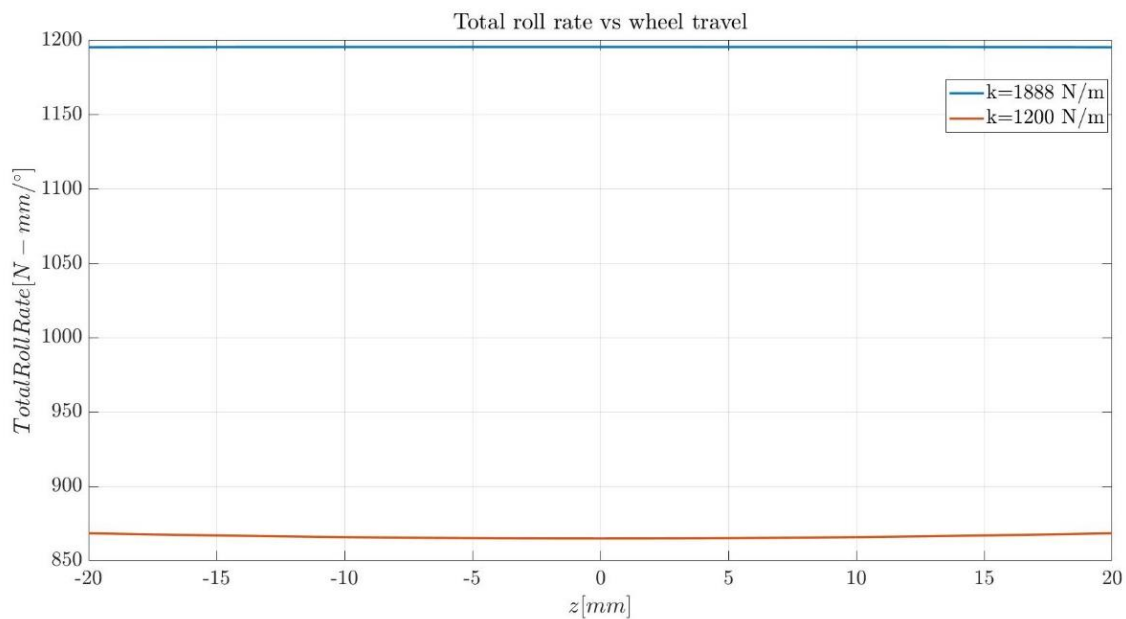


Figure 6.17 – Tire normal forces for rear suspension with different spring stiffnesses vs wheel travel

The plot above shows the decrease in the tire normal forces when softer springs are introduced in the suspension. Both the baseline and the suspension with softer springs are equipped with ARBs during the simulations. These plots are made from the opposite wheel travel results of front and rear suspensions respectively.



**Figure 6.18 – Variation in total roll rate for different springs in front suspension vs wheel travel**



**Figure 6.19 – variation in total roll rate for rear suspension with different spring stiffnesses vs wheel travel**

Softer springs also offer subjectively lesser stiffness characteristics, and this can be brought to evidence by the total roll rate plot against the baseline, which offers a higher degree of stiffness. Once again, these are graphically presented from the simulation data related to the front and rear suspension assemblies respectively.

### 6.1.3. Steering simulation results:

The steering simulation was performed to understand the transfer of motion from the steering input to the wheels. The setup, which has been explained in the previous chapter, yielded the following results.

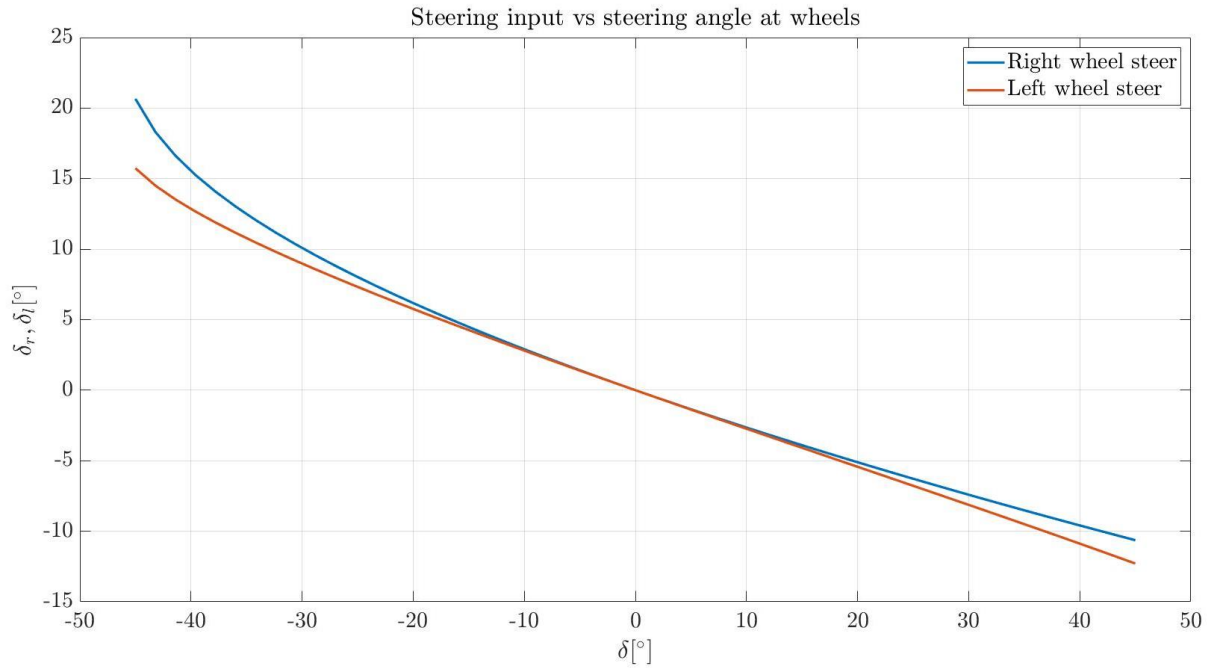


**Figure 6.20 – Steering input vs steering angle at wheels**

Here it is seen that for the current model, at low steering angles, the right and left tires are steered identically for a given input. But the slope changes towards the extremities, which sees a greater steering of the right wheel in comparison to the left wheel when the steering angle is negative and vice versa when the steering angle is positive. This is a result of the geometry of the current model and can be altered to exhibit a different behaviour.

## 6.2. Full vehicle assembly results:

### 6.2.1. Static equilibrium test:

The static equilibrium test, as already stated, helps in tuning the vehicle in terms of its static position and the tuning is done with changing the installed length of the springs according to the stiffnesses. For the configurations that have been discussed, the following table gives the details of the installed lengths for the front and rear cases in each of the cases.

**Table 6.1 – Installed spring lengths for each full vehicle configuration**

Configuration	Front spring installed length [mm]	Rear spring installed length [mm]
Baseline	75	115
2	78	110
3	90	82

### 6.2.2. Ramp steer results:

The results of the ramp steer simulation performed according to the setup explained earlier will now be discussed. It is to be noted that the simulations were performed only on the ‘baseline’ configuration discussed above for both the ARB and non-ARB versions of the full vehicle

assembly. For discussing ramp steer results, some important parameters are lateral acceleration, steering input angle, sideslip angle, and roll angle of the chassis. Here, the steering input, sideslip angle for both assembly versions will be against the lateral acceleration while the temporal evolution of the chassis roll angle has been depicted. But firstly, the variation of wheel loads during the manoeuvre has been explained.

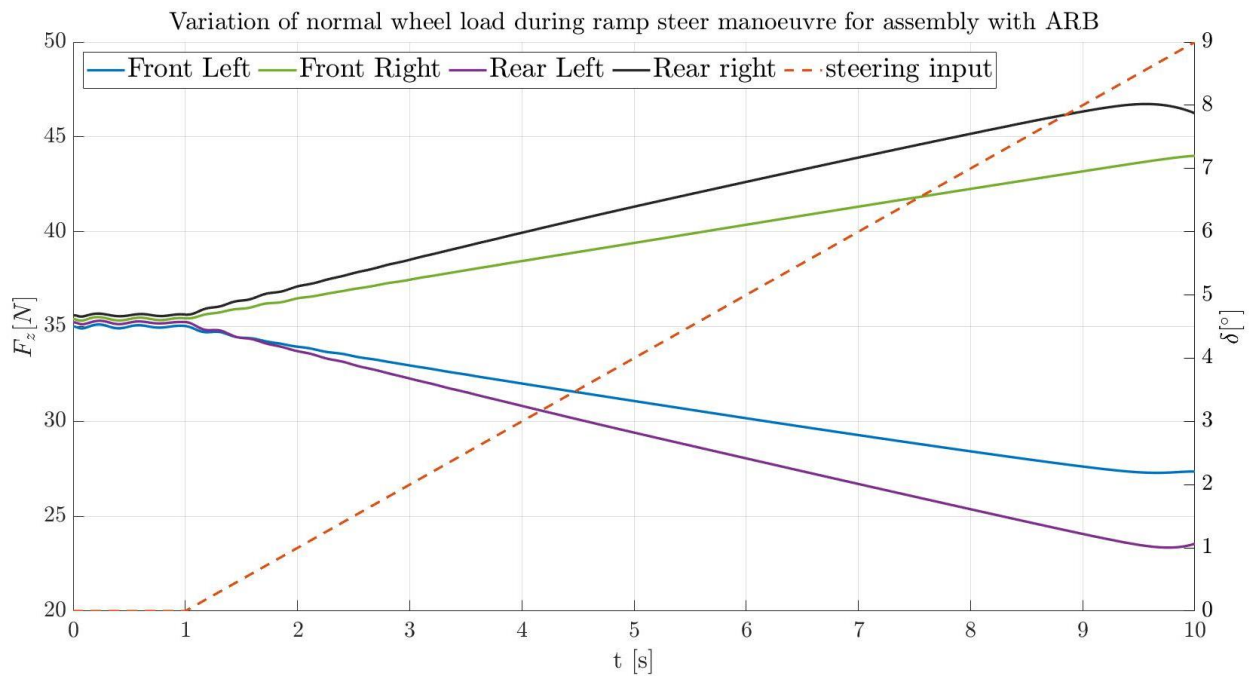


**Figure 6.21 – Wheel load variation in ramp steer manoeuvre with ARB**

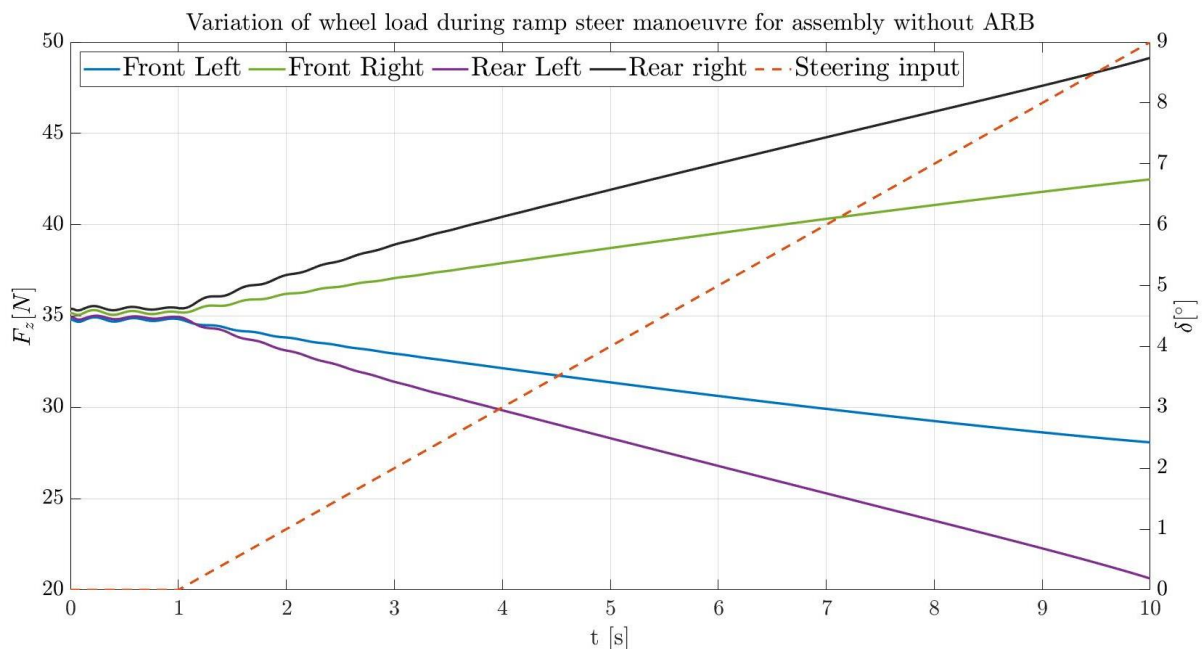


**Figure 6.22 – Wheel load variation in ramp steer manoeuvre without ARB**

From the two plots, it is evident that when taking a left turn, the maximum load acts on the right-hand side wheels. In particular, in both cases, the rear right experiences the highest load.

When comparing the front right wheels of both the ARB and non-ARB versions of the assembly, we see that in the assembly with ARB, the front right tire experiences more normal load than its non-ARB counterpart. This indicates that without ARBs the vehicle tends to be less understeering considering the distribution of the normal load on the tires. This can be attributed to the reduced stiffness in the suspension system as a whole due to the absence of ARBs. This point will be explored further in the results pertaining to the step steer manoeuvres.

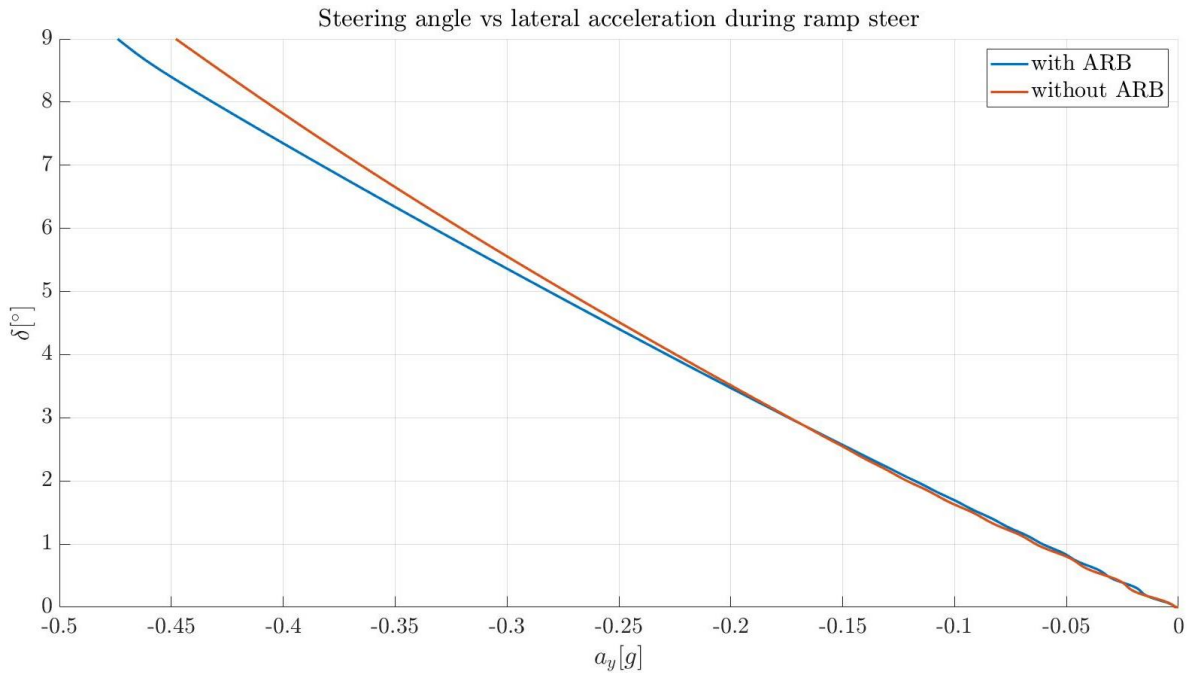


**Figure 6.23 – Steering angle vs lateral acceleration during ramp steer**

The lateral acceleration vs steering wheel angle plots for the ARB and non-ARB configurations are depicted above. The plots show that for the same value of steering angle, the ARB assembly reaches higher values of lateral acceleration in terms of absolute values. This is again attributed to the effect of greater load transfer to the outside when taking a turn due to the effect of the ARBs. It is worth noting that since the vehicle took a left-hand turn, the values of lateral acceleration are provided in negative values in the result set. The same applies for the trends of sideslip and roll that will be described next.



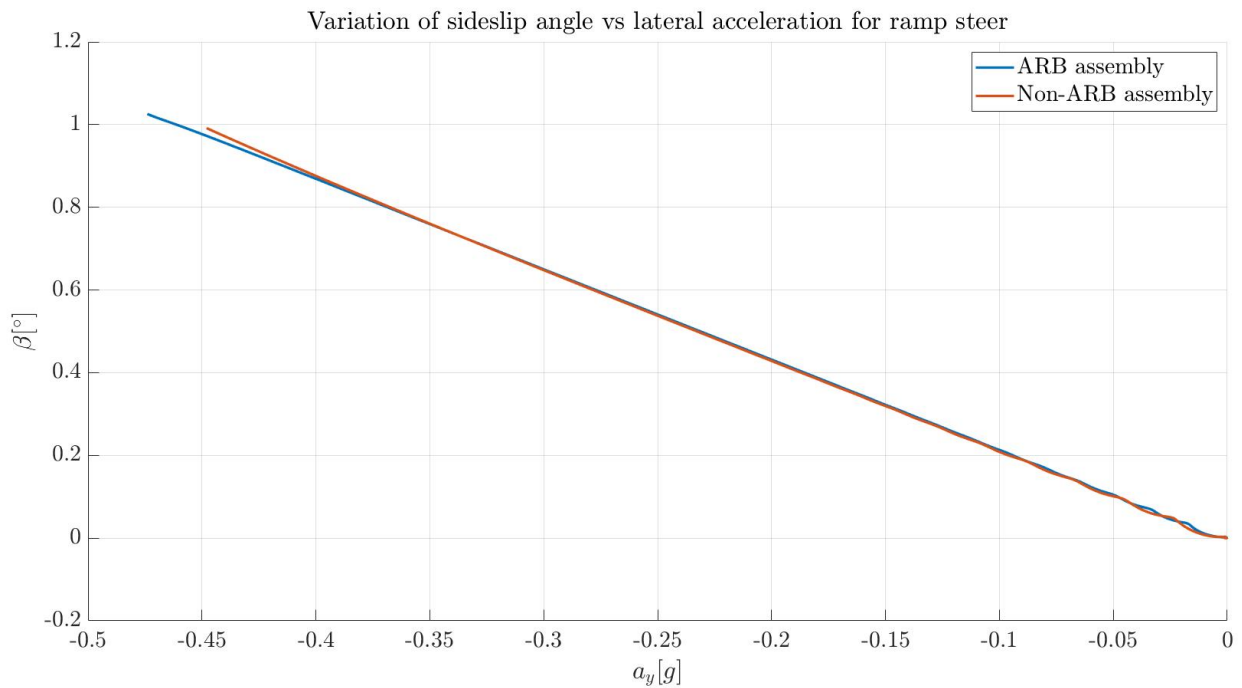


**Figure 6.24 – Sideslip angle vs lateral acceleration during ramp steer manoeuvre**

From the sideslip plots, it is seen that the ARB assembly reaches a higher value of sideslip angle in terms of final values at the end of the simulation. Even though for a given lateral acceleration, the sideslip angles are almost identical, when looked at from the perspective of steering angle input, the more understeering behaviour of the assembly with ARB is highlighted.

Next the results pertaining to roll of the vehicle are discussed in order to fully comprehend the role of ARBs in this assembly.

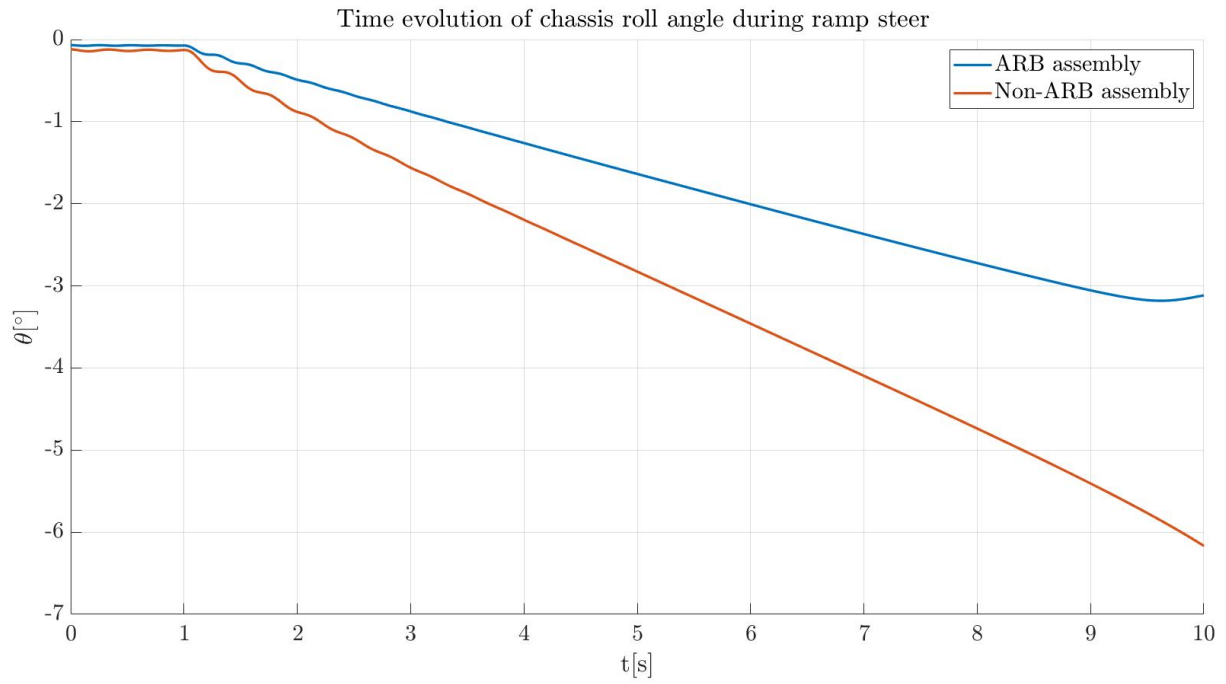


**Figure 6.25 – Time evolution of chassis roll angle during ramp steer**

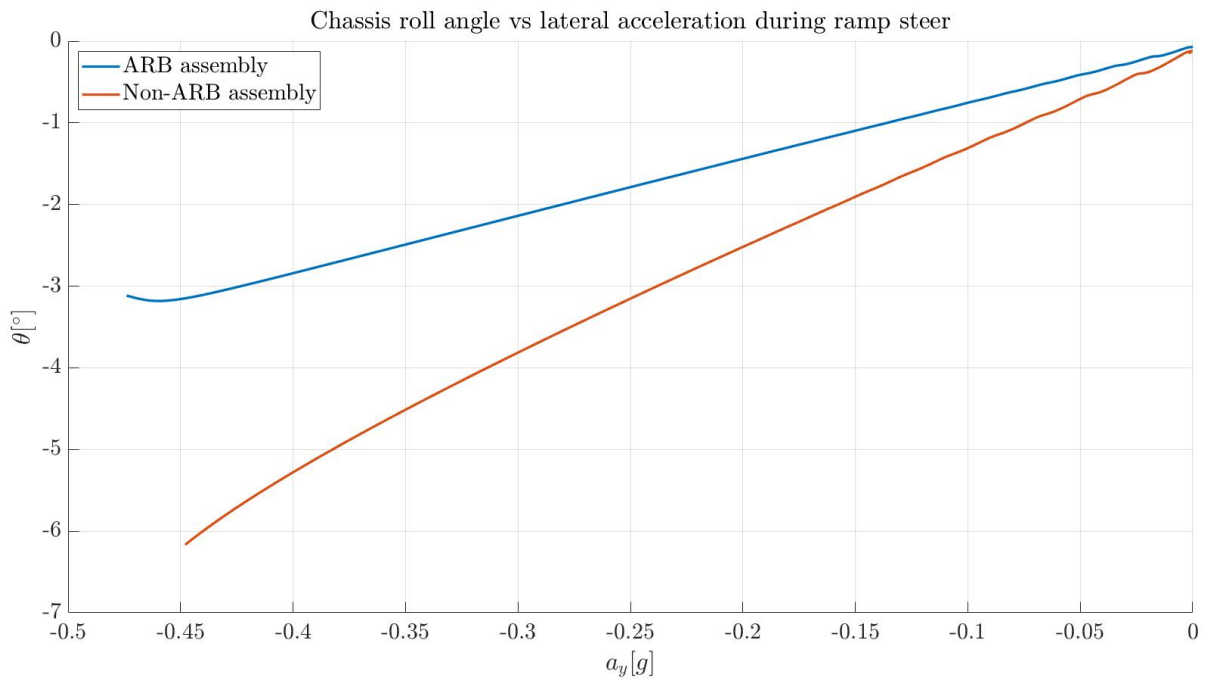


**Figure 6.26 – Chassis roll angle vs lateral acceleration during ramp steer manoeuvre**

Firstly the time evolution of the roll angle is depicted and then the trend of lateral acceleration vs the roll angle is plotted to give the reader a small glimpse of the impact of the ARB, whose primary function is to limit the roll of the vehicle. A more detailed analysis of the same will be done in the results of the step steer simulations, but for now the interpretations of these two plots are listed.

As expected, the chassis rolls more for the assembly without anti-roll bars than the one with them due to the reduction in stiffness in the suspensions that are offered by the bars. It is interesting to note that in this particular case of simulation setup, the roll angle at the end of the simulation for the non-ARB assembly is almost double that of the assembly with ARB, highlighting the impact that the bars have in vehicle handling. From the second plot, it can be inferred that for the same value of lateral acceleration, the non-ARB assembly rolls more than its counterpart, and thus even though the ARB assembly experiences more lateral acceleration, it rolls less, and it can be said that the objective of including the ARBs is met.

### 6.2.3. Step steer results:

The results of the step steer analysis have been categorized as described in the previous chapter. Firstly, the effect of spring stiffnesses will be discussed through the plots and then the effect of ARBs will be studied and evaluated. From the setup of step steer explained in chapter 5, the simulation was done to make the vehicle turn to the right-hand side, and therefore the values all the values are accurate in this subsection in magnitude and also in direction.

#### 6.2.3.1. Influence of spring stiffnesses:

In the baseline configuration, as already stated, the rear springs are slightly stiffer than the front springs and in the other two configurations, the front springs are stiffer. The effect of this can be easily understood with the following plots.

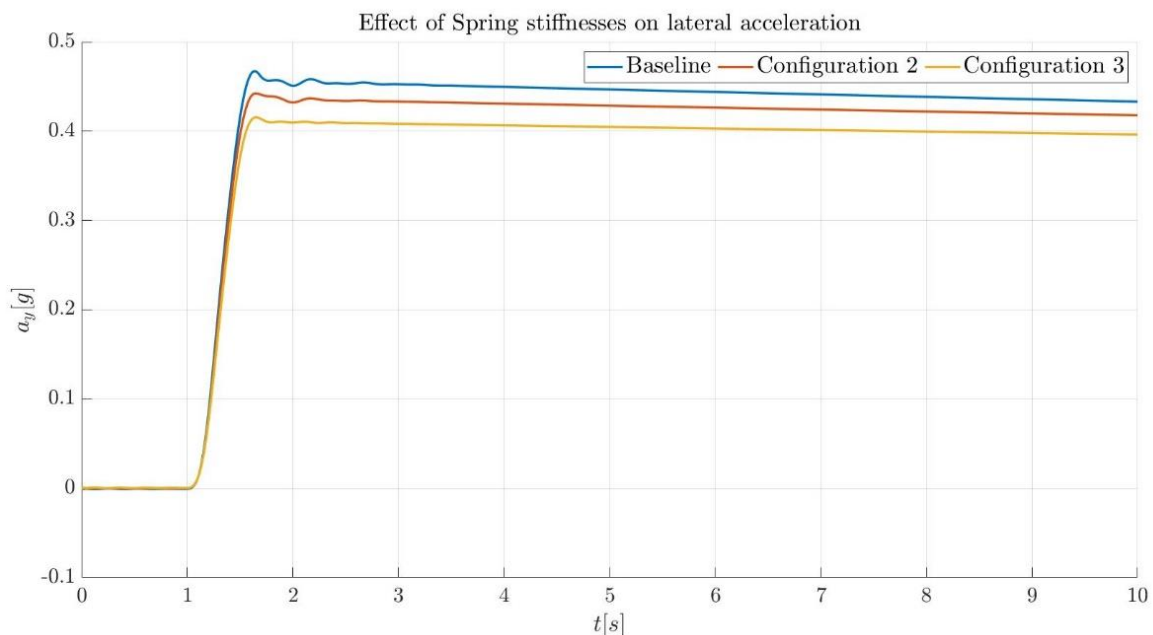
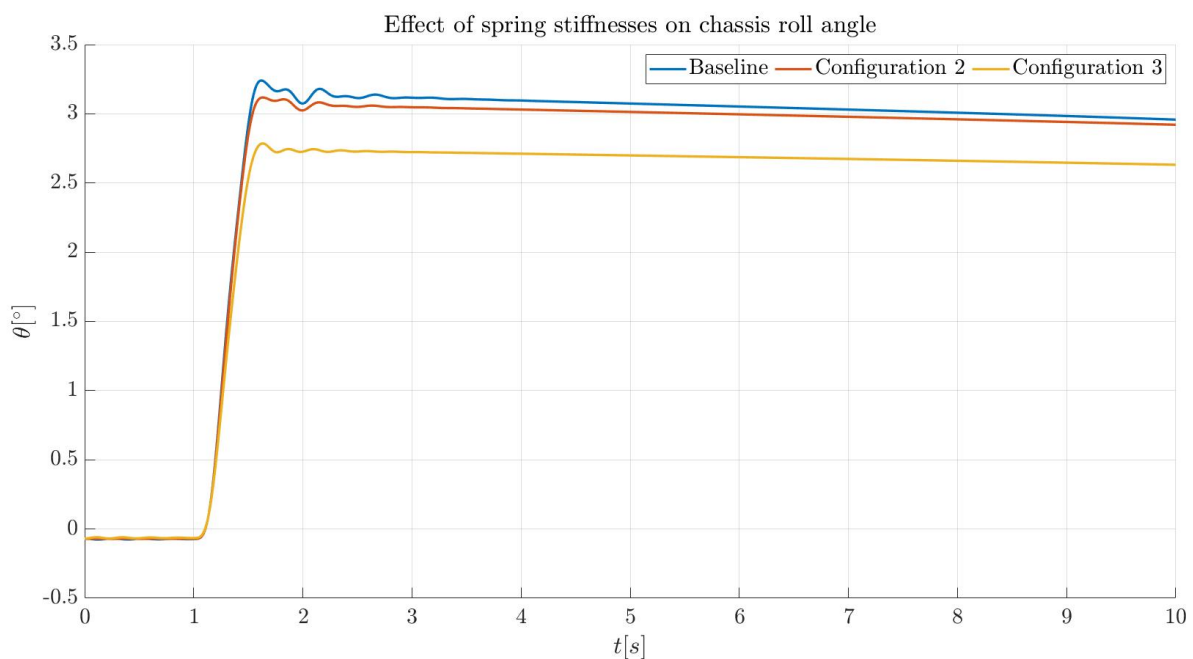


Figure 6.6 – Time evolution of lateral acceleration during step steer manoeuvre for different spring stiffnesses

As shown in the plot, the baseline reaches highest values of lateral acceleration which implies the effect of softer front springs. In terms of stiffness ratio between the front and the rear, the third configuration is the highest as the front springs are almost twice as stiff as the rear in this. And the effect is that there is lesser lateral acceleration, and a more understeer behaviour for the vehicle as a whole, with the stiffness properties of the front suspension higher than that of the rear suspension. In comparison the baseline experiences more oversteering or less understeering.

Once again, this can be observed in the trends of the chassis roll angle for the three configurations. Considering the stiffer front suspensions both objectively and in relation to the rear, the chassis roll is the least for the third configuration and the highest for the baseline, in which the fronts are objectively softer than the rear springs.



**Figure 6.7 - Time evolution of chassis roll angle during step steer manoeuvre for different spring stiffnesses**

The same can be said for the impact of the suspension stiffnesses on the pitch and sideslip angles of the vehicle. The stiffer front suspensions allow for lesser pitching motion experienced by the vehicle and this is in line with the other trends and consequent conclusions arrived at previously in this analysis.

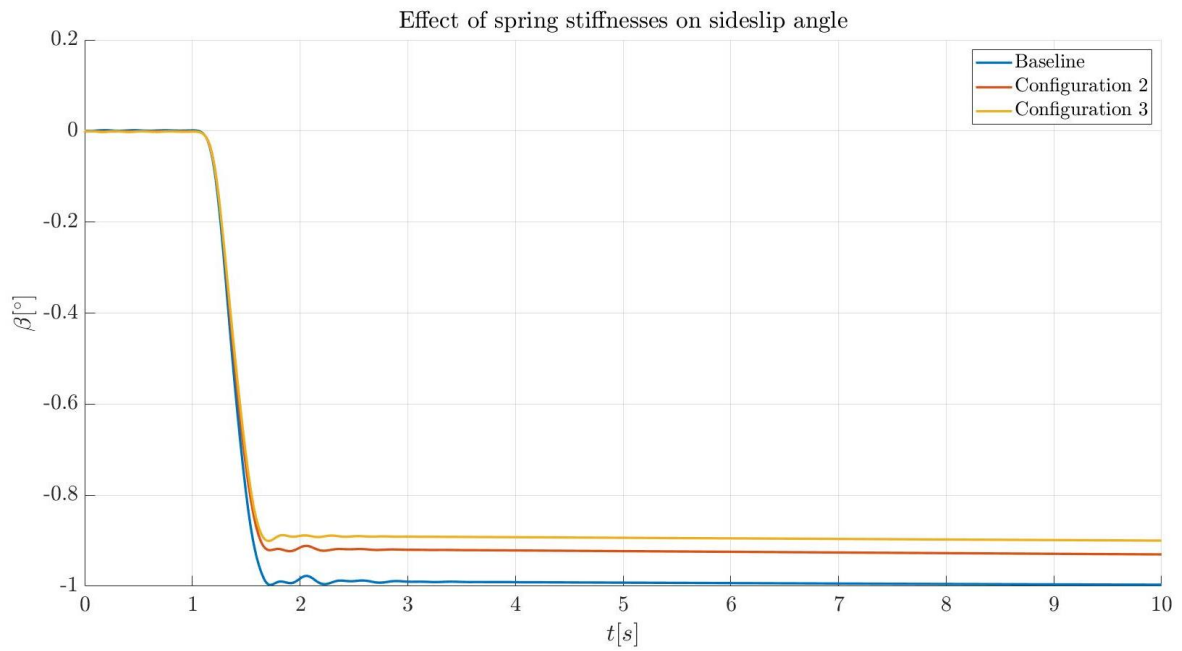


**Figure 6.8 - Time evolution of sideslip angle during step steer manoeuvre for different spring stiffnesses**

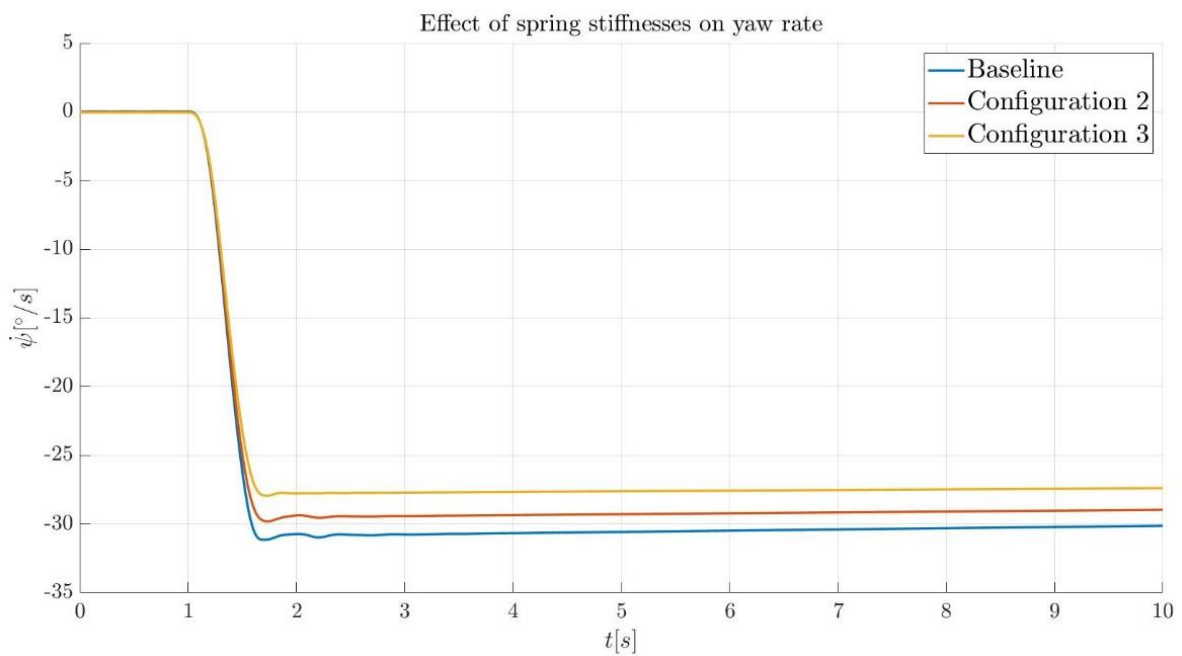


**Figure 6.9 - Time evolution of yaw rate during step steer manoeuvre for different spring stiffnesses**

Finally, the yaw rate evolution confirms the observations made thus far while analysing the effects of spring stiffnesses in the suspensions with respect to handling. The third configuration experiences the least yaw rate in comparison to the other two.

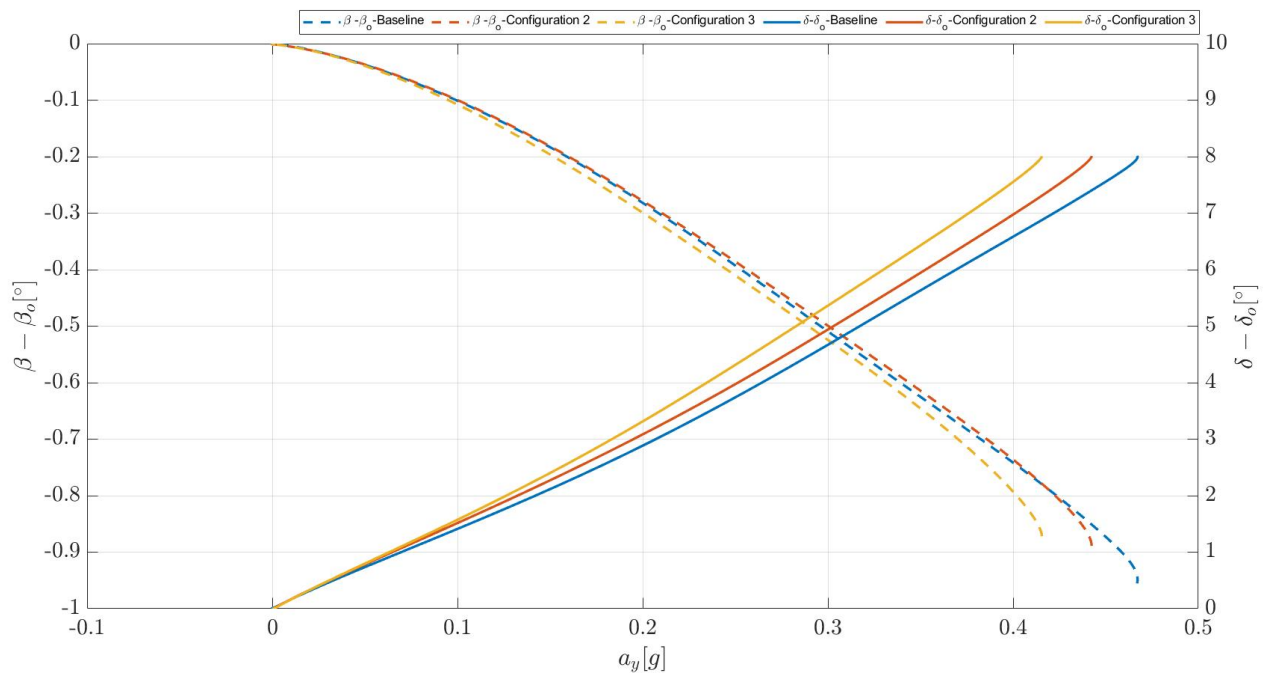


**Figure 6.10 – Handling diagram depicting the steer angles (solid lines) and corresponding sideslip angles(dashed lines) for the analysis of effect of spring stiffness**

The handling diagram for the analysis of spring stiffness effect is presented in the picture above. The diagram helps the reader understand whether a vehicle is exhibiting understeering or oversteering behaviour. In our case, for all stiffness configurations, the understeer behaviour is exhibited as the steering angle difference from an initial value, increases in the positive direction whereas the sideslip angles have increase negatively from an initial value, when plotted against the lateral acceleration. For oversteer, this negative growth of sideslip angle occurs along with the decrease in steering angle or a negative increase from a given reference. For our setup, the initial values of steering angle and sideslip angles are zero and hence the values of  $\beta$  and  $\delta$  are plotted as is against the lateral acceleration in the x-axis.

Now to understand and confirm which of the configurations are more understeer, it can be observed that the baseline experiences the most lateral acceleration and sideslip angle increase and therefore has less understeering behaviour than the others. The most understeering configuration hence is configuration 3, aligning with the explanations given after the temporal evolution plots of different parameters earlier.

### 6.2.3.2. Influence of ARBs:

In this sub-section, an effort has been made to describe the temporal evolution of the parameters discussed in previous sections and how they are affected by the anti-roll bar and the

corresponding handling diagram has been provided towards the end. The baseline assembly with ARBs was modified to allow the following different configurations for this purpose:

- (i) Assembly with front ARB only
- (ii) Assembly with rear ARB only

The fourth configuration for this study was the assembly without any ARB which has already been described earlier.

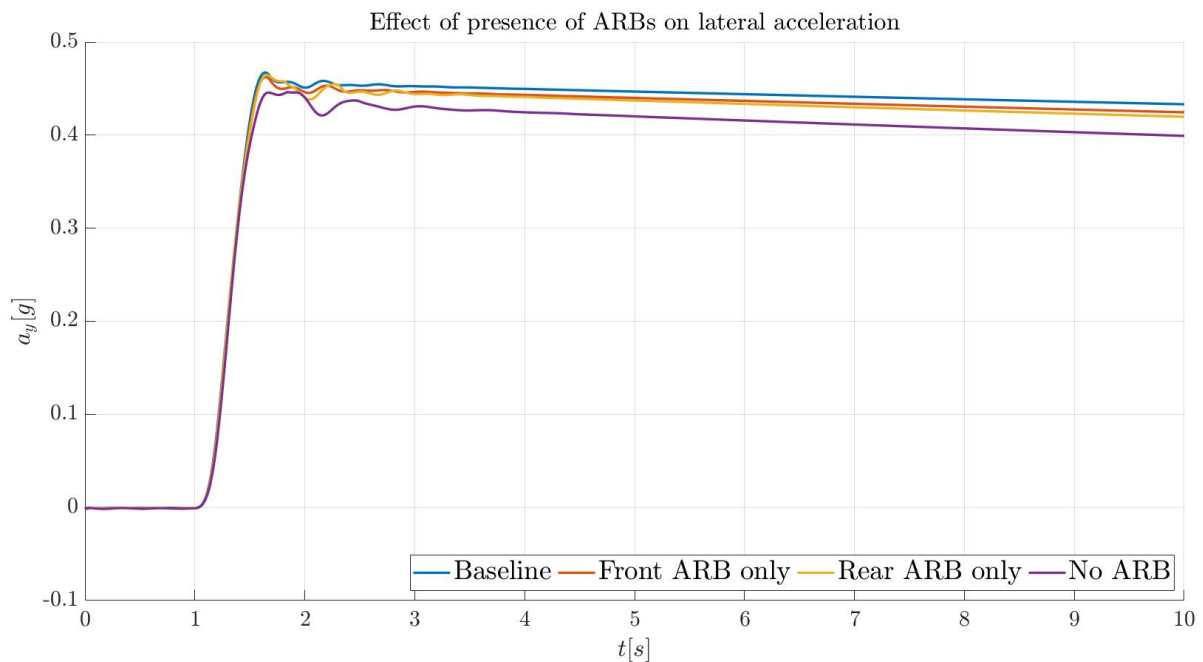


*Figure 6.11 – Effect of ARB on temporal evolution of lateral acceleration for step steer manoeuvre*

In the plot with the temporal evolution of lateral acceleration, we see that, predictably, the baseline reaches the lowest lateral acceleration and the non-ARB experiences it the most. Now, if the curves associated with the other two configurations are observed, it is seen that with only the front ARB, the lateral acceleration is lesser on the vehicle than with only the rear ARB. This is a direct result of the reduced stiffness in the front, and it can also be seen that the front ARB only assembly reaches a steady state value of lateral acceleration quickly while the rear ARB only assembly barely reaches it within the simulation duration. In relation to a case where only a single ARB is present in a vehicle, it can be interpreted that in terms of handling, the presence of the front ARB increases the understeer behaviour and subsequently the stability is higher, while the increase in rear stiffness due to the presence of ARB only in the rear can lead to higher lateral acceleration and can also cause instability at higher steering angles and velocities.

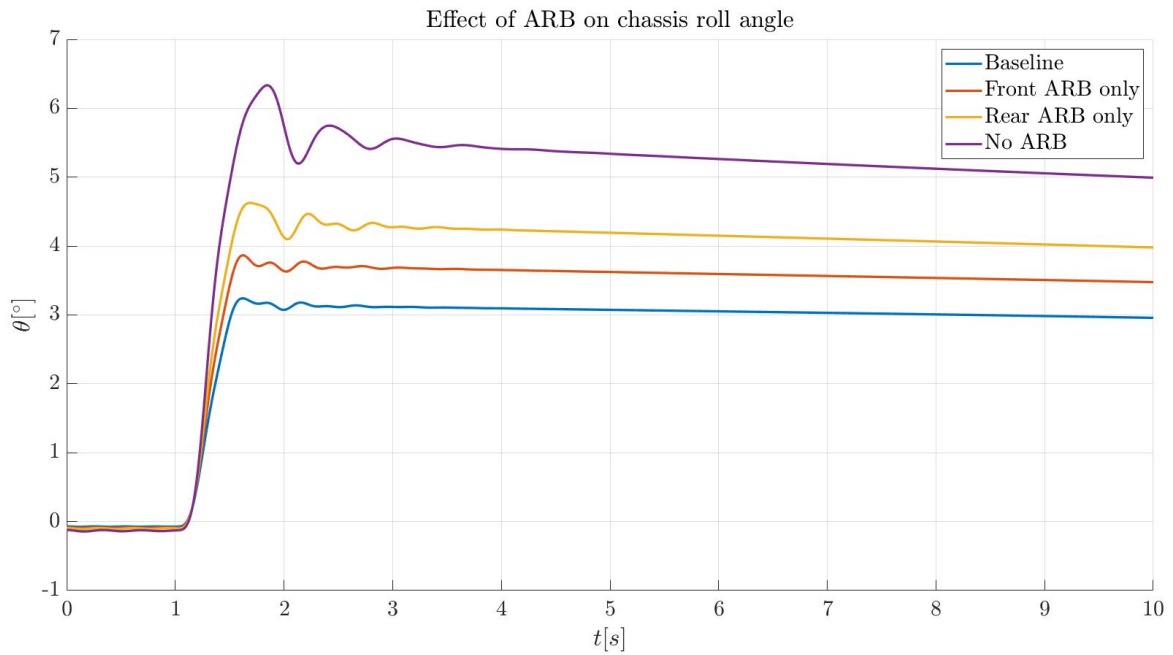


**Figure 6.12 - Effect of ARB on temporal evolution of chassis roll for step steer manoeuvre**

Similar trends are observed when plotting the chassis roll angle and the pitch angle of each of the configurations which emphasise the role of ARB in the vehicle model. The baseline experiences the least roll and pitch motions while the non-ARB experiences the most roll angle and pitching motion. The behaviour of the vehicle in terms of handling is stablest for baseline and when the single ARB configurations are compared, it is seen that the vehicle is stablest and exhibits relatively more understeer if ARB is present in the front only than in the rear alone.

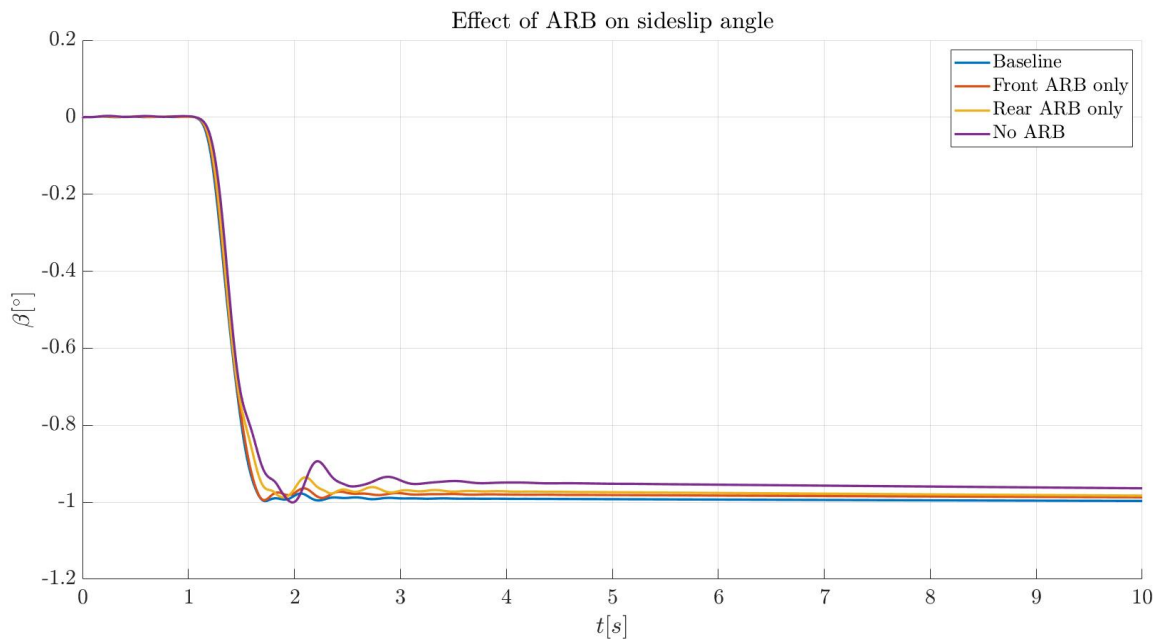


**Figure 6.13 – Effect of ARB on the temporal evolution of sideslip angle during step steer manoeuvre**



The findings are consistent with the trends of the sideslip angle shown above. The angle is greatest for the baseline implying the slipping and more loss of grip of the wheels, and this confirms it experiences more understeering behaviour. The opposite is true for the with neither ARB present.

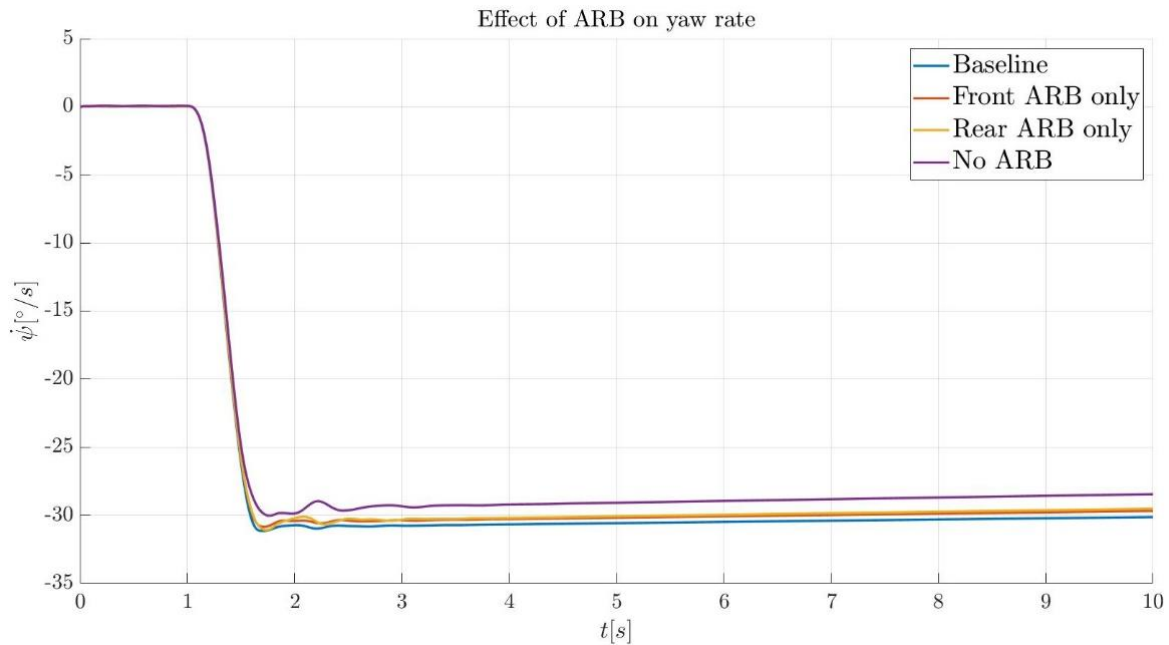


**Figure 6.14 - Effect of ARB on temporal evolution of yaw rate for step steer manoeuvre**

The findings and interpretations made so far are consistent with the trends of the yaw rate evolution shown above. Here, once again, the most yaw rate is observed for the baseline, and the evolution is the smoothest in comparison to the other curves, meaning the vehicle yaws the most in the opposite direction for baseline during a turn, thus once again underlining its higher stability and understeer attributes.

As a final measure, for this analysis of the impact of ARBs, the handling diagram associated with it is presented as a final step. It is then established, by the same logic used for explaining the handling diagram associated with the analysis of stiffness effect on handling, that the baseline once again has the most understeering effect in the vehicle. The configurations with singular ARBs, while experiencing almost identical magnitudes of lateral acceleration, exhibit slightly different behaviours, with the front ARB configuration proving to experience more understeer than the rear ARB only configuration going by the evolution of sideslip angles against the lateral acceleration in the figure. The least amount of understeer is experienced by the configuration with the least stiffness, the no ARB configuration and it is the most unstable of the four configurations and has the highest tendency to roll-over amongst them.

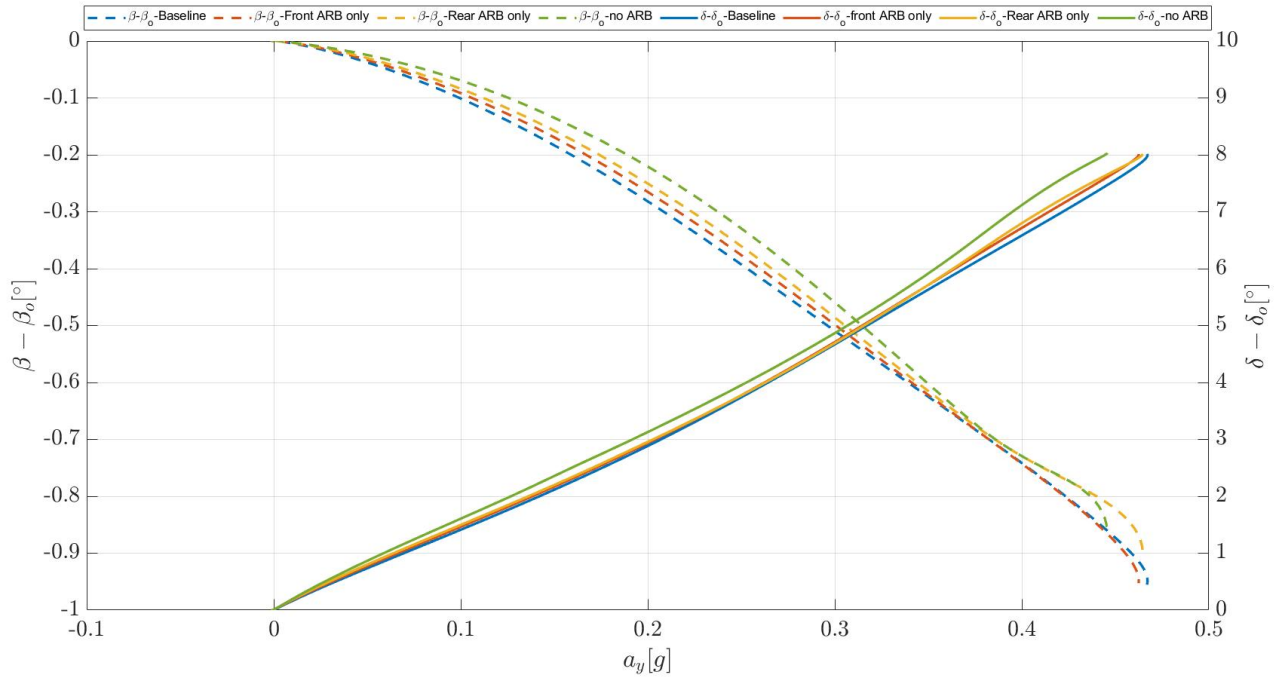


**Figure 6.15 – Handling diagram for the analysis on the effect of ARB during step steer with steer angles (solid lines) and sideslip angles (dashed lines) vs lateral acceleration**

## **Conclusions and further scope of work**

The various parts of the scaled vehicle have been successfully replicated in the multibody environment and have been used in suspension and full vehicle assemblies to analyse its behaviour and get a glimpse of its handling capabilities, while also verifying the accuracy of the model in terms of being in line with vehicle dynamics parameters. The effects of spring stiffnesses and ARBs have been studied as extensively as possible, as they are key in tuning the handling behaviour of vehicles. The future of scope of work for this model are many; further analysis related to handling based on suspension geometries like camber and toe angles can be done. The results obtained from both the body of this work and the effect of camber and toe on handling can be compared with the data available from the actual scaled vehicle once tests are performed. This can help in tuning the vehicle even more in terms of mass and geometrical properties and can lead to results that are as consistent as possible. This work can form a basis of comparison for such studies, on which other attempts can be built. Furthermore, FE part anti-roll bar included in this model can be studied extensively as a separate topic to understand the forces developed in it. This FE part method could then be extended to replicate other parts more realistically and understand the loads and stresses in these parts, particularly for the suspension control arms, uprights and the steering tie-rod. More extensive tests related to straight line events like acceleration and braking and also related to cornering can be performed to have a holistic picture of the functioning of the model.

An attempt can also be made to develop a dedicated tire model, based on experiments, which is consistent with the Losi tires as this can help in understanding the tire mechanics for tires as unique as in the vehicle and can also be useful for durability analysis, considering that the Losi 5ive T2.0 is a scaled off-road truck. Once a compatible tire model is developed, the study can proceed in this direction and can also be correlated with experimental data from the functioning of the vehicle. The tests can be carried out on the predefined road files in ADAMS and also on user defined road files according to needs. The redefined road files in ADAMS already include roads or tracks replicating the behaviour of soft soil for example, which could be of interest with respect to this model in the future to understand the durability of and ride characteristics of the model.

## Appendix

### A.1. 3D beam formulation:

This part is once again a brief of the discussion extracted from “Welcome to the FE Part” [3] by MSC.

The 3D beam formulation by ADAMS is derived from the Absolute Nodal Coordinate Formulation (ANCF) [5] shear deformation beam theory as well as the geometrically exact beam formulation theories present in literature [6-10]. The beam description depends on the centroid line  $r(x,t)$  and the cross section moving frame  $A(x,t)$ , where  $A = [n \ t1 \ t2]$  is the transformation matrix from the moving frame to the global coordinate system.

The following picture depicts the geometrical depiction of a beam particle.

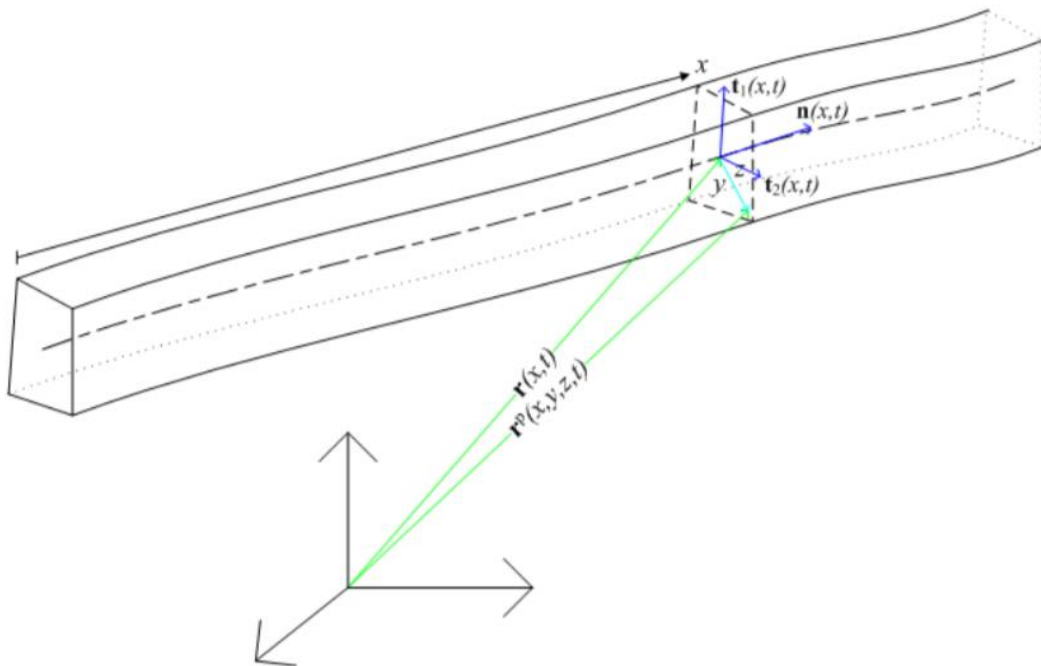


**Fig. A.1 – 3D beam particle depiction**

$r^p$  defines the co-ordinates of a particle P on the beam. It is given by

$$r^p(x, y, z, t) = r(x, t) + A(x, t)d \quad (A.1)$$

Where  $d = (0 \ y \ z)^T$  is used to define the particle's co-ordinates in the cross-sectional frame of reference.

The matrix A requires a rotation matrix  $\Theta$  for its definition. A is defined as

$$A = I + f(\theta)\theta + g(\theta)\theta^2 \quad (\text{A.2})$$

And  $I$  is a 3 x 3 identity matrix and,

$$\theta = \|\theta\| = \sqrt{\theta_1^2 + \theta_2^2 + \theta_3^2} \quad (\text{A.3})$$

$$\theta = \begin{pmatrix} 0 & -\theta_3 & \theta_2 \\ \theta_3 & 0 & -\theta_1 \\ -\theta_2 & \theta_1 & 0 \end{pmatrix} \quad (\text{A.4})$$

$$f(\theta) = \begin{cases} \frac{\sin\theta}{\theta}, & |\theta| \geq 0.01 \\ 1 - \frac{\theta^2}{3!} + \frac{\theta^4}{5!} - \frac{\theta^6}{7!} + \dots, & |\theta| < 0.01 \end{cases} \quad \text{and } g(\theta) = \frac{1}{2}f^2\left(\frac{\theta}{2}\right) \quad (\text{A.5})$$

The position vectors of the centroid line  $r(x, t)$  and the rotation vectors of the moving frames  $\theta(x, t)$  are independently interpolated in each element and are given by

$$r(x, t) = (1 - 3\xi^2 + 2\xi^3)r_0(t) + l(\xi - 2\xi^2 + \xi^3)r'_0(t) + (3\xi^2 - 2\xi^3)r_1(t) + l(\xi^3 - \xi^2)r'_1(t) \quad (\text{A.6})$$

$$\theta(x, t) = (1 - 3\xi + 2\xi^2)\theta_0(t) + 4\xi(1 - \xi)\theta_m(t) + \xi(2\xi - 2)\theta_1(t) \quad (\text{A.7})$$

Where the length of the element is given by  $l$  and  $\xi = x/l$  is the normalized arc-length coordinate.

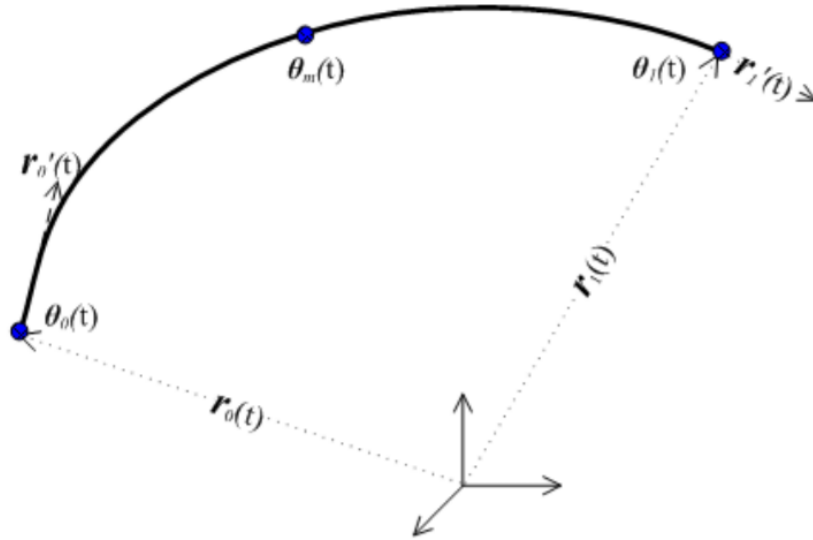


*Fig. A.2 – Depiction of coordinates of beam element*

Then,  $q$  represents the generalized coordinates of the beam element and is given by

$$q = (r_0^T \ r'_0{}^T \ \theta_0^T \ \theta_m^T \ r_1^T \ r'_1{}^T \ \theta_1^T)^T \quad (\text{A.8})$$

This results in 21 generalized coordinates for each beam element. The beam equation is then derived from the Lagrange's equation

$$\frac{d}{dt} \left( \frac{\partial T}{\partial \dot{q}_i} \right) - \frac{\partial T}{\partial q_i} + \frac{\partial V}{\partial q_i} + \frac{\partial \Psi^T}{\partial q_i} \lambda = Q_i \quad (\text{A.9})$$

And  $T$  is the kinetic energy,  $V$  is the potential energy,  $\Psi$  represents equations denoting the constraints and  $\lambda$  denotes the corresponding Lagrange multipliers for the constraints.  $Q$  is the representation of the generalized applied forces.

For an arbitrary nth element, the kinetic energy is given by

$$T^n = \frac{1}{2} \int_0^1 (\rho A \dot{r}^T \dot{r} + \omega^T J \omega) dx \quad (\text{A.10})$$

Where  $\omega = B\dot{\theta}$  and  $B = I - g(\theta) \theta = h(\theta) \theta^2$  and,

$$h(\theta) = \begin{cases} \frac{\theta - \sin\theta}{\theta^3} & |\theta| \geq 0.01 \\ \frac{1}{3!} - \frac{\theta^2}{5!} + \frac{\theta^4}{7!} - \frac{\theta^6}{9!} + \dots & |\theta| < 0.01 \end{cases} \quad (\text{A.11})$$

$\rho$  = density of the beam

$A$  = area

$J$  = rotary inertia of the cross section

$\omega$  = angular velocity of the moving frame

Likewise, the elastic potential energy of the nth element is

$$V^n = \frac{1}{2} \int_0^1 [\gamma^T C_A \gamma + (\kappa - \kappa_0)^T C_I (\kappa - \kappa_0)] dx \quad (\text{A.12})$$

where,

$$\gamma = A^T r' - A_0^T r'_0, \quad \kappa = B\theta' \quad (\text{A.13})$$

$\gamma$  = strains of the centroid line

$\kappa$  = the moving frame's curvature

$C_A$  = stiffness matrix of strain

$C_I$  = curvature stiffness matrix

The matrices  $C_A$  and  $C_I$  are defined as follows

$$C_A = \begin{bmatrix} c_1 & c_2 & c_3 \\ c_2 & c_4 & c_5 \\ c_3 & c_5 & c_6 \end{bmatrix} \quad (\text{A.14})$$

and,

$$C_I = \begin{bmatrix} c_4 + c_6 I_{zz} + 2c_5 I_{yz} & -c_4 I_{yy} - c_5 I_{yz} & -c_4 I_{yy} - c_5 I_{yz} \\ -c_4 I_{yy} - c_5 I_{yz} & c_1 I_{yy} & c_1 I_{yz} \\ -c_4 I_{yz} - c_5 I_{zz} & c_1 I_{yz} & c_1 I_{zz} \end{bmatrix} \quad (\text{A.15})$$

with,

$$I_{yy} = \int_A z^2 da \quad (\text{A.16})$$

$$I_{zz} = \int_A y^2 da \quad (\text{A.17})$$

$$I_{yz} = - \int_A yz da \quad (\text{A.18})$$

The values of  $C_A$  and  $C_I$  matrices depend on whether the material considered is isotropic or orthotropic.

The virtual work done by the  $n^{th}$  equation is given by

$$\delta W^n = \int_0^l [\delta r^T(x, t) f(x, t) + \delta \Pi^T(x, t) t(x, t)] dx = \delta q^T Q \quad (\text{A.19})$$

And

$$\delta \Pi = B^T \delta \theta \quad (\text{A.20})$$

## References

1. “Overview of how to use ADAMS/Solver” – Notes from the Course “Advanced Mechanical Design”, University of Rochester
2. “ADAMS/Solver Primer”, Dan Negrut, Andrew Dyer, MSC Software (2004)
3. “Welcome to the FE Part”, MSC Software
4. “Race Car Vehicle Dynamics”, Milliken and Milliken, Society of Automotive Engineers (SAE) International, (1995).
5. “ADAMS Online Help” (2013), Hexagon MI Documentation Centre
6. “The Absolute Nodal Coordinate Formulation (ANCF)”, Antonio Recuero and Dan Negrut, – Project Chrono Technical Documentation (2016)
7. “A Finite Strain Beam Formulation, the three-dimensional Problem. Part I. Comp. Meth. Mech. Eng.”, Vol.49, pp. 55-70, Simo, J. C. (1985)
8. “Three-dimensional Finite Strain Rod Model. Part II: Computational Aspects. Comp. Meth. Mech. Eng.”, Vol.58, pp. 79-116, Simo, J. C., (1986)
9. “A Computationally Efficient and Robust Geometrically Exact Curved Beam Formulation for Multibody Systems” Ren, H. -7th Asian Conference on Multibody Dynamics, Busan, Korea (2014).
10. “A Shear-Locking Free Model of Timoshenko Beams with Large Deformation and Large Rotation” Ren, H., N. Khude, J. Ortiz, M. Collingridge., -ECCOMAS Thematic Conference. Zagreb, Croatia, 2013
11. “The Multibody systems approach to Vehicle Dynamics”, Mike Blundell and Damian Harty, Butterworth-Heinemann (2004)



## Acknowledgements

“கேடுஇல் விழுச்செல்வம் கல்வி ஒருவற்கு மாடுஅல்ல மற்றை யவை”

The 2000-year-old couplet above roughly translates to “*Education is the truest imperishable wealth in comparison to everything else*”. During my journey here at Politecnico di Torino in pursuit of this wealth, I have had the fortune of having many a person by my side, supporting me and egging me on to achieve whatever I set out to do. This little note is an ode to all of those who have stood by me in this journey.

Firstly, I place on record my gratitude and love for my parents, without whose support this would not have been possible. They have allowed me to dream and achieve those dreams and have always been my strongest pillars of support and I will be forever grateful for it. My thanks are due to my family members, who have all helped me in one way or another right from when I decided to pursue this course. I owe them my sincerest gratitude.

I would like to sincerely thank Prof. Alessandro Vigliani for trusting me and giving me this opportunity to work on this thesis which has helped me deepen my learning on aspects related to the study of vehicle dynamics using multibody simulations. It has been a period of genuine learning and I feel like I have become a better engineer through the course of completion of this thesis.

I would also like to sincerely thank Ing. Daniele Catelani and Ing. Mauro Vesco from Hexagon, without whose constant support and teaching, this thesis work would not have come to fruition. Thank you for always being there and helping me out, nudging me in the right direction to finish this work.

I would also like to place on record my sincerest thanks to Ing. Angelo Vella, who has been a great guide for me since the day I began working on this thesis. Thank you for your constant inputs and suggestions which have ultimately made my work better.

To Karthi, my best friend who also embarked on this journey to Italy to successfully pursue his master’s degree, thank you for being there and trusting me, brother. Your support through all the highs and lows of being a student away from home is invaluable and I am forever grateful for it.

To Sudharshana, who has been a ray of light and has picked me up each time I felt I hit a roadblock; thank you from the bottom of my heart. Your support means the world and I know that I couldn’t have done this without you. Here’s to many more achievements and celebrations that are in store.

I would like to thank Harsha, Nitin and Rohan, who have been my batchmates and my housemates and great friends in this period of study, for all their support. It has been a memorable journey and I am grateful for you all and I will always root for you.

Last, but not the least, a big thank you to all the friends I have made here in Torino and back home in India. I will always be grateful for the love and support.

